

Doctoral Thesis ETH No. 18'276

# Enzymatic Amplification Schemes towards Electronic Biosensing

A dissertation submitted to the  
ETH ZURICH

for the degree of  
Doctor of Sciences  
(Dr. sc. ETH Zürich)

presented by  
Dorothea Niederberger  
Dipl. Werkstoff-Ing. ETH  
born on February 23, 1981  
citizen of Schaffhausen SH, Hallau SH and Dallenwil NW

accepted on the recommendation of  
Prof. Dr. Janos Vörös, examiner  
Dr. Erik Reimhult, co-examiner  
Dr. Thomas Hirt, co-examiner

23. March 2009



FOR RETO AND MY PARENTS



*The only source of knowledge is experience.*

ALBERT EINSTEIN



---

## Acknowledgements

---

It is my great pleasure to hereby thank all the people who have supported me during my project, scientifically as well as personally.

First of all, I would like to thank Prof. Dr. Janos Vörös for giving me the opportunity to perform my PhD thesis in his group and for being my Doctor father. Janos, I highly appreciate your support throughout the thesis. You gave me freedom in planning and performing my project but at the same time the necessary motivation and inputs.

I would also like to thank my two co-referees, Dr. Erik Reimhult from ETH Zurich and Dr. Thomas Hirt from BioCure Inc. Erik, especially in the beginning of my thesis your advice and knowledge was really helpful to me. You always had time for me, even though, I know, you are generally very busy. Thomas, in the later stage of my thesis the collaboration with you broadened my horizon and you convinced me that finally my research might be used in a "real" product.

Prof. Dr. Marcus Textor offered me the possibility to work in his labs until the new LBB labs were finished. Marcus, also thanks to your motivation I decided to stay at ETH for some more years after finishing my studies - a decision I definitely do not regret.

During a semester thesis and at the beginning of my PhD thesis, Dr. Brigitte Städler introduced me to the world of vesicle based sensing. Brigitte, your knowledge and patience in answering all my questions were essential for a successful start of my project.

I would also like to thank my colleagues from the LBB. Marta for being my office mate since the beginning, having fun together at conferences and scientific cooperation; Bink for helping with my 1001 questions about the computer and having fun in the office; Orane for being my office mate and having extended, interesting discussions about PEMs; Elsa for her Swedish cookies and helping me with my first (and only) cell experiment of

my life; Röbi for being the LBB language expert and acrobat; Mike for being patient when the confocal did not like me; Takumi for helping with complicated equipment and theories; Norma for being multi-talented and entertaining in playing the flute, losing and finding keys and updating the coffee stock; Raphael for continuing my PEM project; Tomaso for always being friendly and helpful; Kaori for watching funny movies together; Pascal for quickly organizing a Christmas cake; Alex for making sure we all get to know the best French wine; Esther for taking care of all the administrative issues; Dominik for knowing a practical solution in every situation and finally the cell lab and FACS lab people for joining the coffee break once in a while. Of course, also the former LBB members need to be added to this list: Tinu for building the lab and still joining LBB events together with Blädi and Huwi. And to all of you, thanks a lot for the friendly and helpful atmosphere in our group, not only in the lab but also during ski weekends and other events.

Paul Lüthi and Stephen Wheeler from the mechanics shop did a great job. Paul and Stephen, your work was not only precise, you also took your time for emergency repairs.

Victoria de Lange and David Joos were my students. Both of you did a good job and made a nice contribution to my thesis.

Our collaborators from Strasbourg are acknowledged for their input and support. Dr. Fouzia Boulmedais for discussions and help in writing a paper; Dr. Vincent Ball for performing the FTIR experiments for this paper; Prof. Dr. Pierre Schaaf and Prof. Dr. Jean-Claude Voegel for giving valuable advice and for keeping an eye on our activities.

Dr. Svetlana Litvinchuk and Dr. Arthur Lu from BioCure Inc. are acknowledged for synthesizing the polymeric vesicles.

Finally, I would like to thank Reto and our families. Reto, I know it was not always easy for you, especially when my experiments took long (and still did not work...) or when I worked on the weekend. I highly appreciate your respect and understanding. Mutti and Vati, you always supported me. Without you I would not be where I am now. Katrin, thanks to your 7-year old students I finally know what I am: an "inventor". Ruth and Tony, I know it was difficult for you to understand what I am working on. Nevertheless, you always respected my decision and showed interest in my work. Special thanks go to you Ruth for the proof-reading.

Last but not least I would like to thank ETH Zurich for the financial support of my project.



---

## Abstract

---

Biosensors provide a powerful tool to detect the concentrations of various analytes. Since 1962, when the first glucose test for diabetes patients was introduced, numerous other attempts have been designed. A wide variety of (future) applications are constantly being developed, whereas one main focus of today's research is on the increasing number of people suffering from cancer. Currently, when the disease is diagnosed, it is seldom in an early stage. Therefore, it is essential to provide possibilities for early diagnoses that are cheap and fast. Ideally, such biosensors are built in a way that can easily be multiplied because nowadays more and more cancer (and other) antigens are being identified. The task is now to construct sensors which enable highly sensitive detection of such antigen molecules at very low concentrations.

Most approaches are based on fluorescent or enzymatic detection of the target molecules. Fluorescence is widely spread in high-throughput screening applications, but also enzymes are often used (e.g. in ELISA). Enzymatic detection, however, is dominating the point-of-care and home diagnostics market. The enzymatic sensors can be classified into two categories. Either they perform a reaction causing a colour change, or they generate products that can be detected with electrochemical techniques. In order to be detectable, the antigens need to be connected to enzymes. The most common techniques are sandwich based assays, where the antigen is captured by a surface immobilized antibody and detected by an enzyme labelled, secondary antibody. The sensitivity of such assays is based on the amplification by the enzyme, because that way many enzymatic reaction cycles can be coupled to a single recognition event. However, sometimes even this amplification is not enough and further improvement is necessary, e.g. by linking more than one enzyme to a single recognition event.

This thesis deals with such novel concepts that should allow for bridging the gap between the mM detection limit of existing hand-held enzymatic biosensors and the required pM sensitivity for a future cancer marker sensor.

As an introduction to the field, the most common electrochemical detection techniques are listed along with other emerging electronic sensors, such as nanowires. Although the long-term goal of this work is to achieve a hand-held electronic sensing device, during the development it is often necessary to obtain additional information about the system. Therefore, complementary biosensor techniques that can be combined with electrochemical detection are also described and the most common biosensing surface architectures are introduced.

The first biosensor type presented in this thesis is based on a sandwich assay with vesicles for signal amplification. Vesicles, coupled to secondary antibodies, significantly increased the QCM-D signal because of their large mass and accordingly high viscoelasticity. With this quite simple setup, sensitivities in the critical concentration range of the cancer marker prostate specific antigen (PSA) could be achieved.

In order to benefit from the signal enhancement principle from the QCM-D sensor, enzymes have been implemented into our system to allow for electrochemical detection. These requirements have been achieved by covering the vesicle surfaces with enzymes, meaning every detected antigen finally induced a signal corresponding to thousands of enzymes. With this electrochemically detectable signal enhancement method even lower detection limits than with the vesicle amplified QCM-D biosensor could be achieved. Thus, this system has the potential to be used in biosensors detecting cancer antigens with even much lower abundance than PSA.

For potential applications the stability, the compatibility with biological samples and the shelf-life of the sensor are essential parameters. In order to improve these aspects, the fragile lipidic vesicles were exchanged with more robust polymeric vesicles or solid particles. Besides from their improved shelf-life through better chemical stability and resistance, the polymeric vesicles offer the possibility of incorporating enzymes, accessible through membrane pores.

Another sensor type, situated at the interface between electroactive polymers and polyelectrolyte multilayers (PEMs), has been developed within the frame of this thesis in addition. PEM films containing ferrocyanide ions, were found to show a swelling/deswelling behaviour upon application and removal of a low electric potential.

The deformation occurs instantly and is completely reversible. This setup also allowed for incorporation of the enzyme glucose oxidase into the film or on top of the latter. Like this, the swelling/deswelling effect could be combined with electrochemical detection and activation of enzymes.

Overall, in this thesis a biosensor platform for highly sensitive enzymatic detection of antigens from serum or glucose in sophisticated environments has been developed.



---

## Zusammenfassung

---

Biosensoren sind ein aussagekräftiges Instrument, um Konzentrationen verschiedener Analyten zu messen. Seit 1962 der erste Glukosetest für Diabetiker eingeführt wurde, sind viele weitere Versuche unternommen worden. Eine breite Palette von Anwendungen wird laufend entwickelt. Ein Hauptfokus der aktuellen Forschung liegt dabei auf der steigenden Anzahl von Menschen, die an Krebs leiden. Da die Krankheit heutzutage nur selten in einem frühen Stadium erkannt wird, ist es wichtig, schnelle und kostengünstige Methoden für frühe Diagnosen zu entwickeln. Idealerweise sind solche Sensoren so gebaut, dass sie einfach multipliziert werden können; insbesondere, weil immer mehr Krebs- (und andere) Antigene identifiziert werden. Die Aufgabe ist nun, Sensoren zu entwickeln, die es ermöglichen, Antigene in sehr tiefen Konzentrationen mit hoher Sensitivität zu detektieren.

Die meisten Ansätze basieren auf fluoreszenter oder enzymatischer Detektion der Zielmoleküle. Fluoreszenz wird häufig in Anwendungen mit hohem Durchsatz eingesetzt, aber auch Enzyme sind weit verbreitet (z.B. in ELISA). Bei tragbaren Biosensoren, oder solchen die zu Hause verwendet werden, dominieren jedoch die enzymbasierten Systeme. Dabei gibt es zwei Arten von enzymatischen Sensoren; die einen induzieren eine Farbänderung, während die anderen eine chemische Reaktion auslösen, deren Produkte anschliessend elektrochemisch detektiert werden. Um Antigene zu detektieren, müssen sie an Enzyme gebunden werden. In den meisten Fällen werden auf der Sandwichtechnik basierende Assays verwendet. Dabei wird das Antigen von einem auf die Oberfläche adsorbierten Antikörper gebunden und von einem zweiten Antikörper, welcher an ein Enzym gebunden ist, detektiert. Die Sensitivität eines solchen Sensors basiert auf der Vervielfachung des Signals, da ein einzelnes Enzym mehrere Reaktionszyklen durchläuft. In manchen Fällen reicht diese Signalverstärkung jedoch nicht aus, und es müssen weite-

re Massnahmen getroffen werden, z.B. indem man mehrere Enzyme an einen einzelnen Antikörper bindet.

Heutige tragbare Geräte mit integrierten enzymatischen Biosensoren operieren im mM-Detektionsbereich. In dieser Dissertation wurden neue Konzepte entwickelt, um in den pM Sensitivitätsbereich zukünftiger Sensoren für Krebsmarker zu gelangen.

Als Einleitung ins Gebiet werden die gebräuchlichsten Detektionsverfahren vorgestellt, sowie neuere elektronische Sensoren wie z.B. Nanodrähte besprochen. Obwohl das langfristige Ziel dieser Arbeit ein tragbares, elektronisches Gerät ist, ist es während der Entwicklungsphase oft notwendig, zusätzliche Informationen über das System zu erhalten. Daher werden auch alternative Biosensortechniken beschrieben, welche mit elektrochemischer Detektion kombiniert werden können. Ausserdem werden die gebräuchlichsten Architekturen von Biosensor Oberflächen vorgestellt.

Die erste Art von Biosensoren, welche in dieser Dissertation vorgestellt wird, basiert auf einem Sandwichassay mit Vesikeln zur Signalverstärkung. Lipide Vesikel, die an die sekundären Antikörper gebunden sind, erhöhen durch ihre grosse Masse und die entsprechend hohe Viskoelastizität das Signal der Quartzkristall Mikrowaage (QCM-D) erheblich. Gleichzeitig wird beim QCM-D auch die Dissipation gemessen, welche durch die Vesikel ebenfalls signifikant erhöht wird. Mit diesem einfachen Versuchsaufbau konnten Sensitivitäten erreicht werden, die ausreichen, um den Krebsmarker PSA (Prostata-spezifisches Antigen) zu messen.

Um die elektrochemische Detektion zu ermöglichen, wurde das Prinzip der Signalverstärkung vom QCM-D Sensor weiter entwickelt, indem das System mit Enzymen erweitert wurde. Diese Auflagen wurden durch Funktionalisierung der Vesikeloberflächen erfüllt. Dabei induzierte jedes detektierte Antigen ein Signal, welches Tausenden von Enzymen entspricht. Mit diesem elektrochemisch detektierbaren Signal wurden sogar noch höhere Sensitivitäten erreicht als mit den Vesikeln im QCM-D. Daher hat die elektrochemische Methode das Potential, in einem Biosensor zur Detektion von Krebsmarkern eingesetzt zu werden, welche in deutlich tieferen Konzentrationen als PSA vorkommen.

Für potenzielle Anwendungen sind Kompatibilität mit anderen biologischen Proben, Stabilität, sowie die Haltbarkeit des Sensors wichtige Parameter. Um den Sensor diesbezüglich zu verbessern, wurden die fragilen lipiden Vesikel durch robustere, polymerische Vesikel oder Mikropartikel ersetzt. Neben ihrer besseren Haltbarkeit durch verbesserte chemische Stabilität ermöglichen es polymerische Vesikel auch, Enzyme in ihrem Innern einzuschliessen. Diese sind dann via Membranporen zugänglich.

Eine neue Art von Sensoren, an der Schnittstelle von elektroaktiven Polymeren und polyelektrolytischen, mehrschichtigen Filmen, wurde im Rahmen dieser Doktorarbeit ebenfalls entwickelt. Wenn diese Filme aus einer bestimmten Kombination von Polymeren aufgebaut wurden und Ferrocyanid enthielten, zeigten sie eine Änderung der Dicke, wenn ein kleines elektrisches Potential angelegt und wieder entfernt wurde. Die Änderung der Dicke erfolgte augenblicklich und war vollständig reversibel. Im Weiteren war es auch möglich, Enzyme in diese Filme einzubauen oder sie auf deren Oberfläche zu adsorbieren. Auf diese Weise wurde der Effekt der Änderung der Dicke mit der elektrochemischen Detektion und Aktivierung von Enzymen kombiniert.

In der vorliegenden Dissertation wurde eine Biosensor-Plattform für hochsensitive enzymatische Detektion von Antigenen in Serum oder Glukose in anspruchsvollen Umgebungen entwickelt.





---

## Contents

---

<b>1</b>	<b>Introduction: Principles &amp; Architectures of Electrochemical Biosensors</b>	<b>3</b>
1.1	Introduction . . . . .	4
1.2	Devices . . . . .	7
1.2.1	Electrochemical Detection Techniques . . . . .	8
1.2.2	Nanowires . . . . .	11
1.2.3	Electrochemistry in Combination with Complementary Biosensor Techniques . . . . .	12
1.3	Surface Architecture . . . . .	17
1.3.1	Surface Materials and Modifications . . . . .	18
1.3.2	Electrochemical Signal Transduction . . . . .	19
1.3.3	Enzymes . . . . .	20
1.3.4	Recognition Elements . . . . .	22
1.3.5	Encapsulation of Enzymes . . . . .	24
1.3.6	Supported Lipid Bilayer Sensor Architectures . . . . .	26
1.4	Summary of the Biosensor State of the Art . . . . .	29
<b>2</b>	<b>Scope of the Thesis</b>	<b>33</b>
<b>3</b>	<b>Materials and Methods</b>	<b>37</b>
3.1	Materials . . . . .	37
3.1.1	Buffer . . . . .	37
3.1.2	Proteins . . . . .	37
3.1.3	Enzymes and Substrate . . . . .	38
3.1.4	Antibodies . . . . .	38
3.1.5	Lipids . . . . .	38
3.1.6	Polymers for Multilayers . . . . .	39

---

3.1.7	Mediators . . . . .	40
3.1.8	Substrates, Surfaces . . . . .	40
3.1.9	Particles . . . . .	40
3.2	Methods . . . . .	41
3.2.1	Electrochemistry . . . . .	41
3.2.2	Instruments . . . . .	42
3.2.3	Vesicle Fabrication . . . . .	45
3.2.4	Biosensing Experiments . . . . .	46
3.2.5	Polyelectrolyte Multilayers (PEMs) . . . . .	48
<b>4</b>	<b>Vesicles for Signal Amplification in a Sandwich based Biosensor</b>	<b>51</b>
4.1	Sensor Buildup . . . . .	51
4.2	Optimizing the Sensor . . . . .	56
4.3	Polymeric Vesicles for Increased Stability . . . . .	57
4.4	Conclusion . . . . .	59
<b>5</b>	<b>Enzymatic Biosensors with Electrochemical Detection</b>	<b>61</b>
5.1	Mediators and their Detection Principles . . . . .	61
5.1.1	Ferrocyanide . . . . .	62
5.1.2	Ferrocene . . . . .	63
5.2	Enzyme Functionalized Vesicles for Signal Amplification . . . . .	67
5.2.1	Vesicle Adsorption . . . . .	67
5.2.2	Evaluation of Electrochemical Detection Schemes . . . . .	71
5.3	Sandwich Assays with Enzymatic Detection . . . . .	79
5.3.1	Surface Modification . . . . .	79
5.3.2	Enzymatic Detection . . . . .	79
5.3.3	Polymeric Vesicles for Increased Stability . . . . .	82
5.4	Particles as Enzyme Carriers . . . . .	85
5.5	Conclusion . . . . .	87
<b>6</b>	<b>Enzymes Incorporated into Electroactive Polyelectrolyte Multilayers</b>	<b>91</b>
6.1	Swelling and Deswelling . . . . .	92
6.2	Incorporation of Enzymes . . . . .	107
6.3	Conclusion . . . . .	112
<b>7</b>	<b>Summary</b>	<b>113</b>

---

<b>8 Outlook</b>	<b>117</b>
<b>References</b>	<b>119</b>
<b>A PEM Coated Particles and PEM Capsules</b>	<b>135</b>
A.1 Calcium Carbonate Particles . . . . .	135
A.2 Polystyrene Particles . . . . .	138
A.3 Melamine Formaldehyde Particles . . . . .	139
A.4 Conclusion and Outlook . . . . .	141
<b>Curriculum Vitae</b>	<b>143</b>



---

## Abbreviations

---

AB	Antibody
AFM	Atomic force microscopy
AG	Antigen
BSA	Bovine serum albumin
CE	Counter electrode
CLSM	Confocal laser scanning microscope
CV	Cyclic voltammetry
DOPE/b	1,2-Dioleoyl-sn-Glycero-3-Phosphoethanolamine-N-(Biotinyl)
EAP	Electroactive polymer
EC	Electrochemical
EIS	Electrochemical impedance spectroscopy
FBAR	Film bulk acoustic resonator
FC	Ferrocyanide (general)
FCIV	Ferrocyanide (with focus on 4- charge) ( $\text{Fe}^{2+}$ )
FCIII	Ferricyanide (with focus on 3- charge) ( $\text{Fe}^{3+}$ )
FE	Ferrocene
FET	Field-effect transistor
FTIR	Fourier transform infrared spectroscopy
GO	Glucose
GOx	Glucose oxidase
GOx/b	Biotinylated GOx
HRP	Horseradish peroxidase
IgG	Immunoglobulin G
ITO	Indium tin oxide
LbL	Layer-by-layer
MF	Melamine formaldehyde

---

MW	Molecular weight
NA	NeutrAvidin
OCP	Open circuit potential
OmpF	Outer membrane protein F
OWLS	Optical waveguide lightmode spectroscopy
PAH	Poly(allylamine hydrochloride)
PDMS	Poly(dimethylsiloxane)
PEI	Polyethyleneimine
PEM	Polyelectrolyte multilayer
PE-rhod	1,2-Dioleoyl-sn-Glycero-3-Phosphoethanolamine-N-(Lissamine Rhodamine B Sulfonyl)
PGA	Poly(L-glutamic acid)
PLL	Poly(L-lysine)
PLL- <i>g</i> -PEG/TRITC	Poly(L-lysine)- <i>graft</i> -poly(ethylene glycol) functionalized with TRITC
PLL- <i>g</i> -PEG/b	Poly(L-lysine)- <i>graft</i> -poly(ethylene glycol) functionalized with biotin
PMOXA	Poly(2-methyloxazoline)
POPC	1-Palmitoyl-2-Oleoyl-sn-Glycero-3-Phosphocholine
PS	Polystyrene
PSS	Poly(sodium 4-styrenesulfonate)
QCM-D	Quartz crystal microbalance with dissipation monitoring
RE	Reference electrode
SAM	Self-assembled monolayer
SDS	Sodium dodecyl sulfate
SPR	Surface-plasmon resonance
THF	Tetrahydrofuran
TRITC	Tetramethylrhodamine isothiocyanate
WE	Working electrode

---

## Introduction to Sensor Principles and Architectures of Electrochemical Biosensors<sup>1</sup>

---

Quantification of biological or biochemical processes are of utmost importance for medical, biological and biotechnological applications. However, converting the biological information to an easily processable electronic signal is challenging due to the complexity of connecting an electronic device directly to a biological environment. Electrochemical biosensors provide an attractive means to analyze the content of a biological sample due to the direct conversion of a biological event to an electronic signal. Over the past decades several sensing concepts and related devices have been developed. In this chapter, the most common traditional techniques, such as cyclic voltammetry, chronoamperometry, chronopotentiometry, impedance spectroscopy, and field-effect transistor based methods are presented along with selected promising novel approaches, such as nanowire-based biosensing. Additional measurement techniques, which have been shown useful in combination with electrochemical detection, are also summarized, such as the electrochemical versions of surface plasmon resonance, optical waveguide lightmode spectroscopy, ellipsometry, quartz crystal microbalance, and scanning probe microscopy.

The signal transduction and the general performance of electrochemical sensors are often determined by the surface architectures that connect the sensing element to the biological sample at the nanometer scale. The most common surface modification techniques, the various electrochemical transduction mechanisms, and the choice of the recognition receptor molecules all influence the ultimate sensitivity of the sensor. New

---

<sup>1</sup>D. Grieshaber, R. MacKenzie, J. Vörös, and E. Reimhult, *Electrochemical Biosensors - Sensor Principles and Architectures*, *Sensors*, **8**(3): 1400-1458, 2008.

nanotechnology-based approaches, such as the use of engineered ion-channels in lipid bilayers, the encapsulation of enzymes into vesicles, polymersomes, or polyelectrolyte capsules provide additional possibilities for signal amplification.

In particular, this chapter highlights the importance of the precise control over the delicate interplay between surface nano-architectures, surface functionalization and the chosen sensor transducer principle, as well as the usefulness of complementary characterization tools to interpret and to optimize the sensor response.

## 1.1 Introduction

Biosensor-related research has experienced explosive growth over the last two decades. A biosensor is generally defined as an analytical device which converts a biological response into a quantifiable and processable signal [1]. Figure 1.1 shows schematically the parts comprising a typical biosensor: a) bioreceptors that specifically bind to the analyte; b) an interface architecture where a specific biological event takes place and gives rise to a signal picked up by c) the transducer element. The transducer signal (which could be anything from the in-coupling angle of a laser beam to the current produced at an electrode) is converted to an electronic signal and amplified by a detector circuit using the appropriate reference and sent for processing by, e.g., d) computer software to be converted to a meaningful physical parameter describing the process being investigated. Finally, the resulting quantity has to be presented through e) an interface to the human operator. Biosensors can be applied to a large variety of samples including body fluids, food samples and cell cultures and can be used to analyze environmental samples.

In order to construct a successful biosensor for the non-specialist market, a number of conditions must be met:

1. The biocatalyst must be highly specific for the purpose of the analysis, be stable under normal storage conditions and show a low variation between assays.
2. The reaction should be independently manageable from physical parameters such as stirring, pH and temperature. This will allow analysis of samples with minimal pre-treatment. If the reaction involves cofactors or coenzymes these should, preferably, also be co-immobilized with the enzyme.



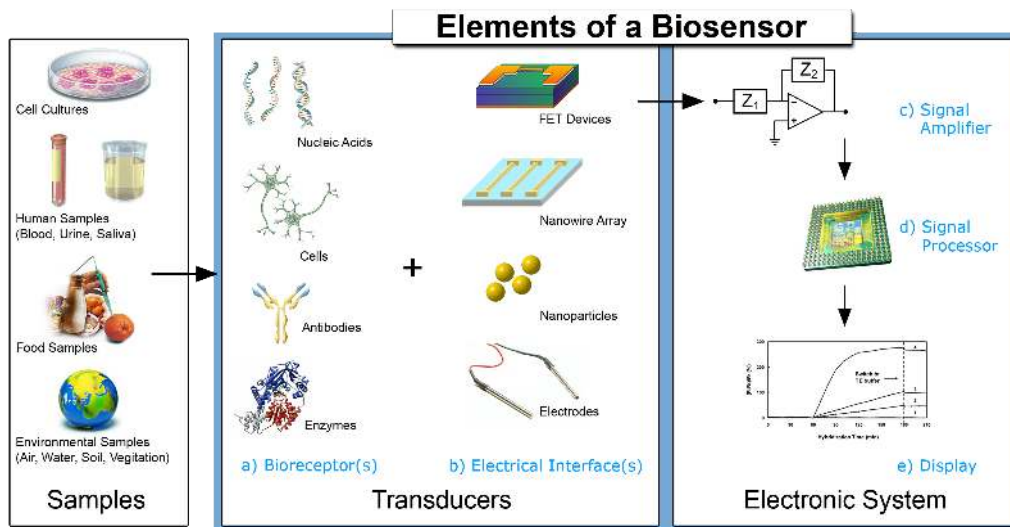


**Figure 1.1:** Elements and selected components of a typical biosensor [1–3].

3. The response should be accurate, precise, reproducible and linear over the concentration range of interest, without dilution or concentration. It should also be free from electrical or other transducer induced noise.
4. If the biosensor is to be used for invasive monitoring in clinical situations, the probe must be tiny and biocompatible, having no toxic or antigenic effects. Furthermore, the biosensor should not be prone to inactivation or proteolysis.
5. For rapid measurements of analytes from human samples it is desirable that the biosensor can provide real-time analysis.
6. The complete biosensor should be cheap, small, portable and capable of being used by semi-skilled operators.

Designed for the purpose, biosensors are generally highly selective due to the possibility to tailor the specific interaction of compounds by immobilizing biological recognition elements on the sensor substrate, that have a specific binding affinity to the desired molecule [4]. Typical recognition elements used in biosensors are: enzymes, nucleic acids, antibodies, whole cells, and receptors. Of these, enzymes are among the most common [3]. To fully exploit the specific interaction through biorecognition, the surface architecture of the sensor also must suppress any non-specific interaction. A tremendous research effort has been invested to find surface modifications with specific interaction capabilities over prolonged periods of time in biological fluids [5].

Today, a multitude of instruments referred to as biosensors can be found in labs around the world and there is a growing number of biosensors being used as diagnostic tools in point-of-care testing, but the realization of cheap handheld devices is so far limited to one well-known example: the glucose sensor [6]. In many cases the main limitation in realizing point-of-care testing/sensing devices is the ability to miniaturize the transduction principle and the lack of a cost-effective production method. Thus, they have to be confined to expert users of high-cost equipment in a lab environment and cannot be used by patients themselves or doctors in the field.

The whole area of biosensors started with the introduction of the first generation glucose oxidase (GOx) biosensor in 1962 [7]. The GOx sensor is still the most widely used, although many improvements (generations) have been added since the 1960's [8]. As exemplified by the glucose sensor, electrochemical biosensors do not suffer the drawback of high sensor setup complexity and cost. This is due to their close link to developments in low-cost production of microelectronic circuits and their easy interface with normal electronic read-out and processing. Other inherent advantages of electrochemical biosensors are their robustness, easy miniaturization, excellent detection limits, also with small analyte volumes, and ability to be used in turbid biofluids with optically absorbing and fluorescing compounds [9, 10]. However, several aspects could be considered to have held back the emergence of additional breakthrough applications built on electrochemical biosensing.

Electrochemical biosensors have suffered from a lack of surface architectures allowing high enough sensitivity and unique identification of the response with the desired biochemical event. For example, pH and ionic strength in biofluids can differ significantly, which affects the response of important classes of biosensors such as immunosensors [10]. Thus, there has recently been an increased emphasis on using nanotechnology to shrink the dimensions of electrochemical sensor elements to sizes which can increase the signal-to-noise ratio for processes designed to occur at the interface of the device and to find ways of using e.g. multiple enzymatic labels to increase the signal per event. The combination of knowledge in bio- and electrochemistry, solid-state and surface physics, bioengineering, integrated circuit silicon technology and data processing offers the possibility of a new generation of highly specific, sensitive, selective and reliable micro (bio-)chemical sensors and sensor arrays addressing these remaining issues [11]. It is thus timely to summarize recent progress in this diverse field and to discuss its future prospects for development.

After introducing the many incarnations of electrochemical biosensors we will discuss how electrochemistry has been and can be combined with complementary sensor techniques to enhance data interpretation. The latter we believe to be very important to optimize given biosensor designs and also for the increased use of electrochemical sensors to characterize biointerfaces. Emerging devices for electrochemical biosensors inspired by advances in microelectronics and nanotechnology like the bio-field effect transistors, nanowires and other "near-molecular scale devices" will be introduced. The last part of this chapter will address surface architectures and modifications used in electrochemical biosensors to improve sensitivity and biospecificity, as well as discuss the emergence of new devices from the multi-disciplinary field where nanotechnology, material science and biology converge.

## 1.2 Devices

Biosensor-related publications were sparse in the early 20th century. The early era of biosensing research and development was first sparked with the defining paper by Clark [12, 13] and his invention of the oxygen electrode in 1955/56. The subsequent modification of the oxygen electrode led up to another publication in 1962 [7], which reported the development of the first glucose sensor and the enhancement of electrochemical sensors (e.g. polarographic, potentiometric and conductometric) with enzyme-based transducers. Clark's work and the subsequent transfer of his technology to the Yellow Spring Instrument Company led to the successful commercial launch of the first dedicated glucose biosensor in 1975 [14].

Since then, various forms of glucose biosensors have been developed, as well as many other sensing technologies and biosensing devices. This section attempts to describe operating principles of electrochemically-based biosensors by reviewing representative devices and their techniques from the aforementioned categories. Although the general topic of this chapter is electrochemical biosensing devices, a detailed overview is given in this section of various combinations of electrochemical sensing with other well-established sensing techniques and biosensor devices. Therefore, special attention is given to aspects of complementary techniques and their advantage of independent, simultaneous measurements with (bio-)electrochemistry. A selection of specific biorecognition elements, structural components and various forms of surface architectures will be summarized in the following section.

### 1.2.1 Electrochemical Detection Techniques

In biosensing the measurement of electrical properties for extracting information from biological systems is normally electrochemical in nature, whereby a bioelectrochemical component serves as the main transduction element. Although biosensing devices employ a variety of recognition elements, electrochemical detection techniques use predominantly enzymes. This is mostly due to their specific binding capabilities and biocatalytic activity [3, 10, 11]. Other biorecognition elements are e.g. antibodies, nucleic acids, cells and micro-organisms [3, 4]. An immunosensor uses antibodies, antibody fragments or antigens to monitor binding events in bioelectrochemical reactions. Detailed information about surface architectures and biorecognition elements is provided in Section 1.3.

Typically, in (bio-)electrochemistry the reaction under investigation would either generate a measurable current when a constant (*amperometric*) or a cyclic (*cyclic voltammetry*) potential is applied, a measurable potential or charge accumulation (*potentiometric*) or measurably alter the conductive properties of a medium (*conductometric*) between electrodes [4]. References are also made to other types of electrochemical detection techniques, such as *impedimetric*, which measures impedance (both resistance and reactance) [15, 16], and *field-effect*, which uses transistor technology to measure current as a result of a potentiometric effect at a gate electrode [2].

Since reactions are generally detected only in close proximity to the electrode surface, the electrodes themselves play a crucial role in the performance of electrochemical biosensors. Based on the chosen function of a specific electrode, the electrode material, its surface modification or its dimensions greatly influence its detection ability. Electrochemical sensing usually requires a *reference* electrode, a *counter* or auxiliary electrode and a *working* electrode, also known as the sensing or redox electrode. The reference electrode, commonly made from Ag/AgCl, is kept at a distance from the reaction site in order to maintain a known and stable potential. The working electrode serves as the transduction element in the biochemical reaction, while the counter electrode establishes a connection to the electrolytic solution so that a current can be applied to the working electrode. These electrodes should be both conductive and chemically stable. Therefore, platinum, gold, carbon (e.g. graphite) and silicon compounds are commonly used, depending on the analyte [4, 17]. An excellent summary of the characteristics, such as the varying detection limits, of electrochemical biosensors is provided in a review by Mehrvar *et al.* [18].

Synergies in nanotechnology and bioelectronics have revealed new possibilities to miniaturize and to optimize existing microscale devices at the nanoscale. It is becoming possible to more accurately measure specific electrical properties in combination with various electrochemical transducers. The higher surface-to-volume ratio of nano-objects makes their electrical properties increasingly susceptible to external influences, especially as these structures continue to shrink toward the atomic limit. Since the nanometer dimensions of these objects are comparable to the size of the target biomolecules, higher measurement sensitivity may result [19], and sensitivity may also increase due to higher capture efficiency [20]. Nanostructures already represent important new components in recently developed electrochemical biosensors, such as the use of nanoparticles as electrochemical labels for DNA sensing [21, 22]. Nanowires, carbon nanotubes, nanoparticles and nanorods are merely some of the familiar objects that are emerging as candidates to become crucial elements of future bioelectronic devices and biosensors [23, 24]. The use of nanowires in biosensing is described in detail in Section 1.2.2.

**Amperometric devices** are a type of electrochemical sensor, since they continuously measure current resulting from the oxidation or reduction of an electroactive species in a biochemical reaction [3, 6]. Clark oxygen electrodes perhaps represent the basis for the simplest forms of amperometric biosensors, where a current is produced in proportion to the oxygen concentration. This is measured by the reduction of oxygen at a platinum working electrode in reference to an Ag/AgCl reference electrode at a given potential [4]. Typically, the current is measured at a constant potential and this is referred to as *amperometry*. If a current is measured during controlled variations of the potential, this is referred to as *voltammetry*.

**Cyclic Voltammetry (CV)** belongs to a category of electro-analytical methods, through which information about an analyte is obtained by varying a potential and then measuring the resulting current. It is, therefore, an amperometric technique. Since there are many ways to vary a potential, there are also many forms of voltammetry, such as: polarography (DC Voltage) [25], linear sweep, differential staircase, normal pulse, reverse pulse, differential pulse and more [3, 26]. *Cyclic voltammetry* is one of the most widely used forms and it is useful to obtain information about the redox potential and electrochemical reaction rates (e.g. the chemical rate constant) of analyte solutions. In this case, the voltage is cycled between two values at a fixed rate, however, when the voltage reaches  $V_2$  the scan is reversed and the voltage is swept back to  $V_1$ . The scan rate,  $(V_2 - V_1)/(t_2 - t_1)$ , is a critical factor, since the duration of a scan must provide suf-

ficient time to allow for a meaningful chemical reaction to occur. Varying the scan rate, therefore, yields correspondingly varied results [3, 27].

The shape of the voltammogram for a given compound depends not only on the scan rate and the electrode surface, which is different after each adsorption step, but can also depend on the catalyst concentration. For example, increasing the concentration of reaction specific enzymes at a given scan rate will result in a higher current compared to the non-catalyzed reaction [27–29].

**Potentiometric devices** measure the accumulation of a charge potential at the working electrode compared to the reference electrode in an electrochemical cell when zero or no significant current flows between them [3, 4, 10]. In other words, potentiometry provides information about the ion activity in an electrochemical reaction [30].

**Conductometric devices** measure the ability of an analyte (e.g. electrolyte solutions) or a medium (e.g. nanowires) to conduct an electrical current between electrodes or reference nodes. In most cases, conductometric devices have been strongly associated with enzymes, where the ionic strength, and thus the conductivity, of a solution between two electrodes changes as a result of an enzymatic reaction. Thus, conductometric devices can be used to study enzymatic reactions that produce changes in the concentration of charged species in a solution [10].

**Electrochemical Impedance Spectroscopy (EIS)** The first publication of electrochemical impedance spectroscopy dates back to 1975 [31]. Through the application of a small sinusoidally varying potential  $U$ , one measures the resulting current response  $I$  [26, 32]. By varying the excitation frequency  $f$  of the applied potential over a range of frequencies, one can calculate the complex impedance, sum of the real and imaginary impedance components, of the system as a function of the frequency (i.e. angular frequency  $\omega$ ). Therefore, EIS combines the analysis of both real and imaginary components of impedance, namely the electrical resistance and reactance, as shown in Equation 1.1 [29, 33].

$$Z(j\omega) = \frac{U(j\omega)}{I(j\omega)} = Z_r(\omega) + jZ_i(\omega); \quad \omega = 2\pi f \quad (1.1)$$

**Field-Effect Transistor (FET)** is a type of transistor that uses an electric field to control the conductivity of a channel (i.e. a region depleted of charge carriers) between two electrodes (i.e. the *source* and *drain*) in a semiconducting material. Control of the

conductivity is achieved by varying the electric field potential, relative to the source and drain electrode, at a third electrode, known as the *gate*. Depending on the configuration and doping of the semiconducting material, the presence of a sufficient positive or negative potential at the gate electrode would either attract charge carriers (e.g. electrons) or repel charge carriers in the conduction channel. This would either fill or empty the depletion region of charge carriers and thus form or deform the effective electrical dimensions of the conducting channel. This controls the conductance between the source and drain electrodes. In linear mode, when drain-to-source voltage is much less than the gate-to-source voltage, an FET operates much like a variable resistor to switch between conductive and non-conductive states. Alternatively, in saturation mode an FET operates as a constant-current source and is often used as a voltage amplifier. In this mode the level of constant current is determined by the gate-to-source voltage. FET devices are preferred for weak-signal and/or high impedance applications, hence their widespread use in the growing field of electrochemical biosensing [6, 34].

### 1.2.2 Nanowires

Nanowires belong to a growing family of nano-objects, which also includes e.g. nanotubes, nanoparticles, nanorods, nanobelts, nanosprings, thin films and more [21–23, 35–37]. Nanowires are not only used in electrochemical biosensing, but also in bio- and nanoelectronic applications. They are increasingly being used as building blocks for biosensing techniques. Their implementation as highly-sensitive electrodes is one obvious example, such as the platinum electrode network proposed by Wang *et al.* for glucose detection [38]. As immediately suggested by their name, nanowires have diameters in the nanometer range. Thus, their diameters have a length scale comparable to the atoms of which they are comprised and are sometimes referred to as quantum wires. Additionally, nanowires are referred to as one-dimensional structures, since their lengths are orders of magnitude larger than their diameters. Nonetheless, one might still pose the question why wires with nanometer dimensions are more suitable or more sensitive than larger wires for sensing applications. As a wire decreases in diameter to the nanometer regime, the ratio of surface atoms compared to interior atoms, i.e. the surface-to-volume ratio, drastically increases. Therefore, external influences by charged particles or biological species increasingly influence the conduction both on the wire surface and in the wire interior.

Nanowires represent very attractive bioelectrochemical transducer components since their diameters are comparable to the size of the biochemical analytes under analysis and

since their conductance is sensitive to surface perturbations. They have already been incorporated into FET devices for biosensing purposes, such as the detection of pH, protein and DNA binding, viral and cancer markers. The Lieber group has also reported attempts to interconnect nanowires with neurons to study their electrical behaviour [19, 39, 40]. Yeh *et al.* have used a combination of gold nanowires and nanoparticles to increase the electron transfer rates in redox enzymes [41]. To overcome the problems of large-scale nanowire production electrically insulating pore-suspending membranes on highly ordered porous alumina obtained from vesicle spreading have combined Extreme Ultraviolet Light Interference Lithography (EUV-IL) with biological patterning to produce high density line arrays of self-assembling DNA-tagged gold nanowires.[24]

### 1.2.3 Electrochemistry in Combination with Complementary Biosensor Techniques

Obviously, all sensing techniques demonstrate specific strengths in different, yet sometimes overlapping, areas of application. For example, both, electrochemical and optical sensing techniques, can allow for real-time, *in situ*, non-destructive and label-free analysis of solutions, bilayers, surfaces, thin films, bulk materials and interfaces [42–44]. On one hand, electrochemical techniques, such as CV, enable the *in situ* monitoring of e.g. redox reactions, system electrical response and reaction reversibility. On the other hand, optical techniques are known for their ability to measure mass adsorption kinetics (e.g. optical waveguide lightmode spectroscopy (OWLS), surface plasmon resonance (SPR) and ellipsometry). Gravimetric techniques like the quartz crystal microbalance with dissipation monitoring (QCM-D) and imaging techniques like scanning probe microscopies, such as AFM, and fluorescent microscopies, such as confocal laser scanning microscopy (CLSM) can also be successfully combined with electrochemical techniques to enhance understanding of biointerfacial phenomena. These techniques provide high sensitivity close to the surface of the transducing element (electrode, waveguide, tip, etc.). The shared high interfacial sensitivity of electrochemical and other types of biosensor results in the simultaneous extraction of a richer set of initial data in addition to the benefit of increased control over the sensing environment.

The following paragraphs will provide an overview of the combination of electrochemical sensing setups with representative biosensor techniques.



### **Electrochemical Surface-Plasmon Resonance (EC-SPR)**

In SPR configurations the surface between two mediums of differing refractive indexes is coated with a thin film of conducting material, which is often a noble metal, such as Ag, Au or Cu. If this thin film is irradiated by light of a certain wavelength at a specific incident angle, termed the SPR angle, the evanescent field wave from Total Internal Reflection (TIR) can excite an electron wave, known as a surface plasmon, which propagates along the metal surface [45, 46]. The coupled electromagnetic evanescent field extends typically  $\sim 200$  nm from the conductive surface (e.g. Au excited at red wavelengths) as its intensity decays exponentially. Therefore, the sensing mechanism of SPR spectroscopy is based on the measurement of small changes in the refractive index in the vicinity of the surface of a conductive thin film [45, 47–49].

For use as a biosensor, the changes in refractive index in the vicinity of the conductive thin film surface (i.e. within the evanescent field) can be induced by the presence of biomolecules. The surface concentration or mass coverage of them can then be calculated using the de Feijter formula [50, 51]. SPR biosensors can be used in the determination of a number of surface binding interactions, such as: small molecule adsorption [49], protein adsorption on self-assembled monolayers, antibody-antigen binding, DNA and RNA hybridization [52, 53], protein-DNA interactions [46], binding kinetics, affinity constants, equilibrium constants, as well as receptor-ligand interactions in immunosensing [45, 54] and many more.

In EC-SPR, the combination of electrochemistry and SPR, the thin metal film on the substrate serves not only to excite surface plasmons, but also acts as a working electrode for electrochemical detection or control [55]. One advantage of the EC-SPR configuration is the ability to simultaneously obtain information about the electrochemical and optical properties of films with thicknesses in the nanometer range. EC-SPR has often been applied to study the formation and the properties of thin films and mono-/multi-biayers using, for example, self-assembly or electro-polymerization methods [56–58].

### **Waveguide based Techniques and Electrochemistry**

Waveguide based optical evanescent sensors have equivalent sensitivity to small numbers of adsorbed analytes compared to most other biosensors. However, because of the need for both, an optically transparent substrate and a conductive interface (electrode), fewer

combinations of waveguide spectroscopy and electrochemistry to SPR and electrochemistry have been made, since optically transparent electrodes are rare. Optical Waveguide Lightmode Spectroscopy (OWLS) is a label-free technique that allows for *in situ* measuring of adsorption, desorption, adhesion and biospecific binding processes [51, 59]. This technique is based on linearly polarized laser light that is coupled into a waveguide at two well-defined incident angles. These incoupling angles are sensitive to changes in the refractive index within the evanescent field above the surface of the waveguide. Monitoring of the changes in the incoupling angles enables determination of the adsorbed mass and the number of adsorbed molecules [59] using de Feijter's formula [50, 51].

Electrochemical OWLS (EC-OWLS) combines evanescent-field optical sensing with the electrochemical control of surface adsorption processes. It gives the possibility to directly observe mass adsorption as a function of an applied potential [60, 61].

An example of such a combined experiment is given in Figure 1.2. First, cyclic voltammetry was performed in order to get stable electrochemical conditions. Then, a three step adsorption was performed. Poly(L-lysine)-*grafted*-poly(ethylene glycol) with 50 % of the side chains conjugated with biotin was adsorbed first, followed by neutravidin and biotin conjugated GOx. Subsequently, a potential of 1 Volt was applied several times in order to measure the current generated by the enzymes at different substrate concentrations.

### **Ellipsometry and Electrochemistry**

Classic ellipsometry is focused on the external reflection of a light beam from a reflective surface, where linearly-polarized light of a known orientation is reflected as elliptically-polarized light. From the changes in the ellipsometric angles ( $\Psi$ ,  $\Delta$ ), the optical properties, thickness, morphology or roughness of layers or films on the surface can be calculated [6, 42, 43] and used to determine e.g. the amount of adsorbed protein on a surface [43, 44].

Since ellipsometry can be performed on most reflective substrates it can be easily conducted on an electrode surface and combined with electrochemistry. Ying *et al.* have used ellipsometry and electrochemical methods to study protein adsorption on metal surfaces and specifically human serum albumin on gold surfaces [62]. Chronoamperometry and ellipsometry were combined for the study of immunosensor interfaces based on methods of Immunoglobulin G adsorption onto mixed self-assembled monolayers [63].

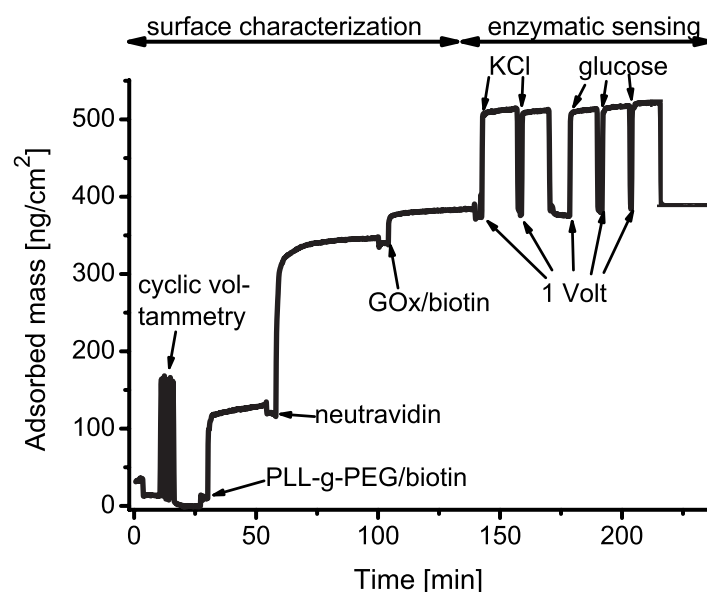


**Figure 1.2:** EC-OWLS curve showing adsorption as a function of time. Additionally, the signal also reacts to an applied potential. Prior to the adsorption steps the system was electrically cycled to obtain stable conditions. PLL-g-PEG/biotin, neutravidin and biotin conjugated GOx were adsorbed in three steps with buffer rinsing in between. After completing the adsorption, a potential of 1 V was applied several times in order to measure the current generated by the enzymes at different substrate concentrations.

### Electrochemical Quartz Crystal Microbalance with Dissipation Monitoring (EC-QCM-D)

The Quartz Crystal Microbalance with Dissipation monitoring measures changes in the frequency  $f$  and dissipation factor  $D$  of an oscillating quartz crystal upon adsorption of a viscoelastic layer [64]. The oscillation is based on the piezoelectric effect and the crystals typically have a fundamental resonance frequency of 5 MHz, which decreases upon mass adsorption. Modern versions of QCM, like the QCM-D, are insensitive to potentials applied at the solution interface and to local changes in ionic strength [65] and can thus be readily combined with electrochemical sensing.

The measured mass includes hydrodynamically coupled water such as water associated with the hydration layer of e.g. proteins and/or water moved in cavities or by rough features in the film [66, 67]. The dissipation factor is a measure of energy loss and increases with higher viscosity of the solution or of adlayers. The main advantages compared to other common methods for measuring biomolecule adsorption, such as ellipsometry or surface plasmon resonance, are the flexibility to use virtually any surface coating and the information about the viscoelastic properties of the adlayer obtained through

simultaneous measurements of both  $f$  and  $D$ . This includes any electrode material of interest. As with SPR or ellipsometry no labelling is required [64].

By using a conductive surface coating on the working electrode of the crystal itself, QCM allows for simultaneous electrochemical experiments [64, 68]. For electrochemical QCM a specially designed flowcell is required; typically the QCM-crystal acts as the working electrode, Ag/AgCl on the upper side of the flowcell as the reference electrode and a platinum wire in the outlet tube as the counter electrode [64, 69]. The same setup is also used for adsorption steps that are sensitive to an applied potential [64].

The main applications to date have been in the fields of polyelectrolyte multilayers [70], corrosion [71], enzymatic and nucleic acid based biosensors [64].

### **Scanning Probe Microscopy (SPM)**

The invention of the scanning tunnelling microscope (STM) [72, 73] in the early 1980's has inspired various forms of SPM techniques. Despite the now diverse palette of SPM techniques, STM remains a promising technique for experiments combined with electrochemistry, such as used by Bae *et al.* [74].

Perhaps the most commonly employed techniques of SPM for imaging and characterization is Atomic Force Microscopy (AFM) [75]. AFM devices have evolved into versatile and powerful tools, which enable the investigation and imaging of surfaces with even molecular resolution. This is accomplished by monitoring the interaction force between the sample surface and a probe, i.e. a sharp tip, which is attached to the end of a force-sensing cantilever. For further details and theory of AFM operation the reader is referred to other sources [76–78]. One area of investigation with generic EC-AFM methods is the study of electrode surface modification or performance under certain electrochemical conditions [56, 79, 80], which is important in application-specific electrode development for bio- and chemosensors.

The development of ultramicroelectrodes (UMEs) and their combination with the SPM also paved the way for an SPM technique known as scanning electrochemical microscopy (SECM) [81–83]. SECM is used to locally investigate the electrochemical activity and/or the topography of a surface. Designed for either amperometric or potentiometric measurements, a UME probe, which is normally in the shape of a tip, is scanned along the surface of interest and is used to induce chemical changes and to collect electro-

chemical information. SECM has proven useful in the detection and imaging of heterogeneous electron transfer reactions at metal/solution interfaces, electron transfer kinetics at solid/liquid interfaces, various electrocatalytic reactions, predominately the hydrogen oxidation reaction (HOR) and the oxygen reduction reaction (ORR), lateral charge and mass transfers and biological cells.[84–86]

AFM-SECM is capable of obtaining simultaneous electrochemical and topographical information at high spatial resolution through the integration of an electrode into the AFM probe. In other words, the structural information is simultaneously correlated with chemical activity of the substrate [87]. These hybrid probes are, therefore, quite effective for the identification and chemical mapping of active surface sites [88]. Critical to the resulting synergy of AFM-SECM is the proper modification of the probe. Kreung *et al.* have mapped glucose oxidase (GOx) activity on a micropatterned surface and through a synthetic membrane [89, 90]. The same group has imaged immobilized horseradish peroxidase with the same techniques [91].

## 1.3 Surface Architecture

In this section the different components of an electronic biosensor are discussed. It starts with the sensor surface that needs to be conductive and, depending on the detection technique, also transparent. A surface coating has to provide inertness and/or functional groups for tethering of the recognition element, which is often an antibody. The recognition elements are surface immobilized to specifically catch biologically relevant molecules (antigens for an antibody based sensor) that need to be detected. Many biosensors with some notable exceptions employ labelling to quantify the binding, e.g., the binding of an additional antibody with a fluorescent label in the case of ELISA. In electrochemical biosensors the label is usually an enzyme that catalyzes certain reactions in cases where the bound molecule in itself does not significantly alter the charge transfer process across the electrode interface. Finally, the electrons, generated during the recognition event or usually the enzymatic label reaction with a substrate, also need to be detected. If the reaction takes place away from the electrode interface, mediators can be used to shuttle the electrons between the reaction site and the surface.

### 1.3.1 Surface Materials and Modifications

Nowadays, a wide variety of different materials is used for the preparation of surfaces for biosensing applications. Depending on the measurement technique, they need to fulfill special requirements, such as electrical conductivity for electrochemical techniques or transparency for optical devices. Most commonly used are glass and other oxide surfaces because of their favourable characteristics, especially their optical characteristics [92]. Widely used are also gold, microporous gold, graphite, glass carbon [93, 94] and Indium Tin Oxide (ITO) [95].

Electrodes are increasingly screen printed. This approach has advantages such as simple and low cost fabrication as well as easy mass production [93].

Another class of materials used for fabricating electrochemical biosensors are various conducting polymers. These include polyaniline, polypyrrole and polystyrene, which can be coated onto other sensor substrates. Typically, the polymers are adsorbed to gold surfaces. This leads to surfaces with good stability, excellent redox recyclability and easy handling [4, 92, 96].

Gold and other metallic surfaces are also coated with self-assembled monolayers (SAMs) of sulfides (thiols) and disulfides. Molecules with a thiol foot can form highly ordered and well-organized structures functionalized with an organic linker [27, 97]. Different end-functionalizations are used to couple biological recognition elements. For example, carboxyl groups often serve for antibody immobilization, esters form amine couplings and biotin coupling can be used to bind streptavidin and further biotin-functionalized biomolecules [27]. In electrochemical applications it is essential that the SAM allows electron or analyte diffusion [97].

Carbon nanotube (CNT) modified electrodes have advantages in terms of their high surface area, mechanical strength, excellent electrical conductivity and good chemical stability. They are especially interesting because enzymes can be entrapped in the inner cavity [98, 99].

In a more unique approach, glassy carbon electrodes were modified with gold nanocrystals. Gold nanoparticles were then bound via cysteamine. The whole procedure leads to high efficiency of the enzyme immobilization [100]. Others have used gold nanorods, which can be flat on a surface or perpendicular to it. They have a diameter of about 20 nm and a length of up to 2  $\mu\text{m}$  [101, 102]. Also semiconductors such as ZnO

have been used to fabricate nanorods. They have been functionalized with e.g. biotin [103].

### 1.3.2 Electrochemical Signal Transduction

Electrochemical biosensors are mostly based on the principle of direct transduction of the reaction rate into a current [4]. The way has been long from the first electrode-based biosensors to today's state of the art. The first generation were simple oxygen based sensors. In the presence of glucose oxidase (GOx) glucose and oxygen undergo a reaction in which gluconic acid and hydrogen peroxide are formed. The drawback of this electrode setup is the dependence on the oxygen concentration which is difficult to maintain at a constant level. In the second generation, the oxygen was replaced by other, reversible, oxidizing reagents also known as mediators. They are often based on iron, e.g. ferro/ferricyanide. In the third generation, denaturation of the enzymes was taken into account. In order to prevent unfolding and inactivation, they were directly coupled to the electrode. In such a configuration no more mediators are required [3].

In general, it is preferable to have the reaction take place as close to the electrode as possible, because the products diffuse in all directions, also away from the surface. This results in a decreasing signal with increasing distance to the surface [104]. Depending on whether or not a mediator is used, one talks about direct or indirect transduction. These are elaborated in the following paragraphs.

In biosensors that are based on direct electron transduction the redox enzyme acts as an electrocatalyst. They are also known as third generation biosensors. Such systems do not require a mediator. The surface immobilized enzyme selectively catalyzes the transformation of a specific substrate. The electrons are directly transferred from the electrode to the substrate molecule or vice versa, as shown in Figure 1.3a. A high efficiency of the enzymatic reaction is required [4, 105].

The direct electron transfer slows down with increasing distance between the enzyme and the electrode surface. This effect reduces the sensitivity of mediatorless sensors. Kuznetsov *et al.* estimated the decrease upon an increasing distance by having a hemoglobin layer between the electrode surface and laccase molecules. They found an exponential decrease of the signal with increasing distance to the surface. Because of charge accumulation, the signal is still detectable also at very low concentrations in the range of 1 nM [104].

In the indirect transduction, the electron transfer mediator shuttles the electrons between the redox center of the enzyme and the electrodes (see Figure 1.3b). Such mediators are defined as artificial electron acceptors with a low oxidation potential. Usually, they can freely diffuse in solution. It is also possible to co-immobilize them with the enzymes [4, 8]. Mediators are small and mobile molecules, which are able to react rapidly with the enzyme. They are oxidized at the electrode and reduced at the reaction site of the enzyme or vice versa. Therefore, they should exhibit reversible heterogeneous kinetics, not react with oxygen and ideally be pH independent. Most commonly used are ferrocene and its derivatives, ferrocyanide, methyleneblue, benzoquinone and N-methyl phenazine [4].

In a similar approach the mediator was replaced by carbon nanotubes (CNTs). Patolsky *et al.* [106] used CNTs to guide electrons between the enzyme and the surface. They immobilized CNTs in an upright position. On the upper end they covalently bound GOx (see Figure 1.3c). In this setup the spacial separation prevents tunnelling effects.

### 1.3.3 Enzymes

Enzymes are proteins that act as powerful catalysts to convert substrates into products [107]. Some enzymes, also known as redox-enzymes, catalyze reactions that produce or consume electrons. Thereby, the substrate is recognized by a binding pocket of the enzyme, similar to the antibody-antigen interaction. Enzymes with such specific binding pockets are used in enzymatic biosensing - where the electrons are detected. Subsequently, from the current density through the interface, the enzyme- or substrate concentration and/or activity can be calculated [32, 108].

The most commonly used enzymes in biosensing are glucose oxidase (GOx) [8] and horseradish peroxidase (HRP) [109]. The corresponding reaction schemes are given in Equation 1.2 for GOx and Equation 1.3 for HRP. Donors for the reaction with HRP are molecules such as phenols, aromatic amines, thioaminoles or iodide [109]. Other, less commonly used enzymes comprise beta-lactamase [110], and urease [10].



One of the major issues when working with enzymes is their stability. This includes shelf life as well as operational stability. Enzymes are very sensitive to their environment.



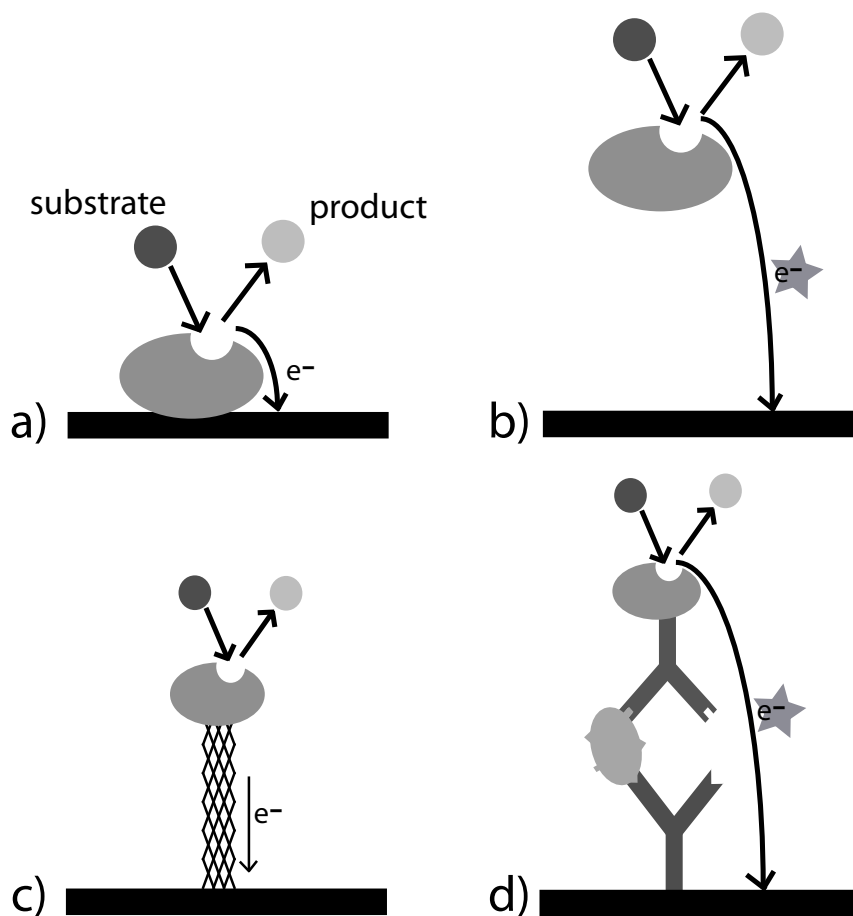


**Figure 1.3:** Scheme of direct and indirect electron transduction. a) Direct transduction: the electrons only generate a measurable current if the reaction takes place close to the surface. b) Indirect transduction: with the help of a mediator, that shuttles the electrons between the reaction site and the surface, much larger distances can be overcome. c) Enzyme bound via conducting CNT. d) ELISA-like sandwich setup, where an enzyme labelled antibody binds to the detected antigen.

Deactivation, inhibition or unfolding upon adsorption and chemical or thermal inactivation are common if no special precautions are applied [111, 112]. The main immobilization strategies that retain the enzymatic activity include encapsulation, covalent immobilization and site-specific mutagenesis. Compared to direct immobilization, encapsulation provides several advantages. This method provides a more natural environment which causes less inactivation. Furthermore, encapsulation opens the possibility to increase the concentration of immobilized enzymes [111–114]. Due to these advantages and major efforts towards their implementation, strategies for encapsulation of enzymes will be treated in more detail in Section 1.3.5. Other stabilization techniques include: enzymes bound to nanoparticles/-fibers or single enzyme nanoparticles [114–116]. Depending on the treat-

ment, different strategies are favourable to inhibit enzyme degradation: e.g. salts, such as sodium chloride, are added to protect the enzymes during freezing processes. Large polyelectrolytes and low molecular weight electrolytes improve the operational stability [111]. The lifetime of enzymatic biosensors is limited by the loss of enzyme activity over time; typically it is limited to 2-8 weeks [10].

### 1.3.4 Recognition Elements

#### Antibodies

Among other recognition elements, antibodies are most widely used because of the high specificity of the antibody-antigen binding. However, they are also very sensitive to their environment. In order to detect antigens, antibodies are surface-immobilized, which can cause a severe loss of their biological activity. Since the activity of surface immobilized antibodies depends on their orientation, it is advantageous to assure that they are not randomly oriented. Other reasons for inactivity include steric hindrance in cases where the density is too high as well as denaturation due to non-specific interactions with the surface [117]. Immobilization techniques include microcontact printing [118], biotin-streptavidin binding [119–122], direct spotting [119], adsorption to a conductive polymer matrix such as polypyrrole or polyaniline [115] as well as covalent binding [123].

Most commonly used is Immunoglobulin G (IgG) which, like typical antibodies, consists of one Fc and two Fab' binding sites. It becomes inactive when the Fab' fragment binds to the surface [117]. Often antibodies help to discover new disease markers [124]. In typical applications, monoclonal antibodies are used as specific capture antibodies for e.g. prostate cancer marker (PSA). In such, so called sandwich assays, one antibody acts as a capture antibody while the second, enzyme-labelled antibody is bound to the PSA [125].

Electrochemical enzymatic biosensors can be built up similar to the enzyme-linked immunosorbent assay (ELISA). After immobilizing antibodies to a surface, an analyte is introduced, to which the antibodies bind specifically. In the most common detection scheme a secondary, labelled antibody then binds to the analyte in order to detect its concentration (see Figure 1.3d). The detection antibodies are coupled to an enzyme, which allows quantitative measurements of the amount of bound antigens by monitoring the electrical signal generated by an enzymatic reaction [126].

A wide variety of antigens, usually in diagnostics, can be detected this way. It is e.g. possible to diagnose Hepatitis C already in an early stage [127]. More recently, capture antigens have also been used to detect cancer markers. Among the most important ones are carcinoembryonic antigen (CEA) [94], carbohydrate antigen 19-9 (CA19-9), carcinoma antigen 125 (CA125), alpha-fetoprotein (AFP), CA15-3, human chorionic gonadotropin (hCG) [93] and prostate specific antigen (PSA) [125], which are used to detect various types of cancer.

### **Antibody Fragments**

Nowadays, antibody fragments are emerging as credible alternatives to antibodies. They provide the same specificity as whole antibodies. Furthermore, they are smaller which can be an advantage for biosensor applications. In their main application field, biosensors and therapeutics, these small, highly specific reagents against target antigens are often used as bi- or trimers [128].

Most commonly used are IgG fragments [117, 118]. Such small, recombinant antibody fragments can be linked to other molecules, for example lipids, drugs and proteins [128]. An antibody that is naturally composed of only heavy chains is the camel antibody. Even though the light chains are missing, it binds very specifically [129]. For other applications, biotinylated fragments are adsorbed to streptavidin coated surfaces [120]. As already mentioned for antibodies, the orientation is of great importance. Lu *et al.* [117] reported on a threefold increase of activation upon proper/controlled orientation. In a more complex approach Vikholm *et al.* adsorbed Fab' fragments directly to gold but embedded them in a protein repellent polymer such that only the antigen binding site stuck out of the polymer [130].

### **Aptamers**

Aptamers are folded single stranded DNA or RNA oligonucleotide sequences with the capacity to recognize various target molecules. They are generated in the SELEX (systematic evolution of ligands by exponential enrichment) process which was first reported by Ellington [131] and Tuerk [132] in 1990. In this approach suitable binding sequences are first isolated from large oligonucleotide libraries and subsequently amplified [6, 133].

The main application for aptamers is in biosensors. While antibodies are used in ELISA, the similar process for aptamers is called ELONA (enzyme linked oligonucleotide

assay) [134]. Aptamers have many advantages over antibodies such as easier deposition on sensing surfaces, higher reproducibility, longer shelf life, easier regeneration and a higher resistance to denaturation. As antibodies, they are characterized by both, their high affinity and specificity to their targets [6, 133].

### 1.3.5 Encapsulation of Enzymes

Several different strategies for enzyme encapsulation to increase signal response and specificity have been envisioned and pursued. Some of the most interesting ones are introduced below.

#### **Polyelectrolyte Multilayer (PEM) Capsules**

These microcapsules were first presented by Caruso and Donath in 1998 [135, 136]. They are fabricated by coating a microparticle with alternating layers of oppositely charged polyelectrolytes, such as the negatively charged poly(sodium styrenesulfonate) (PSS) and the positively charged poly(allylamine hydrochloride) (PAH). The shell thickness can be varied by adjusting the number of layers. Subsequently, the core is dissolved and the material diffuses through the shell into the surrounding solution. The capsules usually have a diameter of 1-10 micrometers [136, 137]. Optionally, coating of poly(L-lysine)-*grafted*-poly(ethylene glycol) can be applied to make them protein resistant [138].

For applications towards electrochemical biosensing, enzymes can be incorporated into PEM capsules. This could be accomplished by adsorbing the enzymes inside the pores of CaCO<sub>3</sub> microparticles where their stability and catalytic activity was successfully maintained [139, 140].

#### **Vesicles**

Liposomes or lipid vesicles consist of bilayer forming amphiphilic molecules such as palmitoyl-oleoylphosphocholine (POPC), called lipids. Liposome sizes vary between 20 nm and several hundred micrometers. Applications are in e.g. drug delivery, cosmetic emulsions, and optical electrochemical biosensing. In the latter case they are loaded with enzymes. Many different encapsulation methods have been developed during the last decade. Among them, the extrusion technique and dehydration-rehydration have been

the most successful ones. The entrapped enzymes catalyze the conversion of substrate molecules into products. Having stable vesicles and enzymes, as well as low enzyme permeability and high substrate permeability are prerequisites for their use in biosensing [141]. However, substrate permeability is typically low, which drastically limits the turnover rate of encapsulated enzymes. To overcome this drawback, membrane channels such as the outer membrane protein F (OmpF) from *Escherichia coli* were incorporated into the membrane [142]. They allow for diffusion of molecules with a molecular weight of up to 400 Da [143]. Hill *et al.* incorporated glucose oxidase, horseradish peroxidase and the combination of both into vesicles. There was no major loss in enzymatic activity [144]. In another application, the enzyme beta-lactamase was incorporated into POPC vesicles [143].

Another class of vesicles are polymeric vesicles made of the triblock copolymer PMOXA-PDMS-PMOXA. They were shown to have a high stability, especially when they are cross-linked [145]. Various functionalizations, such as biotinylation or fluorescent labels can be introduced [146]. Furthermore, they offer the possibility to incorporate OmpF channels [147], which has e.g. been used for substrate diffusion when enzymes were incorporated in the interior [148, 149].

### **Polymeric Micelles**

Polymeric micelles are built from amphiphilic block copolymers. The inner, hydrophobic side usually consists of poly(acrylic acid) (PAA) or polyesters coupled to e.g. hydrophobic drugs; for the outer, hydrophilic shell poly(ethylene glycol) (PEG) is most widely used. Their size can vary between 10 and 100 nm [150–152]. Thurmond *et al.* cross-linked the shells to increase their stability [153]. Even though the main application is in drug delivery where drugs are enclosed, enzymes have also successfully been embedded in the core through electrostatic interaction with polyion complex (PIC) block copolymers [154]. Another way is to PEGylate the enzymes, whereas the PEG is part of the PIC [155]. This allows for potential use in enzymatic biosensing.

### **Hydrogel**

Since encapsulated enzymes do not need to be mobile, hydrogels offer a suitable immobilization technique. Thus, cross-linked polymers form a biocompatible hydrogel that

entraps the enzymes. The water soluble redox polymer should not cross-link too much in order to allow swelling in water. At the same time it mediates electron transfer between the enzymes and the electrode via electron diffusion through electron exchange between mobile polymer segments. In applications, such as electronic biosensors, it is important that the entrapped enzymes are not denatured and remain in their active state. Otherwise, the sensitivity and selectivity of the biosensor is decreased drastically [156–159]. Mao *et al.* introduced a new redox hydrogel, consisting of a polymer with 13-atom-long tethers between the redox centers and the polymer backbone. This led to an electron diffusion coefficient one order of magnitude higher than for previously known systems [160].

### **Sol-Gel**

Like hydrogels, the sol-gel technique is applied directly on surfaces. In the first experiments porous SiO<sub>2</sub> glass was used. Braun *et al.* were the first ones to report about successful enzyme entrapment in a sol-gel matrix [161]. The material is formed via partial or complete hydrolysis of a suitable precursor, usually silanes, mixed with biomolecules. Subsequently, gelation and aging follows. Aging strengthens the network and the drying process simultaneously leads to shrinkage [162, 163]. Tunable pore sizes and pore size distribution, optical transparency, no need of a mediator, mechanical rigidity, chemical inertness, permeability and thermal stability gives them highly desirable properties [163, 164]. Typical applications include selective coatings for optical and electrochemical biosensors [163], for example carbon ceramic composite electrodes (CCE) for amperometric biosensors [164].

### **1.3.6 Supported Lipid Bilayer Sensor Architectures**

Lipid bilayers can be used to build biosensors that make use of the transport process across the membrane. Functional lipid membranes have not yet found as extensive use in biosensor applications [165] as the enzyme or antibody systems described above and are not yet competitive with other screening methods [166]. However, there is a strong desire to use them in particular to probe function of membrane proteins, e.g. in drug screening applications. Lipid bilayers provide the only alternative for sensors aiming to probe or to make use of membrane proteins, which currently comprise > 50% of all drug targets, and many of these proteins are directly involved in charge transfer processes across the membrane [167]. A direct electrical readout of ionic currents generated by ion channels,

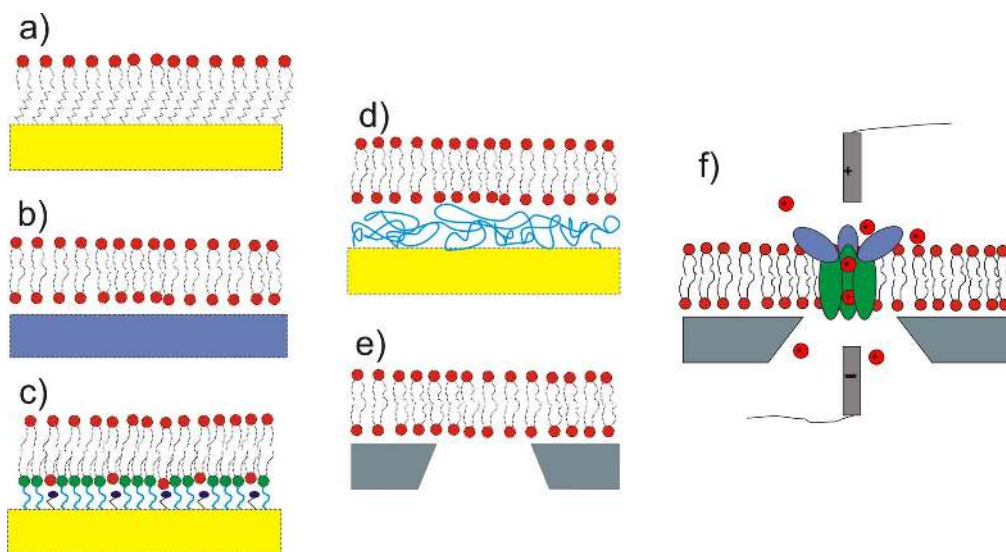


**Figure 1.4:** Schematics of supported lipid bilayer architectures used for sensor applications including electrochemical biosensors: a) hybrid bilayer, b) solid-supported lipid bilayer (SLB), c) tethered lipid bilayer (t-SLB), d) polymer-supported bilayers (pSLB), e) pore-spanning lipid bilayers (nano-BLM) and f) a nano-BLM with an incorporated protein for single channel recordings.

for example, bears the advantage of an amplification of the readout signal of membrane functions without need for labelling compared to current state-of-the-art techniques for membrane protein screening.

While most electrochemical measurements utilizing lipid membranes have been conducted using, so called, black lipid membranes (BLMs), which are formed across apertures separating two aqueous compartments, we will focus on lipid bilayer architectures stabilized by a solid support. Only these can be formed free from solvents and detergents, in a miniaturized format and with sufficient stability to be viable for commercial biosensor applications. There are recent examples of advances in combining nanostructures with lipid bilayers which effectively fuse the approaches of aperture spanning membranes with solid supported lipid bilayers [168, 169]. This combination exploits the advantages of the two approaches. For a further overview of recent advances see Reimhult *et al.* [170]. The main techniques to form lipid bilayers on various, also porous, surfaces include vesicle fusion, painting, detergent dilution and Langmuir-Blodgett deposition [170, 171]. The membranes can be directly adsorbed or tethered to the surface, but also separated from the sensor substrate by a hydrogel [171–173]. When a lipid membrane is adsorbed in close proximity to a solid substrate like an electrode, it is generally referred to as a supported lipid bilayer (SLB), but several different classes can be identified in terms of the

surface architecture. They can be divided into hybrid lipid layers (Figure 1.4a), solid SLB (Figure 1.4b), tethered lipid bilayers (tSLB, Figure 1.4c), polymer-supported lipid bilayers (pSLB, Figure 1.4d) and pore-spanning lipid membranes (nano- or micro-BLM, Figure 1.4e). Of these, the hybrid lipid bilayers have been the ones used the most for electrochemical measurements, because of the ease with which they can be prepared on electrode materials like Au [174]. However, in recent years they have been replaced by the more advanced tSLBs [175, 176], which have two leaflets of lipids and a hydrophilic spacer group between the electrode and the lipid bilayer. This allows incorporation of smaller transmembrane proteins and produces membranes with high resistance.

Using SLBs to study transmembrane protein function or to construct the ion-channel sensors discussed below, requires a lipid bilayer of high integrity to provide a good electrochemical seal. Without a good seal the current to the underlying electrode (or the impedance) is dominated by conduction through defects in the membrane instead of charge transport through the integrated proteins. Incorporation of membrane proteins like ion channels and pumps, which enable the diffusion of charged molecules, allows the study of their transport properties through electrochemical measurements in configurations ranging from cyclic voltammetry to impedance spectroscopy and membrane-FET. Among these, impedance spectroscopy has been the most common characterization method due to the possibility to model the membrane from the impedance characteristics. Examples of such peptides incorporated into the membrane are gramicidin, melittin, alamethicin, and valinomycin [177–181]. Larger proteins forming ion channels, like Outer membrane protein F (OmpF) from *E. Coli*, and other peptides have also been investigated [180, 182–185]. Incorporation is mostly achieved by direct insertion of the small hydrophobic channel proteins directly from solution.

Ion-channels in SLBs have also been exploited as a means of amplifying biorecognition events for electrochemical sensing [173]. Ion channels are membrane proteins with highly selective pores that regulate the transport of inorganic ions, for example  $K^+$ ,  $Na^+$  or  $Ca^{2+}$ , and/or charged molecules creating electrochemical gradients of cell membranes [186]. When an ion channel is triggered to open, the selective pore allows the transport of only the channel-specific ion through the channel. Dependent on the trigger mechanism, this process continues until the potential difference across the membrane (voltage and/or ion concentration) is sufficiently equalized or until the pore closes in response to another stimulus [187]. The most well-known biosensor of this type is the ion channel switch (ICS<sup>TM</sup>) biosensor, developed by Cornell *et al.* [188, 189]. The ion channel switch uses a tSLB and an underlying gold substrate as the working electrode to measure the change in



admittance when dimerization occurs for anchored and gated gramicidin ion channels in a two-dimensional sandwich assay. This clever construction utilizes the fluidity of the lipid bilayer to achieve a  $10^3$  times higher sensitivity to a capture event than if direct binding to the antibody would be used for gating. Since each active gramicidin ion channel allows very high flux of cations ( $\sim 10^7$  ions per second), the amplification per recognition event by the tethered Fab' fragments is amplified by many orders of magnitude. Gramicidin has also been used to construct biosensors by, e.g., Nikolelis *et al.* [190] and Blake *et al.* [191].

## 1.4 Summary of the Biosensor State of the Art

The development and research of (bio)sensors is becoming one of the most popular scientific areas at the intersection of the biological and the engineering sciences. Semiconducting technology has matured so much that we see now a rapid infiltration of new nanotechnology-based approaches in the field of sensors. The resulting new discipline of nano-biosensing is a good example of how engineering sciences, physics, chemistry, and biology coincide at the nanometer scale: The traditional separation between transducers and bioreceptors is being replaced by an integrative approach as the nano-transducers start to take part in the recognition event and as the receptors start to become active transducing elements of the sensors (Figure 1.1).

Another explanation to why (nano)biosensing cuts out a major piece of the nano-bio cake is the need for it. Early, low-cost point-of-care detection of markers for diseases is crucial to diagnose and to manage health problems world wide, especially in the developing world. This has been evident already from the inception of the field when the need for distributed monitoring of diabetes mellitus was - and is - driving both academic and commercial efforts towards developing glucose biosensors. Nanotechnology now promises a solution for integration and high throughput for a vast range of electrochemical sensor applications. Miniaturization, functional sensitivity, simplified read-out and multiplexing are the answers for many current challenges of drug discovery and personalized medical care. In addition, nanotechnology provides new physical phenomena that can be utilized for sensing with a potential to reach the ultimate, single molecule sensitivity. For example, nanowires directly convert a binding event to an electrical signal.

Recently, gene-chip technology has become another prospering industry, which is growing at an impressive rate and opening new areas of application ranging from sys-

tems biology, drug discovery and forensics, to diagnostics [10]. In addition, the first nanobiosensors are also already on the market illustrating that the advancement of nanotechnology also brought a paradigm change into the already mature field of biosensing. It is easy to imagine how related technologies will have a further impact on formats for electrochemical biosensing. The fusion of electrochemical biosensing with nanotechnology and the growing need for inexpensive, mass production of single-use biosensors promises to change the fact that glucose test strips are the sole product of the electrochemical biosensor industry to have achieved commercial success.

This chapter focused on the interplay between the sensors and the corresponding transducer surface nano-architectures with special focus on electronic sensing. In the first section traditional electrical measuring methods that have largely contributed to the current advanced understanding of the existing transduction mechanisms were introduced. After this the use of field-effect transistor technology for biosensing with special focus on the efforts being invested into the combination of existing FET technology and nanotechnology, such as nanowires and carbon nanotubes was discussed [19, 23].

As we approach the nanoscale, the characterization and optimization of the devices becomes more and more difficult. Novel tools that combine different sensing methods can provide the necessary complementary information that is needed to understand the limitations and to optimize the performance of the new techniques. Therefore, we introduced existing methods (e.g. electrochemical SPR, QCM, optical waveguides and AFM) which allow parallel complementary investigations of the biochemical processes that take place at the interface between the devices and the biological sample. Besides their importance in characterization, these techniques also provide unique possibilities for research. It is now possible to manipulate interfaces with electric fields, to study the effect of applied fields onto binding affinities of charged molecules and to control the release of drugs from polyelectrolyte layers or other embedded systems by electronic means [53, 192].

The enormous interest in microarray-based assays originally arose from work using DNA chips [193]. On the other hand, protein microarrays are of general interest for all diagnostic applications where the parallel analysis of several parameters is required [193]. They are mainly used to measure abundances of multiple proteins, usually to discover associations with disease or new biomarkers or to improve the selectivity and specificity of tests [126]. In general, arrays allow for the detection of whole cells and enzyme activity and allow for measuring changes in modification or expression levels of cancer-related proteins [194].

The various generations of enzymatic glucose sensors beautifully demonstrate the integration of transducers, biochemistry, and nanotechnology. In order to eliminate dependence on oxygen levels, the mediator concept was introduced; later nanotechnology-based approaches help to overcome problems with low efficiency of the electron transfer between the enzyme and the sensor electrode (Figure 1.3).

Furthermore, supramolecular architectures enabled unprecedented signal amplification schemes, e.g., incorporating the enzymes into vesicles, polyelectrolyte capsules, sol-gel films or particles. This not only enhanced the stability and improved the shelf-life of sensors, but also improved the sensitivity. However, further new ideas are needed if we want to address new target molecules in the future. While glucose is present in mM concentrations in blood, the diagnosing of cancer markers requires the detection of analytes at pM concentrations. Nanotechnological approaches, both artificial and biologically inspired, which have been demonstrated down to single-molecule sensitivities, are likely to provide the detection schemes that will make this possible.

Natural receptor schemes that operate at such low concentrations (e.g. taste sensing or hormone action) usually involve membrane-based amplification schemes. Ion-channels and G-protein coupled receptors are highly sophisticated nanomachines that successfully solve the problem of selective and efficient amplification of a binding event. Such concepts can be borrowed from nature and used for engineered purposes. Engineered ion-channels embedded in a supported lipid bilayer can be used to amplify the signal of a biosensor. Future approaches include the use of nanoporous substrates to increase the stability of membranes by spanning apertures only 10-100 nm in diameter [170, 195, 196]. These can be miniaturized in a chip format and also allow very sensitive recording of single protein activity by e.g. voltage-clamp electrochemical setups. Such systems are promising for drug discovery since they directly measure membrane protein functionality when they are e.g. exposed to drug candidates.

At present, biosensor research is not only driving the ever-accelerating race to construct smaller, faster, cheaper and more efficient devices, but may also ultimately result in the successful integration of electronic and biological systems. Thus, the future development of highly sensitive, highly specific, multi-analysis, nanoscale biosensors and bioelectronics will require the combination of much interdisciplinary knowledge from areas such as: quantum, solid-state and surface physics, biology and bioengineering, surface biochemistry, medicine and electrical engineering. Any advancement in this field will have an effect on the future of diagnostics and health care. Personalized and pre-

## 321. INTRODUCTION: PRINCIPLES & ARCHITECTURES OF ELECTROCHEMICAL BIOSENSORS

ventive medicine, bedside diagnostics, and drug discovery will all benefit from the novel electronic sensing technologies that were summarized in this chapter.

---

### Scope of the Thesis

---

Biosensors are analytical devices composed of a biological recognition element, a transducer and a readout system. They are used in various fields such as clinical screening and diagnostics [197] or environmental monitoring and detection of pesticides [198, 199].

Because of their ability to detect reagents in very low concentrations, biosensors have a big potential in early diagnostics of cancer and other diseases [200]. Currently, an increasing number of signalling proteins are being identified, e.g. for cancer [93] or for the Alzheimer's disease [201]. An overview of the currently best known and most used cancer antigens, together with their clinically relevant concentrations, is presented in Table 2.1. Normally, biosensors are based on the sandwich principle, where primary antibodies are adsorbed to the surface and specifically capture antigens. In fluorescent assays the antigen concentration is then determined by a fluorescently labelled secondary antibody, specifically binding to the antigen [124]. In enzyme-linked immunosorbent assays (ELISAs) the secondary antibody is coupled to an enzyme which performs an enzymatic reaction that leads to a colour change or drives an electrochemical reaction [4, 202]. Furthermore, these immunoassays can be miniaturized and parallelized to achieve high-throughput devices [124, 197, 203–205].

Several methods exist which require no fluorescent or enzymatic labels. Most of them are highly useful for research, but have a format that is not really suitable for point-of-care diagnostics. Recently, a promising CMOS compatible platform based on film bulk acoustic resonance (FBAR) has emerged which has the potential to enable acoustic techniques to enter the point-of-care diagnostics market [211]. In this study, we used a similar technique, the quartz crystal microbalance with dissipation monitoring (QCM-D).

**Table 2.1:** Overview of critical concentrations and cancer types of the nowadays most investigated cancer antigens.

	Concentrations	Cancer types
PSA (prostate specific antigen)	Normal range: 0-4 ng/ml [206, 207]	Prostatic cancer [206, 207]
CA-125 (carcinoma antigen)	Normal up to 35 units/ml [208], 1.6 ng/ml [209]; >80% of patients have enhanced level [208]	Ovarian cancer; also elevated for endometrial, pancreatic, lung, breast and colon cancer [207]
CA19-9 (carbohydrate antigen)	Healthy up to 35 units/ml [210]	Gastrointestinal cancer; together with CEA also gallbladder neoplasm [210]
CA15-3 (carbohydrate antigen)	Changes in the level to detect breast cancer recurrence (therefore more sensitive than CEA) [207, 210]	Breast cancer; also increased level for colon, lung and hepatic tumours [210]
AFP (alpha-fetoprotein)	High risk patients 100-350 ng/ml, disease >350 ng/ml [210]; up to 10 ng/ml (healthy adult) [207]	Hepatocellular carcinoma [207, 210]
hCG (human chorionic gonadotropin)	-	Gestational tumours [207]

With the QCM-D surface adsorption can be measured *in situ* with a similar sensitivity as with FBARs.

However, the sensitivity of the label-free techniques, including QCM-D and FBAR is not sufficient to detect cancer markers. Therefore, new technique specific amplification systems need to be developed before such devices could enter the point-of-care diagnostics market [204]. The goal of the thesis was to overcome this issue by amplifying the generated signal through a mass increase (QCM-D) or electrochemically with a high number of enzymes per detected antigen. Recently published results with promising sensitivities usually suffer from assay times from hours to days [206]. Thus, another focus of this thesis is to reduce the assay time to allow the use of the sensor in point-of-care diagnostics.

---

A first approach to go one step further and thereby reach the required sensitivity as well as a reduced assay time is described in Chapter 4. It is essential to increase the signal, reduce the background and increase the sensitivity of the detection method itself [212]. Thus, the goal of the presented approach was to lower the detection limit to a sensitivity that is sufficient to assess e.g. cancer antigens, such as prostate specific antigen (PSA), where the diagnostically relevant concentration is in the range of ng/ml [125]. Therefore, the high sensitivity of the QCM-D to dissipative losses was combined with the specific detection strategy of a sandwich assay. In Chapter 4 the signal of the secondary antibodies was increased by coupling them to lipid vesicles. The larger mass and especially the increased viscoelasticity of the vesicles compared with a single antibody pushed the detection limit down to the sub-ng/ml range in human serum. With this it was demonstrated that the detection of cancer markers is possible also with acoustic, label-free techniques.

In order to transfer the approach of the signal enhancement through the vesicles to electrical sensing techniques, the idea was to functionalize the vesicles with a high number of enzymes. Here, we focussed on electrochemical detection because of the availability of non-expensive and small readout systems like the ones already used for glucose monitoring in diabetes care. Within the electrochemical techniques, a suitable detection method was evaluated. Its performance to amplify the signal when enzymes were bound to vesicles needed to be assured before the technique could be transferred to the vesicle based sandwich assay (see Chapter 5).

In summary, the enzyme functionalized vesicles worked similarly to the vesicles for mass amplification in the QCM-D. One drawback of this system is the limited stability of the lipidic vesicles. To improve the shelf-life and the chemical stability of the sensor, we replaced the lipidic- by polymeric vesicles with incorporated enzymes (see Section 5.3.3). Another possibility, where enzymes are bound to microparticles, is shortly introduced in Section 5.4.

In order to further simplify the biosensor, the idea was to include the mediator in the system to prevent an additional injection step. We chose the approach to incorporate it into a polyelectrolyte multilayer (PEM) film, built by the versatile and inexpensive layer-by-layer (LbL) deposition technique. Thereby, films are formed by the alternating adsorption of positively and negatively charged species from aqueous solutions. Because they are held together mainly by electrostatic interactions, we expected the charged mediators to remain in such films. During the development of this system we discovered that these mediator-loaded PEM films showed electroactive behaviour. Upon application of CV

they expanded and contracted reversibly. Furthermore, this shape change was observed under mild conditions, meaning no drastic pH change or high potentials were required (see Chapter 6). Unfortunately, the mediator working for the electrochemical enzyme detection could not be incorporated into the film. Thus, for the enzymatic reaction in and on the film the mediator needed to be present in solution. Nevertheless, the here developed system has the potential to induce a shape deformation of the film without applying an electric potential. With the right parameters, the mediator in the film could be reduced or oxidized by the enzymatic reaction instead.

To conclude, in this thesis a highly sensitive sandwich based biosensor was developed. It allows for the detection of antigens through vesicles for mass enhancement or electrochemical sensing with a high number of enzymes coupled to one binding event. Additionally, an alternative enzymatic biosensor including electroactive PEM films was introduced.



### **3.1 Materials**

#### **3.1.1 Buffer**

All measurements were carried out in a 10 mM 4-(2-hydroxyethyl)piperazine-1-ethanesulfonic acid (Sigma, Switzerland) solution containing 100 mM KCl. The pH of the buffer solution was adjusted to pH = 7.4. The buffer was prepared with ultrapure water (Milli-Q gradient A 10 system, Millipore Corporation, USA) and filtered (0.2  $\mu\text{m}$ ) prior to use.

#### **3.1.2 Proteins**

Albumin from bovine serum (BSA) (Sigma, Switzerland) was used to inhibit unspecific adsorption to the surface. When nothing else is indicated, it was applied at a concentration of 10 mg/ml.

Serum (Precinorm U) was purchased from Roche, Switzerland. To check the specificity of the antigen binding it was applied 10 times diluted. It was only used in the measurements where it is specifically mentioned.

Neutravidin (NA) (Molecular Probes, Netherlands) was used to couple biotinylated reagents together. When nothing else is mentioned, it was applied at a concentration of 20  $\mu\text{g/ml}$ .

Open membrane proteins F (OmpF) were used in the membranes of polymeric vesicles with incorporated enzymes. They allow for the diffusion of molecules with a molecular weight of up to 400 g/mol [148]. The OmpF proteins were supplied by Prof. W. Meier.

### 3.1.3 Enzymes and Substrate

For the various sensors in this thesis the enzyme Glucose oxidase (GOx), Type X-S from *Aspergillus niger*, lyophilized powder was chosen (Sigma, Switzerland). It contains 100'000-250'000 units/g solid (used batch: 146'000 units/g) and is without added oxygen. 1 mg corresponds to 140 units. One unit is defined as the amount that oxidizes 1.0 mmol of  $\beta$ -D-glucose to D-gluconic acid and hydrogen peroxide per minute at pH 5.1 and 35 degrees Celsius. For some experiments biotinylated GOx (GOx/b) was used (Bio-Concept, Switzerland). The supplier does not give any information about the number of biotins per enzyme (usually there are multiple); for calculations no multiple binding was assumed. The variable concentrations (in the range of  $\mu\text{g/ml}$ ) for the individual measurements are given in the experimental part.

The substrate,  $\beta$ -D-glucose (Sigma, Switzerland), was used at a concentration of 200 mM. When a lower concentration was used, it is stated in the corresponding experimental part.

### 3.1.4 Antibodies

For the immunoassay experiments an antibody-antigen-antibody sandwich system was used. The primary antibody (AB) was an Fc specific anti-mouse IgG, the antigen (AG) a purified mouse IgG and the second antibody (2nd AB) an Fab specific anti-mouse IgG biotin conjugate. They were all ordered from Sigma, Switzerland. Unless mentioned differently in the text, they were used at a concentration of 20  $\mu\text{g/ml}$ .

### 3.1.5 Lipids

All lipids were purchased from Avanti (Avanti Polar Lipids Inc., USA). Neutral, unsaturated 1-Palmitoyl-2-Oleoyl-sn-Glycero-3-Phosphocholine (POPC) lipids were used.

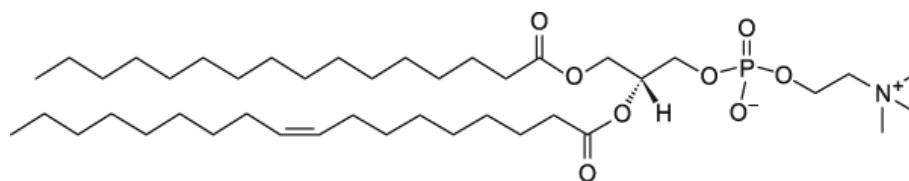


**Figure 3.1:** Molecular structure of a POPC lipid, with hydrophobic tails (left) and hydrophilic head (right).

They have a molecular weight of 760 g/mol and a sum formula of  $C_{42}H_{82}NO_8P$ . Their structure with the hydrophilic head and the hydrophobic tails is shown in Figure 3.1.

Depending on the application different functionalities, such as biotinylated or fluorescent lipids, were introduced by adding 1 % 1,2-Dioleoyl-sn-Glycero-3-Phosphoethanolamine-N-(Biotinyl) (DOPE/biotin) and/or 2 % 1,2-Dioleoyl-sn-Glycero-3-Phosphoethanolamine-N-(Lissamine Rhodamine B Sulfonyl) (PE-rhod) lipids.

### 3.1.6 Polymers for Multilayers

The following polymers were used to build polyelectrolyte multilayers:

- Polyethyleneimine (PEI), MW 25'000 g/mol, branched, initiator layer (positively charged)
- Poly(L-glutamic acid) (PGA), MW 15'000-50'000 g/mol (negatively charged)
- Poly(allylamine hydrochloride) (PAH), MW 70'000 g/mol (positively charged)
- Poly(sodium 4-styrenesulfonate) (PSS), MW 70'000 g/mol (negatively charged)
- Poly(L-lysine) (PLL), MW 15'000 g/mol (positively charged)
- Poly(L-lysine(20 kDa))-g[3.5]-poly(ethylene glycol)(2 kDa)/PEG(3.4 kDa)-biotin (50 %) (PLL-g-PEG/biotin)
- Poly(L-lysine(20 kDa))-g[3.5]-poly(ethylene glycol) (2 kDa)/PEG(3.4 kDa)-TRITC (red label) (PLL-g-PEG/TRITC)

The first five on the list were purchased from Sigma, Switzerland, the last two from SurfaceSolutionS AG, Switzerland. All polyelectrolyte solutions were applied at a concentration of 1 mg/ml buffer. They were filtered (0.2  $\mu$ m) prior to use.

### 3.1.7 Mediators

For the electrochemical measurements two iron based mediators were used. Ferrocyanide and ferricyanide have the same molecular formula, but are differently charged. Ferrocyanide ( $[\text{Fe}(\text{CN})_6]^{4-}$ ) is the reduced form, ferricyanide ( $[\text{Fe}(\text{CN})_6]^{3-}$ ) the oxidized form. Ferrocyanide can be ordered as potassium ferrocyanide, in the form of a salt. The other mediator was (dimethylaminomethyl)ferrocene ( $\text{C}_{13}\text{H}_{17}\text{FeN}$ ), a ferrocene with a dimethylaminomethyl group to make the molecule water soluble.

### 3.1.8 Substrates, Surfaces

For electrochemical measurements, where the substrate acts as the working electrode, only electrically conductive surfaces can be used. QCM-D measurements were performed with 50 nm gold coated sensor crystals (Q-Sense AB, Sweden). Indium tin oxide (ITO) coated surfaces (Microvacuum, Budapest, Hungary) were used for AFM and CLSM measurements. Small interfacial potential differences between ITO and Au were not relevant for the here presented results, because it was only important whether the applied potential was above or below the oxidation potential of the mediator.

Before the experiments a cleaning protocol was applied to the sensor surfaces. They were soaked in a 2% sodium dodecyl sulfate (SDS) (Sigma, Switzerland) solution for 30 minutes, rinsed with Milli-Q water and blown dry under nitrogen. Subsequently, they were put into the UV/Ozone cleaner for another 30 minutes. At the end of the measurement cleaner (Cobas Integra, Roche, Germany) was injected into the flowcell. After half an hour the flowcell was properly rinsed with Milli-Q water. For storage the sensors were removed from the flowcell, rinsed again with Milli-Q water and blown dry under nitrogen.

### 3.1.9 Particles

Polystyrene (PS) particles with a diameter of 1 and 10  $\mu\text{m}$  as well as weakly crosslinked melaminformamid (MF) particles with a diameter of 5  $\mu\text{m}$  were used for particle based assays. They were obtained from Microparticles GmbH, Germany. Calcium carbonate ( $\text{CaCO}_3$ ) particles (5  $\mu\text{m}$  diameter) were ordered from PlasmaChem GmbH, Germany.

## 3.2 Methods

### 3.2.1 Electrochemistry

Together with the QCM-D and the CLSM an IPS Jaissle PGU10V-1A-IMP-S potentiostat/galvanostat (Jaissle Elektronik GmbH, Germany) was used. An AMEL potentiostat/galvanostat (model 2053, AMEL electrochemistry, Italy) was combined with the AFM.

Independent of the instruments, for our measurements flowcells with a three-electrode setup were used (see Figure 3.2). Thereby, the sensor surface was at the same time used as working electrode (WE). The Ag/AgCl reference- (RE) and the platinum counter electrode (CE) were situated on the upper side of the flowcell. The potential was applied between the working and the reference electrode whereas the counter and the working electrode were used to read out the current. In the mode *open circuit potential* (OCP) the cell potential is monitored, but no current is allowed to flow. According to the convention, a positive current means electrons are entering the flowcell through the working electrode; a negative current corresponds to electrons leaving the flowcell at the working electrode.

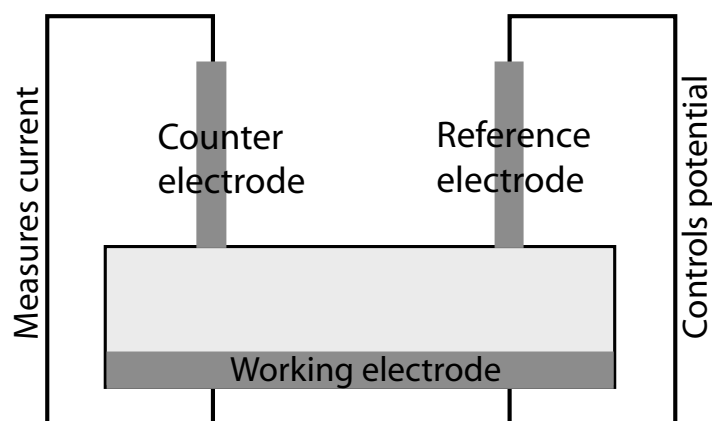


**Figure 3.2:** Setup of our three-electrode flowcells. The working electrode, corresponding to the sensor surface, is connected to the reference electrode to control the potential and to the counter electrode to measure the generated current.

Cyclic voltammetry (CV) was performed prior to the measurements to condition the reference electrode. Therefore, a scan rate of 50 mV/s was used. For the measurements we used CV and/or chronoamperometry. For the former, a cyclic potential was applied with a scan rate ranging from 2-100 mV/s. Normally, 5 cycles were performed, whereas the

last cycle was used for data evaluation. An exception is the CV in ferrocene biosensors, where only 3 cycles were performed when the scan rate was 3 mV/s. For lower scan speeds the system has more time to stabilize, thus 3 cycles are sufficient. The current is plotted as a function of the applied potential. In case of the latter, the chronoamperometry, a constant potential was applied and the output current was recorded as a function of time (see Section 5.1).

### 3.2.2 Instruments

#### Quartz Crystal Microbalance with Dissipation Monitoring (QCM-D)

The Quartz Crystal Microbalance with Dissipation monitoring was used to measure the adsorption of small masses. A detailed description of the technique is given in the Introduction (1.2.3). A schematic view of our EC flowcell is given in Figure 3.3.

The thickness of the PEM layers was estimated by using the viscoelastic Voigt model [213, 214]. As opposed to the Sauerbrey equation [215] this model takes into account the viscoelastic losses obtained from the dissipation monitoring (see Section 6.1).

#### Atomic Force Microscope (AFM)

The Atomic Force Microscope (AFM) is a scanning probe microscope with high resolution. AFM allows to obtain a three-dimensional surface profile of the sample. This is accomplished by monitoring the interaction force between the sample surface and a probe (e.g. a sharp tip), which is attached to the end of a force-sensing cantilever. Therefore, no special surface treatment or probe preparation is required. The AFM experiments in this thesis were performed in liquid.

Experiments were run using a NanoWizard I BioAFM (JPK Instruments, Germany) instrument. A home built EC-cell provided the possibility to perform EC measurements. As shown in Figure 3.4, there is a round cavity for the liquid. The surface on its bottom acts as working electrode. The two circles around the basin are an Ag reference- and a Platinum counter electrode (see Section 6.1).

For the characterization of PEM layers the AFM was used to measure the surface topography and the film thickness in liquid state. For the latter, the film was scratched

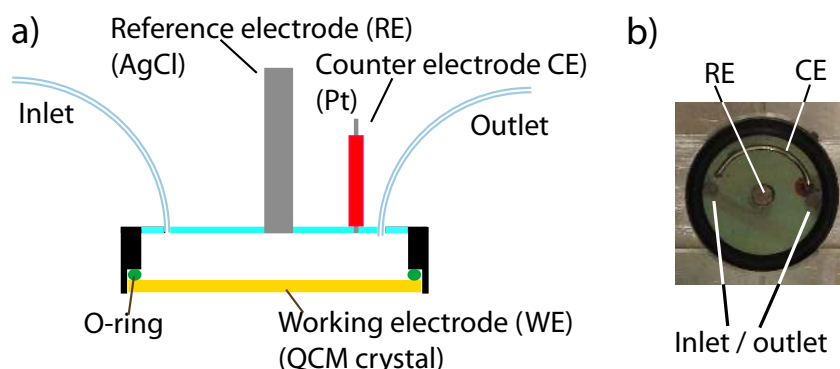


**Figure 3.3:** Electrochemical flowcell of the QCM-D. a) Schematic cross-section of the flowcell. b) Expanded view of the upper side of the flowcell. In the center of the transparent flowcell, that is surrounded by an o-ring, is the reference electrode (RE). The counter electrode (CE) is placed in a groove with the shape of a half circle. Inlet and outlet tubes are on the left and right sides.

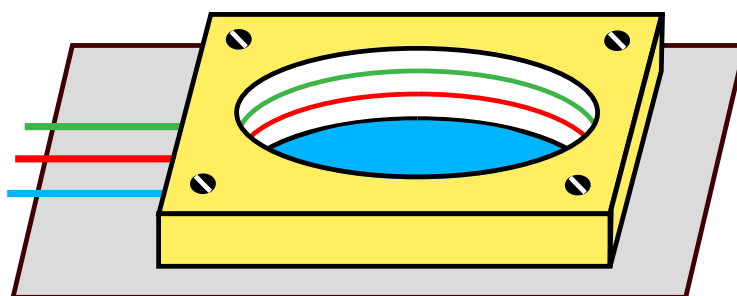


**Figure 3.4:** Schematic view of the EC-AFM cell. The surface acts as WE (blue), counter and reference electrodes (red and green) are around the liquid filled basin.

with a razor blade. In order to prevent damage of the soft film, the AFM was run in the tapping mode. The electrochemical setup allowed us to apply CV and chronoamperometry parallel to the scanning [216].

### Confocal Laser Scanning Microscope (CLSM)

A Zeiss LSM 510 confocal laser scanning microscope (CLSM) was used (Zeiss, Germany). Fluorescent images were taken from samples illuminated with the DPSS-Laser (10 mW,  $\lambda = 561$  nm). The instrument also allows to take conventional bright field images, which were used to obtain information about particle density and agglomeration. The instrument is equipped with 10x (0.3 NA), 20x (0.5 NA), 40x (LD, 0.7 NA) and 63x (oil, 1.4 NA) objectives and the corresponding filter sets. For more detailed information about the basics and the development of the CLSM technique the reader is referred to Jones *et al.* [217].

The CLSM was utilized to test the polymer adsorption on microparticles. Therefore, a fluorescent polymer was adsorbed on top of the others and its presence confirmed by photobleaching experiments (see Appendix A).

Like for the other instruments, a home built EC-flowcell was used in combination with the CLSM. ITO coated, transparent sensor surfaces were used for adsorption and as the working electrode. On the upper side of the polycarbonate cell, thin Ag and Platinum wires were placed as counter- and reference electrode, respectively. Inlet and outlet channels were placed at the short end of the 2 cm x 1 cm sized flowcell. Their special geometry assured the equal distribution of the injected solution in the entire cell. This setup allowed for parallel *in situ* microscopy and EC measurements.

### Fourier Transform Infrared Spectroscopy (FTIR)

Fourier Transform Infrared Spectroscopy (FTIR) was measured with an Equinox 55 (Bruker, France). The films were deposited on a trapezoidal ZnSe crystal (Graseby-Specac, Orpington, UK) located on the bottom of a flow cell (Graseby-Specac, Orpington, UK) by allowing each polyelectrolyte solution to circulate over the substrate during 5 min. Two polyelectrolyte adsorption steps were separated by buffer rinse for 10 min. Polyelectrolyte and buffer circulation was allowed through Tygon tubings by means of a peristaltic pump. The infrared spectra of the film were acquired during each buffer rinse step in the total attenuated reflection mode by accumulating 512 interferograms at a resolution of  $2\text{ cm}^{-1}$ . The signal transmitted through the ZnSe crystal was collected with a liquid nitrogen cooled mercury-cadmium telluride detector. During the deposition of the PEI-(PGA-PAH)<sub>5</sub> multilayer film, the absorption spectrum was calculated as  $-\log(T_{\text{layer}}/T_{\text{PEI}})$ , where  $T_{\text{layer}}$  and  $T_{\text{PEI}}$  are the transmissions in presence of the considered film and when PEI is adsorbed on the native ZnSe crystal, respectively. FCIV ions and PSS/PLL multilayers were adsorbed the same way. The spectra were acquired as for the deposition of the PEI-(PGA-PAH)<sub>5</sub> underlayer. The absorbance was now calculated by taking the transmission of the PEI-(PGA-PAH)<sub>5</sub> stratum as a reference in order to measure the change in ferrocyanide content (the cyanide groups give rise to a strong band centered at  $2033\text{ cm}^{-1}$ ) as well as the deposition of PSS layers (giving rise to elongation peaks due to the sulfonate groups at  $1035$  and  $1007\text{ cm}^{-1}$ ) (see Section 6.1). The FTIR measurements were performed by Vincent Ball.



### 3.2.3 Vesicle Fabrication

#### Lipidic Vesicles

To prepare the vesicles, lipids, dissolved in chloroform and stored at  $-20^{\circ}\text{C}$ , were used. A solution containing 99 % POPC and a 1 % DOPE/biotin was mixed in a round bottom flask. For fluorescent vesicles 2 % PE-rhod lipids were added. Then, the chloroform was evaporated from the lipids using nitrogen gas. Subsequently, buffer was added and the lipid bilayers were removed from the flask by vortexing to form big, multilamellar vesicles. These vesicles were 31 times extruded through polycarbonate membranes with pore sizes of 100, 400 or 1000 nm, whereas only the 100 nm vesicles are unilamellar. Throughout the text lipid vesicles are referred to as vesicles.

#### Polymeric Vesicles

The synthesis of the polymeric vesicles is performed in two steps; first some of the polymer is biotinylated, then the vesicles themselves are formed [145]. (Poly(2-methyloxazoline)-*b*-poly(dimethylsiloxane)-*b*-poly(2-methyloxazoline)), a tri-block copolymer was used to synthesize the vesicles.

Synthesis of biotinylated amphiphilic polymer: Further details for the synthesis of amphiphilic polymers can be found in U.S. Patent No. 6,916,488. 1.0 g of the amphiphilic polymer (HO-PMOXA<sub>13</sub>-PDMS<sub>60</sub>-PMOXA<sub>13</sub>-OH), 200 mg of biotin, and 300 mg of hexamethylenetetramine were added to a 100 ml 2-neck flask and dried under vacuum for 24 h. Then 50 ml of dry trichloromethane was added under nitrogen and the reaction carried out at room temperature for 60 h. Trichloromethane was evaporated under reduced pressure and the polymer was dissolved in an ethanol/water mixture (4/1, v/v). This solution was diafiltrated through a membrane (MW 1000 cut off) to remove unreacted biotin. The solvent was evaporated under reduced pressure. The polymer was dried under vacuum for 24 h and characterized by <sup>1</sup>H NMR (1.2-1.4 ppm, -CH<sub>2</sub>- of biotinyl group).

Synthesis of nanoreactors: 15 mg of HO-PMOXA<sub>7</sub>-PDMS<sub>22</sub>-PMOXA<sub>7</sub>-OH + 1.5 mg of the above biotinylated polymer were placed in a 10 ml flask and dissolved in 2 ml of ethanol, then 20  $\mu\text{l}$  of a solution of the bacterial porin OmpF (1.5 mg/ml) was added. The solution was vortexed for 1 min before ethanol was evaporated under reduced pressure. On the top of the film, an additional 10  $\mu\text{l}$  of OmpF solution was placed, and dried under high vacuum. After film drying for approximately 45 min, 5 ml of GOx (1 mg/ml, or

200 units/ml) in 100 mM acetate buffer pH 5.5 was added. The film was hydrated under shaking for about 12-15 h at 0 C. After film hydration, the vesicle solution was filtered through a 1  $\mu$ m filter once and 11 times through 400 nm filter (Agilent) with a syringe drive system (Agilent) and placed on a Sepharose-4B column for the separation of the nanoreactors from unencapsulated GOx and OmpF. Once prepared, the nanoreactors were kept at 4 C.

Activity testing: 10 mM glucose in 100 mM acetate pH 5.5 buffer, 100 units/ml horseradish peroxidase (in 100 mM AcH/AcNa pH 5.5 buffer), and 100  $\mu$ M Amplex-Red were mixed. The solution was colourless to slightly pink depending on the freshness of the Amplex-Red. 50  $\mu$ l of the nanoreactor formulation was added to the above mixture and the solution turned purple within 1-3 min. Throughout the text these vesicles are referred to as polymeric vesicles.

The polymeric vesicles were synthesized by Svetlana Litvinchuk and Arthur Lu from BioCure Inc.

### 3.2.4 Biosensing Experiments

#### Sensing with Enzyme Functionalized Vesicles

Different NA concentrations were adsorbed to the sensor surface, ranging from 0 to 20  $\mu$ g/ml. To prevent unspecific adsorption of the vesicles, BSA (0.1-10 mg/ml) was injected. In the last step the enzyme functionalized vesicles followed. Prior to injection of the vesicles, the biotinylated GOx were premixed with NA for 10 min (if nothing else is indicated 1:1 ratio). It is possible that several NA and GOx/b are bound to each other or even have the potential to connect vesicles. However, since this does not change their total number and thus not their number per binding point this is not expected to influence the sensor output. Then, the vesicles (100-400 nm, depending on the experiment; 6-250  $\mu$ g/ml) with 1 % biotinylated lipids were added to this solution. After another 10 min they were finally injected. After each adsorption step the system was rinsed with buffer. The scheme of such a sensor with high NA concentration is shown in Figure 3.5. For few experiments no GOx was used. In this case no pre-mixing of the vesicles with NA was required and they were directly injected after the BSA adsorption (see Section 4).

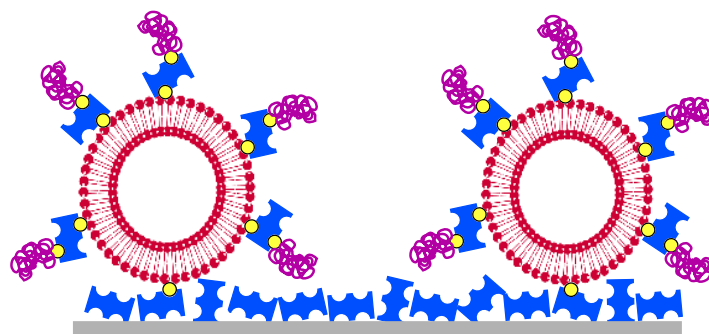


**Figure 3.5:** Scheme of the NA model system with detection through enzyme functionalized vesicles. First, the NA is adsorbed, followed by BSA (especially important for low NA concentrations) and the functionalized vesicles.

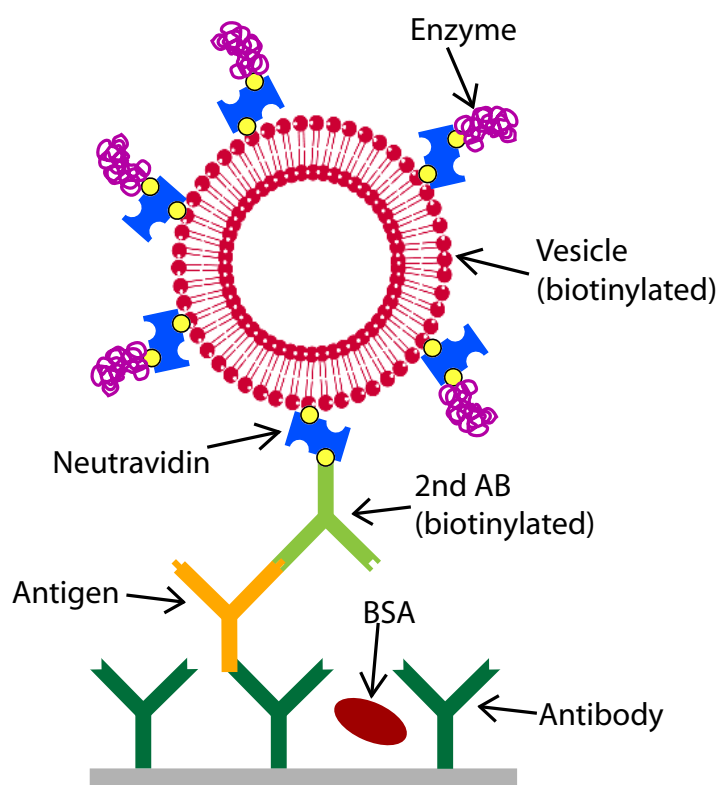


**Figure 3.6:** Scheme of our biosensor. The primary antibody is adsorbed to the substrate. BSA is added to prevent unspecific adsorption before the antigen is captured. Subsequently, the secondary antibody, coupled to the vesicle via biotin/neutravidin, is added. Finally, the vesicles are functionalized with enzymes.

### Enzyme Functionalized Vesicle Enhanced Sandwich Assay (EFVESA)

The assay is built up according to the scheme in Figure 3.6. First, a solution containing 20  $\mu\text{g/ml}$  primary antibodies was injected into the flowcell. In order to inhibit unspecific adsorption, 10 mg/ml BSA was injected in a next step. Then, the antigen to be detected

followed in a low concentration. Finally, the secondary antibodies, bound to vesicles via NA, were injected to enhance the signal of the detected antigens. The last three steps were either performed individually or the three assay solutions were premixed in different orders prior to injection. Each mixing step lasted 10 min. Control experiments were run with serum. In this case, after the BSA adsorption, serum was injected and the antigen was spiked directly into the serum as well. Between the individual steps the system was rinsed with buffer. The vesicles adsorbed for 1 hour. For all the other steps we waited until the adsorption curve reached an equilibrium. A diagnostically relevant assay time of about 30 min was used for the adsorption of low antigen concentrations that could not be seen in the QCM-D curve (see Section 5.3).

For electrochemical measurements involving enzymes, the existing biosensor (see paragraph above) was expanded by introducing enzymes into the system. Therefore, NA (20  $\mu\text{g/ml}$ ) was injected, followed by GOx/b (50  $\mu\text{g/ml}$ ) after a rinsing step. There was also the variation where the enzyme functionalized vesicles were injected in one step. Therefore, GOx/b and NA were premixed for 10 min. Then these complexes were mixed with the vesicles for another 10 min prior to injection. The molar mixing ratio of NA:GOx/b:vesicles(400 nm) was 1000:1000:1. Ratios other than that are indicated in the results section.

### 3.2.5 Polyelectrolyte Multilayers (PEMs)

#### PEM Buildup on Flat Surfaces

Polyelectrolyte multilayer (PEM) films were built up by alternating adsorption of positively and negatively charged polymers onto either a gold or an ITO surface. PEI was used as an initiator layer for all films regardless of their polymer combinations. Subsequently, up to 10 bilayers of PGA/PAH, PSS/PLL or combinations of the two were adsorbed. For multilayers with  $n$  repetitions of one bilayer type the sequence is abbreviated with (polyA-polyB) $_n$ . Each polymer was injected for 5 minutes. For QCM-D measurements the polymers were adsorbed without a buffer rinse between the steps. For AFM measurements the excess was removed and subsequently the system rinsed with a pipette. After extensive rinsing, following the last adsorption step, the film was exposed to 1 mM ferrocyanide for 10 minutes (see Section 6.1).

### Particle Coating

The positively charged PS particles (see Section 3.1.9) were first coated with PEI. Depending on the application, PGA, PAH and PLL-*g*-PEG/biotin or (PGA-PAH)<sub>*n*</sub>-FC followed. To test whether the polyelectrolytes really adsorbed to the particle surfaces, they were coated with the fluorescent PLL-*g*-PEG/rhod as a last layer. PEI, PGA and PAH were all dissolved in buffer at a concentration of 1 mg/ml, PLL-*g*-PEG/rhod at 0.1 mg/ml. Prior to the polymer adsorption, the particles were washed with buffer. The higher concentrated polyelectrolytes were adsorbed for 5 min, PLL-*g*-PEG/rhod for 10 min. Between the individual adsorption steps the coated particles were rinsed with buffer three times. For rinsing, the particles were centrifuged for 30 s at 2'000 rpm. The supernatant was carefully removed with a pipette. After adding the next solution, the mixture was vortexed to avoid coagulation of the particles (see Sections 5.4 and Appendix A). CaCO<sub>3</sub> particles were also first covered with a PEI layer, while the positively charged MF particles were directly coated with the negative polyelectrolyte of the film.



---

## Vesicles for Signal Amplification in a Sandwich based Biosensor<sup>1</sup>

---

The sensitivity of biosensors is often not sufficient to detect diagnostically relevant biomarker concentrations. This chapter describes how a Quartz Crystal Microbalance with Dissipation monitoring (QCM-D) can be utilized to detect dissipative losses induced by the attachment of intact vesicles. We modified a sandwich assay by coupling the secondary antibodies to vesicles. This resulted in an increase of the detection sensitivity, achieving a diagnostically relevant detection limit of 5 ng/ml or 30 pM antigens. In addition, we could combine the individual steps to decrease the total assay time to result in about 30 minutes. Finally, polymeric vesicles were introduced to overcome potential problems related to the limited shelf-life of lipid vesicles.

### 4.1 Sensor Buildup

Prior to the detection of the antigen, the surface was functionalized with a primary antibody and blocked with BSA to prevent unspecific adsorption. Then, the antigen was injected at a given concentration. To enhance the weak signal of the antigen, a secondary antibody, specifically binding to the antigen and functionalized with biotin, was bound, followed by the linker neutravidin and vesicles, functionalized with biotin (see Figure 4.1). A QCM-D curve of this adsorption sequence is shown in Figure 4.2. The

---

<sup>1</sup>Parts of this chapter have been published in: D. Grieshaber, V. de Lange, T. Hirt, Z. Lu and J. Vörös, *Vesicles for Signal Amplification in a Biosensor for the Detection of Low Antigen Concentrations*, *Sensors*, **8**: 7894-7903, 2008.

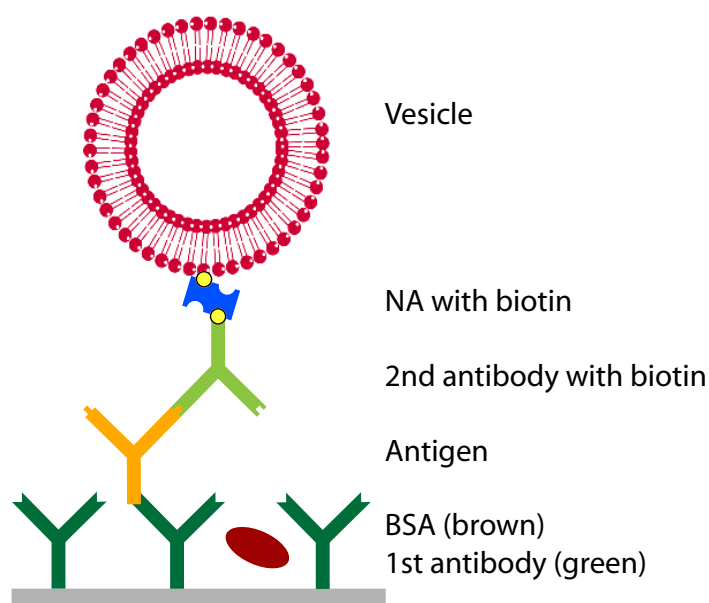


**Figure 4.1:** Scheme of our biosensor. The primary antibody is adsorbed to the substrate. BSA is added to prevent unspecific adsorption before the antigen is captured. Subsequently, the secondary antibody, coupled to the vesicle via biotin/neutravidin, is added.

example represents a curve with an antigen concentration of 400 ng/ml. The adsorption of the primary antibody gave a signal in both the frequency and the dissipation change. Some BSA adsorbed as well, but upon rinsing the loosely bound molecules were rinsed off. The adsorption of the antigen is not visible in the curve because the few molecules did not yield a high enough signal. The secondary antibodies and the neutravidin resulted in a signal, but considering that 400 ng/ml antigen was far above the detection limit, it was quite small (see Figure 4.2 step iv). Finally, the adsorption of the vesicles resulted in a big signal (see Figure 4.2 step vi); a frequency change of 51 Hz and a dissipation change of  $1.4E-5$ . Even at low antigen concentrations, which were not directly detectable with the QCM-D, the vesicles multiplied the signal and allowed for the indirect, quantitative measurement of the antigen concentration. In control experiments containing all steps except from the 2nd AB, the signal upon injection of the vesicles was  $f=-0.8$  and  $D=0.22$ .

The spikes, appearing upon injection or buffer rinse (marked with dotted arrows in Figure 4.2), are an artefact from the temporarily enhanced pressure in the flowcell and are completely reversible.

For different antigen concentrations the changes in frequency and dissipation upon adsorption of the vesicles are depicted in Figure 4.3. For the saturation concentration, meaning the maximal number of antigens that can sterically fit on the surface, the anti-



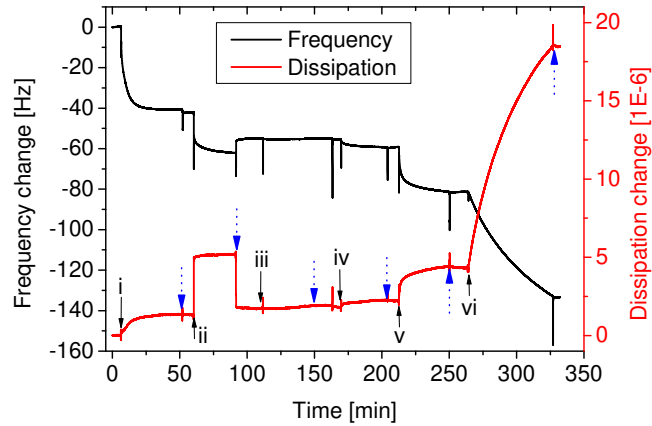


**Figure 4.2:** QCM-D curve showing frequency and dissipation changes during the adsorption steps. i) Primary antibody, ii) BSA (part of it is removed upon rinsing), iii) antigen (400 ng/ml), iv) secondary antibody, v) neutravidin, vi) vesicles. The spikes (marked with dotted arrows) are an artefact upon injection/rinsing.

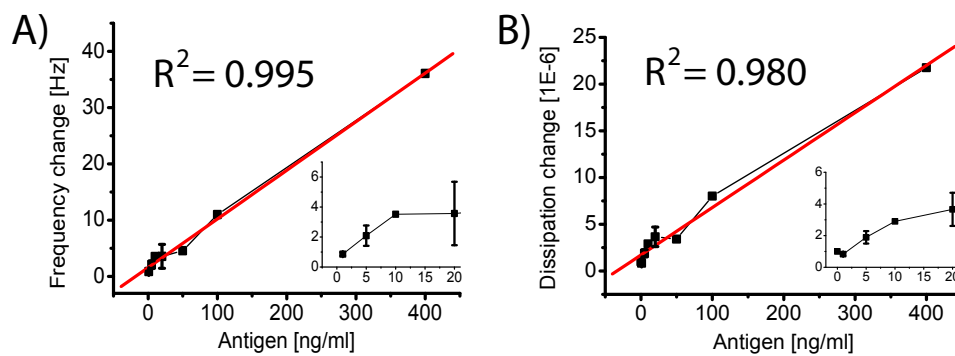


**Figure 4.3:** Vesicle adsorption for low antigen concentrations. A: Frequency change upon adsorption of the vesicles as a function of the antigen concentration. B: Dissipation change upon adsorption of the vesicles as a function of the antigen concentration. The insets show the detection limit at low concentrations.

gens themselves still yielded a small signal in the QCM-D. However, compared to the signal from the vesicles it was 10-20 times smaller, depending on the different concentrations (see example in Figure 4.2). As soon as the antigen concentration was decreased, the direct signal was no longer detectable, whereas the enhanced signal through the vesicle binding was still detectable for significantly lower concentrations. For the dissipation curve, being sensitive to the viscoelastic behaviour of the whole vesicles (including the entrapped buffer), the detection limit, after 30 min exposure to the antigen and few minutes of vesicle adsorption, was around 5 ng/ml or 30 pM (see Figure 4.3B, inset). To recapitulate, the setup of our biosensor made it possible to perform highly sensitive and reproducible measurements. Because of the comparably low mass of the antigen molecules, the signal was significantly increased by specifically binding secondary antibodies linked to vesicles. This amplification scheme enabled us to also detect antigen concentrations that did not give a sufficient signal in the QCM-D before the signal amplification through the vesicles. In the concentration range of interest for potential applications (i.e. ng/ml), the signal increased linearly with increasing antigen concentrations. The curves only started to level off for higher antigen concentrations, i.e.  $\mu\text{g/ml}$  (not shown in Figure 4.3), which is above diagnostically relevant concentrations of cancer markers in blood. This, together with the fact that we could reach saturation with the vesicle adsorption, suggests that for low concentrations every single antigen was detected by a vesicle, i.e. the antibodies were separated far enough so that the vesicles had sufficient space to bind to each of them. The reason why the S/N ratio curves increased fast in the beginning before levelling off could be that after a while most of the specific binding points are occupied and the fraction of unspecific binding increased for the adsorption after several hours. This allows also for the quantitative determination of the antigen concentration. With the currently used antibody-antigen system, the unspecific adsorption of the secondary antibody was the limiting factor. However, this is only a model system and can be further improved, e.g., by additional blocking steps or by using another antibody-antigen system. The direct non-specific adsorption of vesicles or NA was negligible compared to their secondary binding through non-specifically adsorbed secondary antibodies. If we were able to lower the unspecific binding below the current limit of the detection method (e.g. by using an antibody-antigen system with a higher specificity than the current model system or by introducing blocking steps with IgG), we would expect to further lower the detection limit.

For potential applications it is essential to obtain the results within a short time, usually within minutes. To demonstrate the assay time of our sensor, the adsorption of the

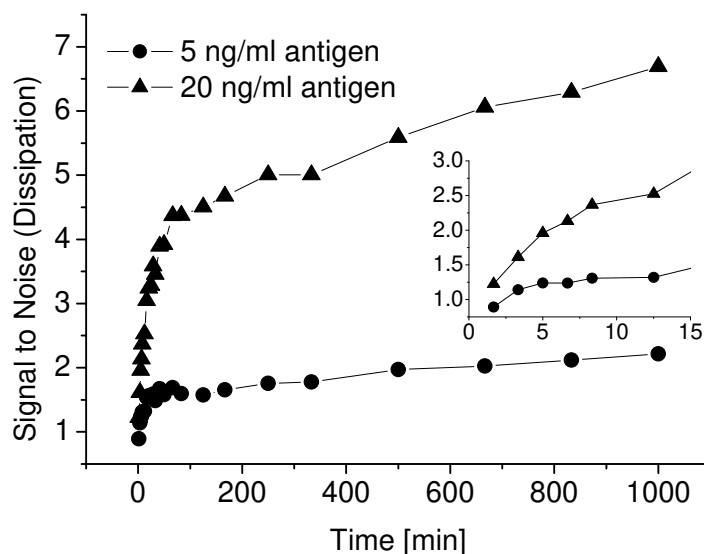


**Figure 4.4:** The S/N ratio of the vesicle adsorption is shown as a function of the incubation time. The inset shows a zoom in of the first 15 minutes.

vesicles as a function of incubation time is shown in Figure 4.4; the adsorption is plotted as a S/N ratio. Signal-to-noise corresponds to a dissipation change upon adsorption of the vesicles in a system with a certain antigen concentration divided by the background signal, obtained from unspecific vesicle adsorption. Thus, for no antigens it remains 1 throughout the measurement. The S/N ratio for the frequency was slightly less sensitive. The main increase in the S/N ratio, and therefore the response of the sensor, occurred during the first hour. Later on, the increase was only marginal. As it can be seen from the inset in Figure 4.4, already after few minutes a quantitative result was obtained even for the low concentration regime. For higher concentrations the curves still had the same shape, but the signal-to-noise ratio was accordingly higher.

The detection limit of the biosensor was determined by the signal-to-background ratio of the dissipation change upon adsorption of the vesicles. With our sensor we have achieved a detection limit as low as 5 ng/ml or 30 pM. To our knowledge, so far the lowest detection limit reached by QCM-D has been published by Larsson *et al.* [218] who detected cholera toxin down to a limit of 750 pM. Thus, our new system is 25 times more sensitive than the one reported by Larsson *et al.* Furthermore, it is 160 times more sensitive than a DNA recognition sensor by Patolsky *et al.* [219] and even 300 times more sensitive than results presented by Yun *et al.* [220] some years ago.

## 4.2 Optimizing the Sensor

To minimize the analysis time we went one step further towards a one-pot assay and premixed secondary antibodies, neutravidin and the vesicles. The concentrations and the order in which the three reagents were mixed together were varied as shown in the example in Figure 4.5. The first four double-bars correspond to different variations of concentrations and mixing order, whereas the double-bar on the right shows the sum of changes in frequency and dissipation when all three reagents were injected separately. When first NA and the vesicles were mixed for 10 min, before adding the secondary antibodies for another 10 min, the adsorption was less than 20 % compared to the single-step adsorption (see first two bars in Figure 4.5). The reason could be that some of the NA molecules did not bind to a vesicle and therefore later on occupied binding sites on the secondary antibodies. On the other hand, if only few NA molecules were used, this would enhance the chance of vesicles being coupled together by NA. In other words, the vesicles would bind to a NA already coupled to another vesicle instead of binding to a free NA. Most likely, in the experiments a mixture of the two phenomena occurred. The procedure was improved by first premixing the NA and the secondary antibodies for 10 min, before the vesicles were added for another 10 min prior to injection (see 3rd and 4th double-bars in Figure 4.5). This mixing order turned out to be significantly better than the previously mentioned one. Depending on the ratio of NA and vesicles, the achieved adsorption ranged between 40 % and 85 % of the multi-step injection. The ideal concentration mixture was found to be  $\text{NA}:2^{nd} \text{AB} = 1:1$  (in number of molecules). It is possible that some vesicles were still connected to each other, but this did not interfere with the measurement. As long as the mixing is always done the same way (mixing order, concentration, mixing time), the results are reproducible. Furthermore, this effect would even increase the sensitivity by increasing the attached mass per detected antigen. Control experiments showed that the unspecific adsorption of premixed NA and vesicles directly on the primary antibody and BSA (without secondary antibody) was even smaller than in the normal system including the secondary antibody.

Combining the optimal concentrations and order of mixing, almost the same sensitivity was reached as by the step-by-step assay. Through this change of the protocol we were able to significantly lower the assay time to 30 minutes. Mixing the NA and the vesicles prior to the addition of the secondary antibody resulted in a low signal. Overall, the presented two-step assay could be performed within 30 minutes, whereas most of the time was needed for the antigen incubation. This means that, although higher vesicle

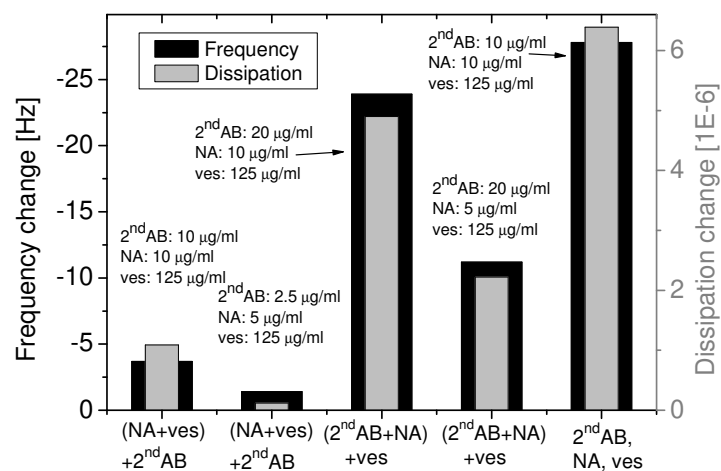


**Figure 4.5:** Frequency and dissipation change upon injection of NA, 2<sup>nd</sup> AB and vesicles as a function of mixing order and concentrations. For the first two measurements (from left to right) prior to injection neutravidin (NA) was first mixed with the vesicles and ten minutes later the secondary antibody (2<sup>nd</sup> AB) was added. In the next two experiments, prior to injection NA and 2<sup>nd</sup> AB were mixed before to the addition of the vesicles. The right bar shows the control where the injection was performed in three individual steps.

concentrations might further decrease the assay time, the limiting factor is already the adsorption of the low abundant antigen.

To further increase the sensitivity, vesicles with a diameter of 400 instead of 100 nm were used. For the step-by-step sensor with the larger vesicles the dissipation was increased up to 20-30 %. When the vesicles were premixed with NA or NA and secondary antibodies, no significant influence of the size was observed.

### 4.3 Polymeric Vesicles for Increased Stability

To increase performance and stability of our biosensor in complex samples, such as blood, the lipid vesicles were replaced by polymeric vesicles, which have a better stability with respect to degradation and against enzymatic attack. Such polymeric nanocontainers were built from the triblock copolymer PMOXA-PDMS-PMOXA.

The performance of the polymeric vesicles was first tested by adsorbing them to NA. Different concentrations were used as shown in Figure 4.6. In the low concentration regime the QCM-D response increased linearly with increasing concentrations; high concentrations were not investigated, because they are not of interest for potential applications. Since there was no unspecific adsorption on a surface coated with antibodies and

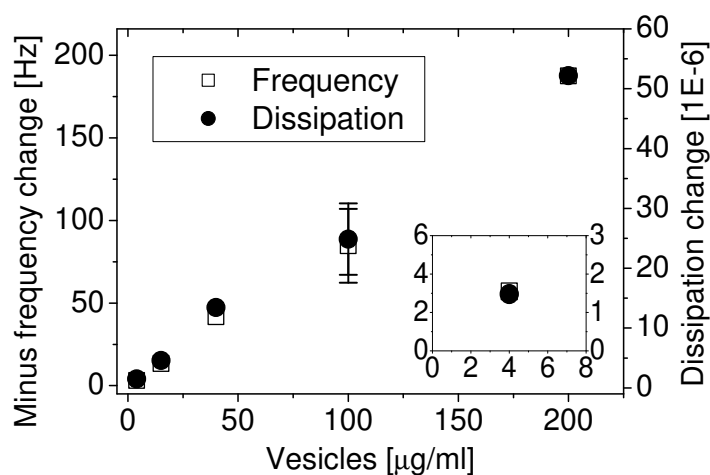


**Figure 4.6:** QCM-D results showing the adsorption of polymeric vesicles on NA as a function of the vesicle concentration.

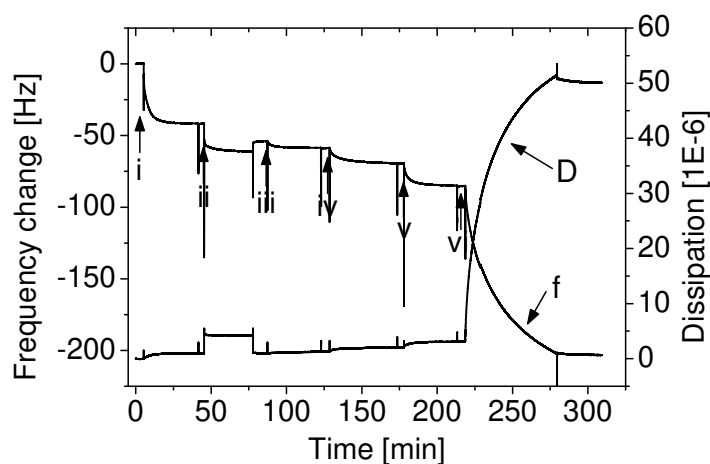


**Figure 4.7:** QCM-D curve showing the buildup of a sandwich based sensor with polymeric vesicles as signal amplification target. i) AB, ii) BSA, iii) AG, iv) 2nd AB (biotinylated), v) NA and vi) biotinylated polymeric vesicles.

blocked with BSA, it is possible to achieve a very low detection limit. From the vesicle size ( $1\ \mu\text{m}$ ), the membrane thickness ( $10\ \text{nm}$ ) and the density ( $1\ \text{g/cm}^3$ ), a vesicle mass of  $3.1 \cdot 10^{-14}\ \text{g}$  was calculated. With the results from Figure 4.6 this results in a sensitivity of  $0.2\ \text{pM}$ .

Then, the polymeric vesicles were integrated into the sandwich sensor with vesicle amplification. The buildup was essentially the same as with lipid vesicles. As it can be seen in the QCM-D adsorption curve in Figure 4.7, the biosensor behaved the same way than with lipid vesicles. The sensor was built in the step-by-step way, with the adsorption steps AB, BSA, AG, 2nd AB (biotinylated), NA and the biotinylated polymeric vesicles.

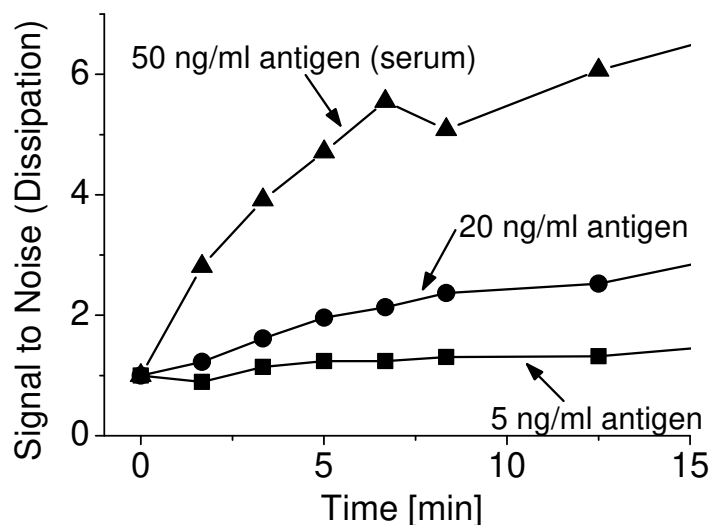


**Figure 4.8:** S/N ratio of vesicle adsorption of polymeric vesicles in a sensor with serum and lipid vesicles in buffer. Note that polymeric vesicles were used for the detection from serum experiment because of their enhanced stability.

The overall sensitivity was also similar when the antigen was detected from serum (see Figure 4.8, serum). Here, a concentration of 50 ng/ml antigen was spiked into 10% serum. Polymeric vesicles were used because of their better stability, i.e. lipid vesicles are easily degraded by the lipase molecules present in serum.

These triblock copolymers show in general very low unspecific adsorption to proteins [146, 221, 222]. In our experiments unspecific adsorption was smaller than the detection limit of the QCM-D.

## 4.4 Conclusion

In this chapter we have described a highly sensitive, *in situ* biosensor. Unlike most existing sandwich assays we used vesicles as a mass and dissipation amplification tool instead of an enzyme-labelled secondary antibody. With lipid vesicles this allowed for detecting antigen concentrations as low as 5 ng/ml or 30 pM, which is sensitive enough to detect e.g. PSA antigens indicating prostate cancer. Compared to other sensors using the QCM technology, we significantly decreased the detection limit by a factor of at least 25. Furthermore, we presented a way to decrease the assay time to about 30 minutes. With the achieved simplicity (easy to use equipment and straight-forward performance), high sensitivity as well as reduced assay time, this type of biosensor has a potential value for

applications in clinical diagnostics. Polymeric vesicles were successfully implemented to enhance the stability of the biosensor. They also showed the potential to further improve the detection limit down to 0.2 pM.



---

## Enzymatic Biosensors with Electrochemical Detection

---

In the first part of this chapter the electrochemical detection methods that have been used in this thesis are evaluated. The two mediators, ferrocyanide and ferrocene, and their reaction schemes are introduced. Solutions containing the species involved in the enzymatic reactions are used to show the principle of the detection methods and the influence of different parameters, such as concentration ratios or scan rates.

A simple model sensor is built to test the enzymatic sensing of adsorbed enzymes, especially in combination with the signal increase when enzymes are coupled to vesicles.

This sensing technique is then combined with the sandwich assay introduced in Chapter 4. For the proof of principle, i.e. to quantify the amount of enzymes bound to the vesicles, the sensor buildup is *in situ* monitored with the QCM-D. Once established, this sensor will allow for electrochemical detection of the antigen concentration independent of the QCM-D.

Finally, experiments are shown where the lipid vesicles are substituted by enzyme containing polymeric vesicles or enzyme functionalized microparticles.

An overview of the different sensor types and the tested electrochemical detection methods is given in Table 5.1.

### 5.1 Mediators and their Detection Principles

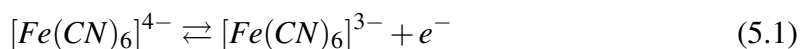
In this section the reaction schemes of the mediators ferrocene and ferrocyanide are introduced. It is shown how they can be used in the measurements of the following sections and what parameters need to be taken into account.

**Table 5.1:** Overview of the different enzymatic sensors and the corresponding electrochemical detection methods.

	FC, hold	FE, CV	FE, hold
Detection principle (GOx in solution)	Section 5.1.1	Section 5.1.2 (1)	Section 5.1.2 (2)
Model assay with NA	Section 5.2.2	Section 5.2.2	Section 5.2.2
Sandwich assay with enzyme functionalized vesicles	Section 5.3.2	Section 5.3.2	
Polymeric vesicles with enzymes	Section 5.3.3		
Microparticles coated with enzymes		Section 5.4	

### 5.1.1 Ferrocyanide

Hexacyanoferrate(II) or ferrocyanide (FC) is available as the salt potassium ferrocyanide  $K_4[Fe(CN)_6]$ . It is water soluble. According to Equation 5.1 it can be oxidized to ferricyanide or hexacyanoferrate(III), whereas the oxidation takes place at 194 mV and the reduction at 110 mV.



In the reaction cycle (see Figure 5.1) glucose reacts with the enzyme GOx, which is reduced during this reaction. Then, in principle the latter should reduce ferricyanide. However, depending on the environment, this reaction is in competition to the reduction of oxygen in the solution. In this case it is converted into  $H_2O_2$ . Independent of the extent of the side reaction, the open circuit potential (OCP) of the system increases through the enzymatic reaction. If we now apply a constant potential (below the oxidation potential of FC) the ferricyanide is constantly reduced to ferrocyanide, which results in a negative current being detected by chronoamperometry. However, the competition of ferrocyanide and oxygen did not allow for the enzymatic readout in CV measurements.

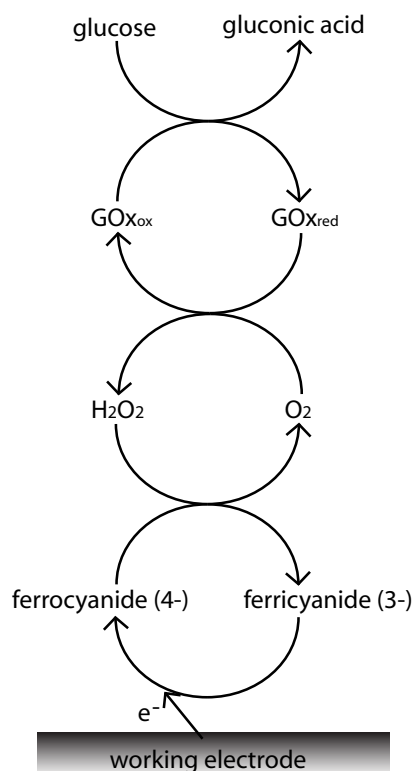
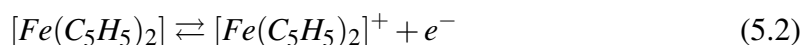


**Figure 5.1:** Possible reaction scheme of ferrocyanide mediated systems. During the reaction with glucose the GOx is reduced, before being oxidized through the reaction with oxygen. The so produced hydrogen peroxide oxidizes the ferrocyanide, which is subsequently reduced at the working electrode.

### 5.1.2 Ferrocene

Ferrocene (FE) is an organometallic compound. As opposed to ferrocyanide it is not soluble in aqueous solutions. Since our experiments are carried out in a water based and ion containing buffer, the water soluble (dimethylaminomethyl)ferrocene was used. The methyl groups slightly shift the oxidation/reduction potential towards the negative or cathodic direction, but for the here presented application this does not interfere with any other reaction, especially not the enzymatic one. The scheme of the enzymatic reaction and the subsequent transport of the produced electrons to the surface via ferrocene is shown in Figure 5.2a. As opposed to ferrocyanide there is no side reaction where oxygen is reduced. The enzyme (GOx) catalyzes the reaction of glucose to gluconic acid, during which it is reduced. In a next step the GOx is oxidized by reducing the ferrocene. The ferrocene itself is oxidized at the working electrode when a potential below its oxidation potential is applied. The reaction of ferrocene is given in Equation 5.2:



A cyclic voltammogram of ferrocene indicating the oxidation and reduction peak is given in Figure 5.2b. The oxidation potential was at 323 mV, the reduction potential at 254 mV. The effect of the enzymatic reaction is illustrated in Figure 5.2c. After adding GOx to the solution the oxidation peak increased, whereas the reduction peak disappeared. Since the enzymatic reaction is constantly reducing the ferrocene, a single molecule can be oxidized more than once during the increase of the potential. While the potential was decreased to 0 mV, the enzymes were also working and quickly reduced the ferrocene before it could be reduced through the applied potential. When less enzymes were present in the solution, the increase of the oxidation peak was only moderate and the reduction peak was smaller but still present. Thus, provided that an excess of glucose is available, the extent of the reduction and oxidation peaks is related to the enzyme concentration. The signal-to-noise (S/N) ratio of such curves is defined as (current with GOx)/(current without GOx) at the maximum potential.

The influence of the scan rate was investigated for constant concentrations of all participating species. We found that the slower the scan rate, the higher the difference between the curves with and without enzymes (i.e. the S/N ratio). This can be explained by the fact that the enzymatic reaction reduces more enzymes per potential cycle when the scan rate is lower, which means, the duration of the individual cycles increased. To obtain the maximal S/N, we went down to 3 mV/s. For higher enzyme concentrations 10 or even 50 mV/s turned out to be sufficient as well. Furthermore, higher scan rates decrease the assay time. Therefore, the scan rate should be chosen as high as possible but as low as necessary.

The other way to influence the generated signal is to adjust the ferrocene concentration. As it can be seen in Figure 5.2c, the enzymes reduce a certain amount of FE. When the overall concentration of the mediator is too high, the fraction of the FE molecules reduced by the enzymes is only small, resulting in a small S/N ratio only. If the mediator concentration is too low, it becomes the limiting step in the reaction scheme because there are simply not enough molecules around to be reduced by the enzymes. Thus, ideally the ferrocene concentration is chosen such that it is as low as possible but still allows for a small reduction peak. Like that, the enzyme concentration resulting in a linear response can be adapted individually.

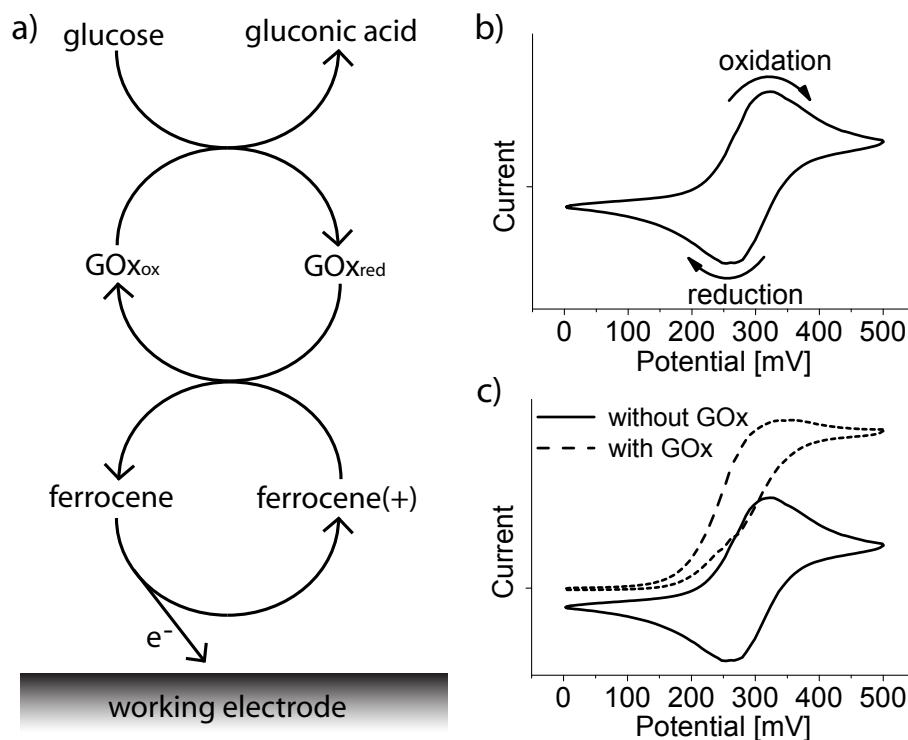


**Figure 5.2:** Reaction scheme of ferrocene. a) GOx is reduced during the reaction with glucose. Then, the reduced GOx is oxidized by reducing the positively charged ferrocene. The ferrocene itself gives electrons to the working electrode. b) Cyclic voltammogram of ferrocene with the oxidation and reduction peak around 320 and 260 mV, respectively. c) Cyclic voltammogram of the reaction cycle depicted in a). The ferrocene is constantly reduced by the enzymatic reaction, which results in a higher oxidation and a lower reduction current.

Like with the ferrocyanide, with the ferrocene it is also possible to perform chronoamperometry. According to the reaction cycle (see Figure 5.2) the ferrocene is reduced by the enzymatic reaction. Therefore, in order to oxidize the reduced ferrocene, a potential above the oxidation peak needs to be applied. Like this, the ferrocene reduced during the enzymatic reaction is constantly oxidized by the applied potential. The oxidation current is proportional to the amount of enzymes. An example of such a curve, where the potential was kept at 500 mV, is given in Figure 5.3. The measurement was started with a buffer rinse (1). At (2) a mixture of 0.5 mM FE and 200 mM GO was injected. Because of the applied potential the FE is oxidized, resulting in a higher current than before. For both injections, (1) and (2), there is a current peak with a fast decay. During the first few milliseconds the current comes from charging the electric double-layer on the electrode surface. This regime then passes into the diffusion controlled reaction with

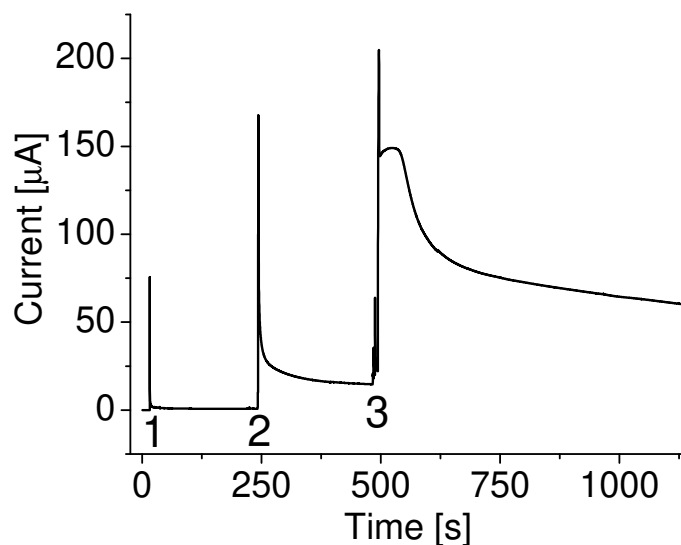


**Figure 5.3:** Chronoamperometry measurement of an FE mediated enzymatic reaction. The applied potential was 500 mV. 1) Buffer rinse, 2) 0.5 mM FE and 200 mM GO, 3) 0.5 mM FE, 200 mM GO and 10  $\mu\text{g/ml}$  GOx. The reducing effect of the enzymatic reaction on the FE induced a positive oxidation current.

the current density proportional to  $t^{-0.5}$  ( $t = \text{time}$ ).<sup>1</sup> Finally, FE and GO were injected at the same concentrations, with additionally 10  $\mu\text{g/ml}$  GOx (3). Upon injection of this mixture, the current significantly increased as a result of the enzymatic reaction.

<sup>1</sup>This equation follows from the Fick's laws and the Nernst Equation. Details of the derivation can be found in [223].

## 5.2 Enzyme Functionalized Vesicles for Signal Amplification

In this section, enzyme functionalized vesicles are used to generate electrical signals in a model biosensing assay. Lipid vesicles, functionalized with enzymes and carrying biotin ligands, were specifically adsorbed to neutravidin (NA) coated surfaces. For this setup, it is first shown how the ideal BSA blocking concentration was determined. The sensitivity of the sensor with enzyme functionalized vesicles as amplification objects is then compared to the direct adsorption of biotinylated GOx to NA. Two mediator systems, ferrocyanide and ferrocene, were applied and compared.

### 5.2.1 Vesicle Adsorption

In order to be able to detect enzyme functionalized vesicles, we first built a simple model system. Therefore, the enzyme loaded, biotinylated vesicles were bound to NA as described in Section 3.2.4.

To find the detection limit of NA (molarity) that can still be detected, different NA concentrations were adsorbed to the gold surface. The adsorption was monitored by QCM-D as shown in Figure 5.4. Subsequently, BSA (10 mg/ml) was adsorbed to inhibit unspecific adsorption of the vesicles. With a higher surface coverage of the NA, the BSA adsorption decreased. Interestingly, the total adsorption reached a minimum at 5  $\mu\text{g/ml}$  NA. Because NA is a soft protein, it is likely that it undergoes slight conformational changes upon adsorption even on a hydrophilic surface. Like this it will proportionally occupy more surface area and therefore decrease the BSA adsorption. In a last step, the biotinylated, enzyme functionalized vesicles were injected. However, when adsorbing low concentrations of NA, e.g. 1  $\mu\text{g/ml}$ , and blocking against unspecific adsorption with BSA we observed that there was no vesicle adsorption. On the other hand, the BSA is really required to inhibit unspecific vesicle binding.

To overcome this issue, we first need to know the reason for this behaviour. When BSA is abundant at a high concentration, a high number of molecules reaches the surface at once. This means, there is no room for relaxation and many of these molecules are in their native conformation. In case of a lower BSA concentration, first few molecules reach the surface. Because BSA is a soft protein, it is partially denaturing upon contact with

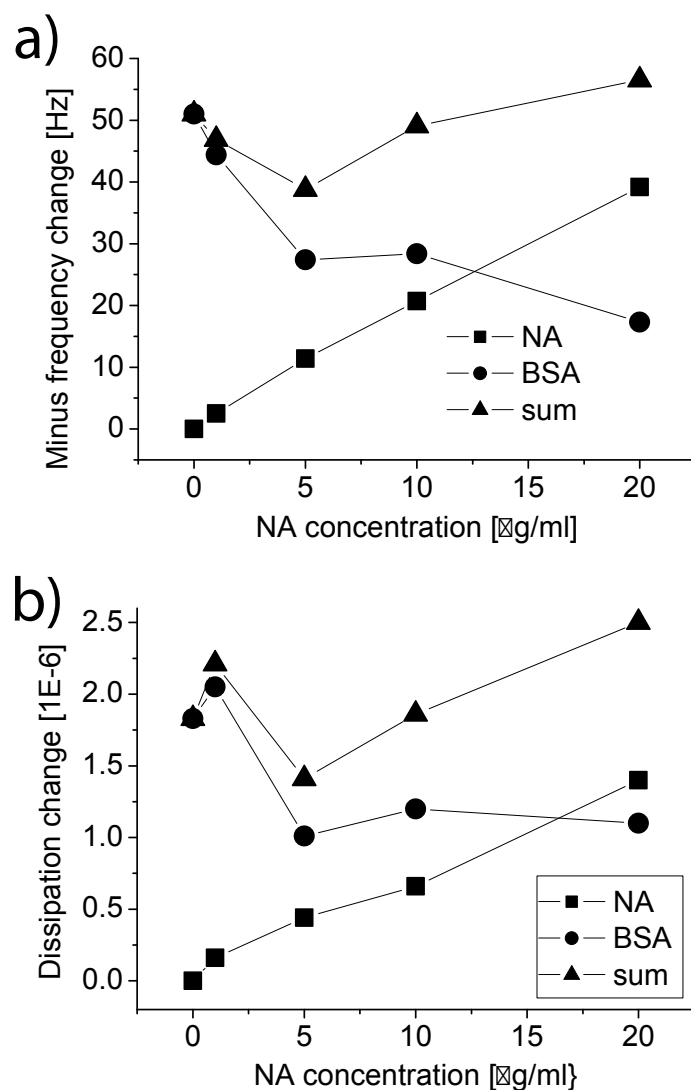


**Figure 5.4:** Adsorption of NA and subsequent blocking with BSA. a) Shows the absolute frequency change, b) the dissipation change upon adsorption of NA, BSA and the total protein adsorption (sum of NA and BSA).

the surface if there is enough time and room for relaxation. Since BSA is known to form only monolayers, this means, fewer molecules adsorb, but the film is more flat. With a flat BSA film around the NA the biotin on the vesicles can easily reach the binding pocket of the NA. However, if the BSA molecules are mainly in their native conformation, flat NAs - adsorbed from low NA concentrations - are not accessible for the biotin any more because the binding pocket of the NA molecules is 0.9 nm deep (see Figure 5.5) [224]. Another reason why the vesicles did not bind could be that the few NA molecules were exchanged by BSA when the latter was injected at a high concentration.



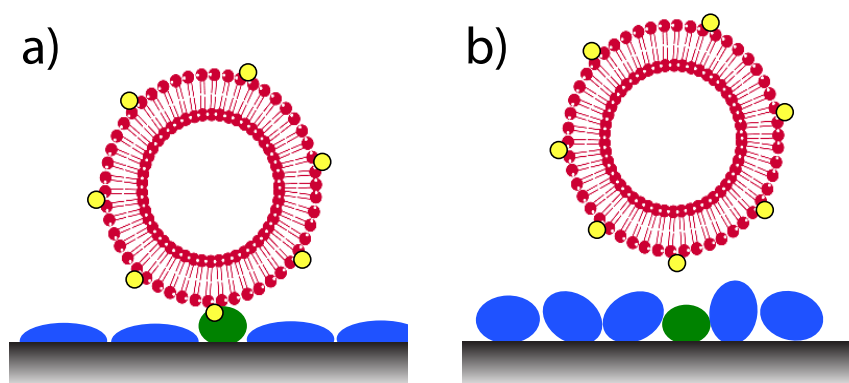


**Figure 5.5:** Scheme of the vesicle adsorption on a surface functionalized with NA and blocked with a) a low and b) a high BSA concentration.

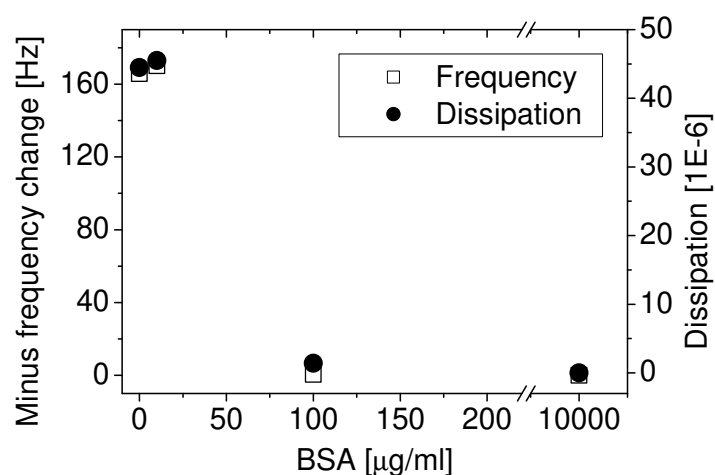


**Figure 5.6:** Unspecific adsorption of liposomes to a BSA coated gold surface. Minus frequency and dissipation changes are shown as a function of the BSA concentration. About  $100 \mu\text{g/ml}$  was required to prevent unspecific vesicle adsorption.

To find the BSA concentration needed to inhibit unspecific adsorption of the vesicles, different concentrations of BSA were adsorbed, followed by the addition of biotinylated vesicles. In this case no NA was involved. As it can be seen in Figure 5.6,  $100 \mu\text{g/ml}$  BSA was sufficient to prevent unspecific vesicle adsorption.

In order to find the highest possible BSA concentration that still allows specific vesicle adsorption, an assay with  $1 \mu\text{g/ml}$  NA was built. The effect on the vesicle binding as a function of BSA concentration is illustrated in Figure 5.7. The tested BSA concentrations were  $100 \mu\text{g/ml}$  and higher. However, as soon as the BSA concentration was significantly higher, there was almost no vesicle adsorption observed. As such, we concluded

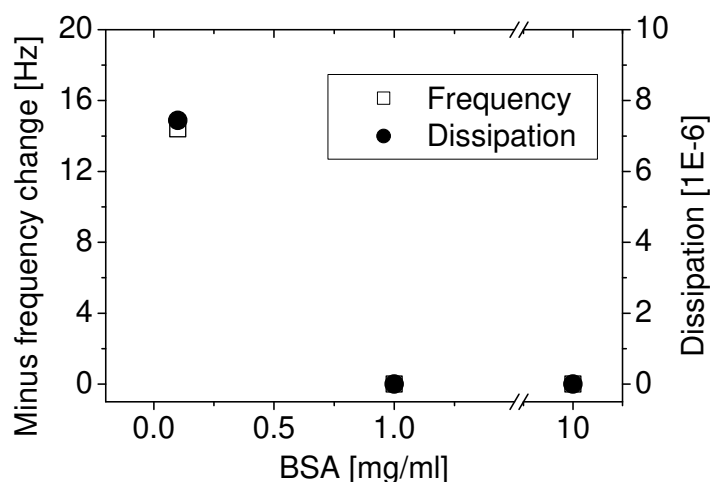


**Figure 5.7:** Adsorption of liposomes to a NA functionalized gold surface blocked with BSA. Minus frequency and dissipation changes are shown as a function of the BSA concentration. BSA concentrations of more than 100  $\mu\text{g/ml}$  inhibited the specific vesicle binding.

that a BSA concentration of 100  $\mu\text{g/ml}$ , sufficiently inhibits the nonspecific binding of biotinylated vesicles to NA, while still allowing specific vesicle binding.

What exactly is happening on the surface when high BSA concentrations are adsorbed is further investigated by Andreas Binkert. For this thesis here, it is sufficient to know the BSA concentration that is required to inhibit unspecific adsorption but still allows the biotinylated vesicles to bind to the NA.

So far it has only been described how the biotinylated vesicles adsorbed to NA. But for the EC measurements they need to be functionalized with enzymes prior to adsorption. Because the enzymes are coupled to the vesicles via biotin-NA, it is not possible to adsorb the vesicles before functionalizing them, especially when a high NA- and a low vesicle concentration is used. In this case, there would be unspecific adsorption of the enzymes on non-occupied NA's on the surface. For the experiments described in this section, NA and GOx molecules were premixed in a 1:1 ratio (number of molecules). Assuming that the vesicles consist of one lipid bilayer, 500 NA/GOx complexes per vesicle will be available. However, since vesicles of this size are multilamellar, the number of vesicles is lower and thus, more than 500 enzymes per vesicle; in case of four bilayers, it would already be 2'000, for eight bilayers 4'000. More than eight bilayers are unlikely, since the threshold between mono- and multilamellar vesicles is around 200 nm diameter [225]. On the other hand, 400 nm lipid vesicles with 1% biotinylated lipids have around 4'000 biotins on their surface, corresponding to the number of available enzymes in case of eight lipid bilayers. The GOx molecules have dimensions of 7.0 x 5.5 x 8.0 nm [226]. Thus, if they were

densely packed on the vesicle surface, around 8'000 would sterically fit. Because this is very unlikely, 4'000 binding points are sufficient. In fact, because the NA and the GOx/b are premixed, it is likely that few NA bind to more than one enzyme, which inhibits them from binding to a vesicle. If the vesicles are completely covered with GOx/NA complexes, due to steric hindrance of the biotin on the vesicles, they will not be able to bind to NA immobilized on a surface. However, it is possible that biotins on the enzymes, bound to the vesicle, bind to the surface immobilized NA.

### 5.2.2 Evaluation of Electrochemical Detection Schemes

Here the EC-signals of the different detection methods (as described in Section 5.1) are compared. Thereby, the focus is on the signal amplification factor through the vesicles as well as on the detection limit.

For all these experiments 400 nm vesicles were used. To estimate the signal amplification factor of the enzyme functionalized vesicles, their signal was compared to GOx/b molecules directly adsorbed to a surface saturated with NA (20  $\mu\text{g/ml}$ ). Because NA and the enzymes have about the same size, most of the NA on the surface will bind to a GOx/b from the supernatant. The vesicles on the other hand are much larger; because of steric hindrance only few of the surface immobilized NA can bind to a vesicle. Overall, one vesicle occupies the area of 1'000-2'000 enzymes (both assumed to be densely packed), which allows for calculating the vesicle induced signal increase.

#### Ferrocene: Cyclic Voltammetry

In this section CV's of ferrocene based biosensors are presented. First, the amplification of enzyme functionalized vesicles is compared to GOx/b directly adsorbed to NA. Then, the parameters of the vesicle sensor are adjusted to obtain the optimal detection limit of the sensor.

A comparison between individually immobilized GOx molecules and enzyme functionalized vesicles is given in Figure 5.8. For both systems the saturating NA concentration of 20  $\mu\text{g/ml}$  NA was adsorbed first, followed by the biotinylated GOx or the enzyme functionalized biotin vesicles. The graphs in Figure 5.8 were obtained from CV with 0.1 mM FE and a scan rate of 3 mV/s. The green curve indicates the CV of a system without GOx, the so called background current from CV of FE. The black and the red

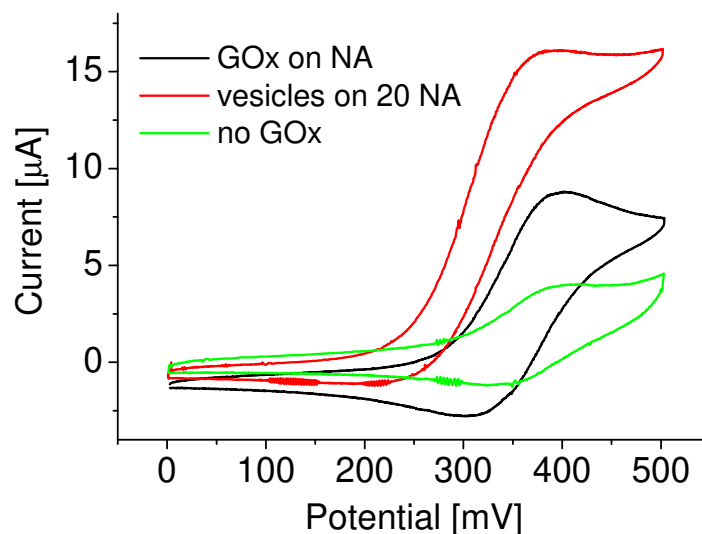


**Figure 5.8:** CV with a scan rate of 3 mV/s and an FE concentration of 0.1 mM. The signals from GOx on NA, GOx on vesicles and no GOx are compared.

curve were measured with only enzymes and enzymes on vesicles, respectively. The signal from the vesicles was around 3.5 times the signal from the GOx. To quantify this result, we assumed the vesicles to be densely packed (hexagonal) on the surface. In this case, their surface is 3.6 times the surface of the sensor itself. Subsequently, the signal from the vesicles is expected to be 3.6 times higher. The correspondence of the calculated and the measured values indicates that the vesicle surfaces were almost fully covered with NA, without inhibiting the vesicles from specifically binding to surface immobilized NA.

The signal of a single vesicle thus corresponds to that of around 3'500 directly immobilized enzymes, but the binding of a vesicle can be connected to a single recognition event on the surface. As such, we can expect a similar signal amplification factor for low abundant analytes with the vesicle system. This signal amplification also corresponds to the above calculated number of enzymes per vesicle (see Section 5.2.1). The fact that it is in the upper range of the calculated value supports the model of the multilamellar vesicles.

After calculating that the signal enhancement through enzyme functionalized vesicles should be at least three orders of magnitude, we now focus on lower concentrations and how the ferrocene concentration can be optimized in order to minimize the detection limit.

To find the detection limit, NA was used as an analyte. Accordingly, it was adsorbed to the surface in different concentrations. To inhibit unspecific vesicle adsorption, the remaining free surface was blocked with BSA (0.1 mg/ml). As described in Section 5.1.2

the sensors are in general more sensitive, when lower FE concentrations are used. In Figure 5.9 300  $\mu\text{M}$  and 30  $\mu\text{M}$  FE are compared. In Figure 5.9a (300  $\mu\text{M}$ ) the main contribution to the current came from the FE itself. During the CV, only a small fraction of the FE was converted by the enzymatic reaction. Thus, the FE concentration was reduced to 30  $\mu\text{M}$  (see Figure 5.9b). Since the overall current was lower, the percentage of the enzyme induced current was accordingly higher. This way it was possible to clearly detect 300 ng/ml NA without flow. Additionally, an experiment where the NA was not injected in a single shot but continuously let flow through the flowcell, was performed. The flow rate was 40  $\mu\text{l}/\text{min}$ , which corresponds to the volume of the flow-chamber. Thus, the NA solution was exchanged 60 times during the one hour of applied flow. The rather high flow-rate was chosen because the NA adsorbs quite fast; but of course this treatment did not enhance the signal by a factor of 60, because not all NA molecules were able to adsorb during one minute. As it can be seen from Figure 5.9b (300 ng/ml NA with and without flow), this procedure significantly improved the performance of the sensor at low concentrations, i.e. it was four times more sensitive. With flow the detection limit is 100 ng/ml.

Because the applied FE concentrations did not lead to saturation (i.e. there were still reduction peaks), we further reduced the FE concentration with the aim to lower the detection limit of the sensor when having less "background" current from the CV of the FE itself. 10  $\mu\text{M}$  and 20  $\mu\text{M}$  FE were used; the corresponding curves are shown in Figure 5.10. However, in both cases, especially in Figure 5.10a with the lower concentration, the typical CV of FE is hardly visible. Only the 1  $\mu\text{g}/\text{ml}$  concentration gave a small signal in Figure 5.10b (20  $\mu\text{M}$  FE). At such low concentrations, the current of the FE is obviously not dominant any more. In fact, the background current from CV on the bare system (electrode, buffer, etc.) becomes comparably too high. Therefore, the FC signal is not pronounced any more. And since only very few FE ions are abundant, only a small enzymatic signal can be generated.

To conclude, the detection limit of FE based sensors when applying CV is around 100 ng/ml NA, which corresponds to 1.7 nM. To further lower the detection limit, a basic system with less background current during CV would need to be developed.

### **Ferrocene: Chronoamperometry**

As described in Section 5.1.2, ferrocene cannot exclusively be used for CV, but also for chronoamperometry. An example of the signal from enzyme functionalized vesicles is

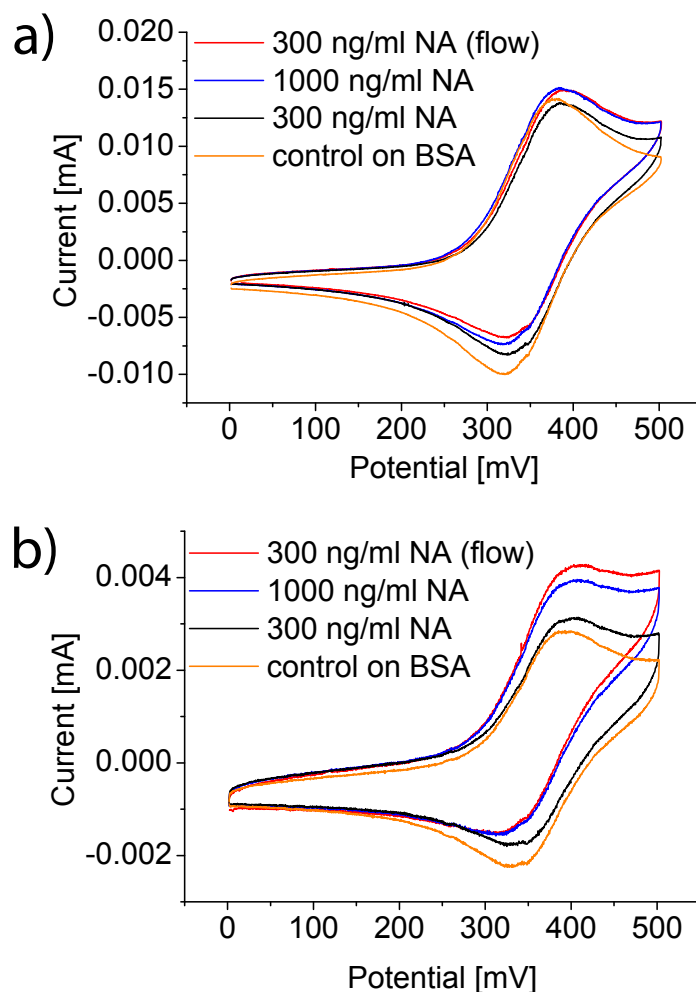


**Figure 5.9:** CV on enzyme-labelled vesicles adsorbed to different NA concentrations. The ferrocene concentration was a) 300  $\mu\text{M}$  and b) 30  $\mu\text{M}$ .

given in Figure 5.11, where the GOx functionalized vesicles adsorbed to surfaces pretreated with different NA concentrations are compared to an empty surface. The black curve represents vesicles adsorbed to a surface saturated with NA (20  $\mu\text{g/ml}$ ), the red curve was obtained from vesicles on 5  $\mu\text{g/ml}$  NA and the blue curve shows the background signal from only GO and FE without any enzymes. In all cases a potential of 500 mV was applied.

This example nicely demonstrates how the principle of chronoamperometry works in a sensor with enzyme functionalized vesicles. However, as can be seen from these curves with high analyte concentrations, this approach is not sensitive enough for possible applications. Compared to the signal, the background is too high. Even at a fairly high, 5  $\mu\text{g/ml}$ , NA concentration the S/N ratio is only around two.

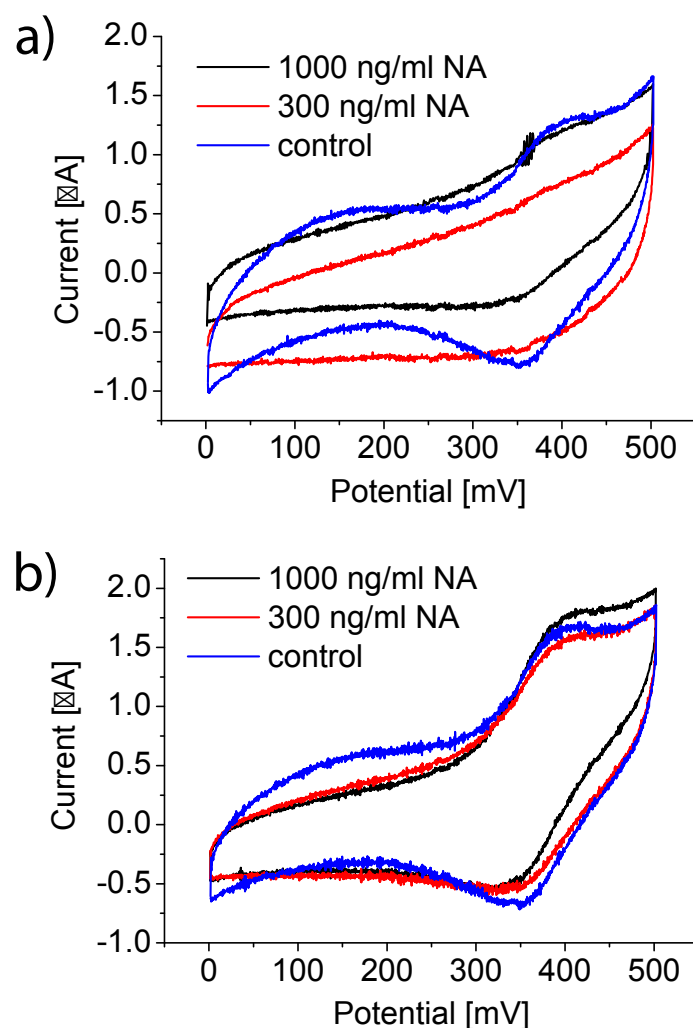


**Figure 5.10:** CV on enzyme-labelled vesicles adsorbed to different NA concentrations. The ferrocene concentration was a)  $10 \mu\text{M}$  and b)  $20 \mu\text{M}$ .

### Ferrocyanide: Chronoamperometry

Here, the evaluation of the detection limit of a ferrocyanide mediated sensor in the chronoamperometry mode is described. Different vesicle concentrations were adsorbed to NA functionalized surfaces. The vesicles were functionalized with enzymes prior to the adsorption.

In the example presented in Figures 5.12-5.14 the vesicles were adsorbed for 10 min only. The concentration dependence of their adsorption to NA is shown in Figure 5.12. The adsorbed amount increased linearly with an increasing concentration. The vesicles were enzyme functionalized as described in Section 3.2.4. In chronoamperometry experiments (see Figure 5.13) a FC concentration of 1 mM was used. The potential was kept

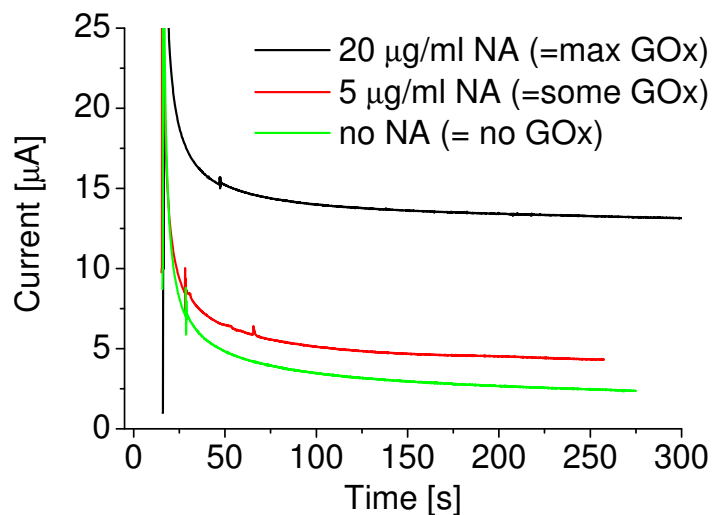


**Figure 5.11:** Chronoamperometry on enzyme-labelled vesicles adsorbed to different NA concentrations. GOx functionalized vesicles were adsorbed to a surface pre-treated with 20 µg/ml (black curve) and 5 µg/ml (red curve) NA. The green curve represents the control experiment without GOx. A potential of 500 mV was applied.

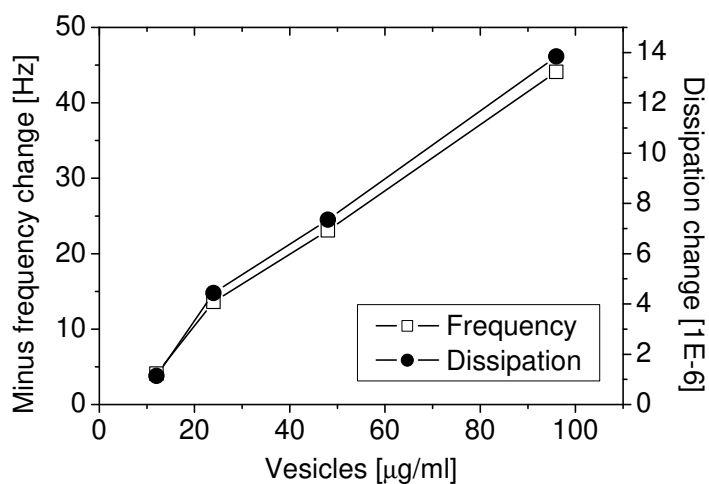


**Figure 5.12:** Frequency and dissipation changes of different vesicle concentrations on NA (20 µg/ml). The vesicles adsorbed for 10 minutes.



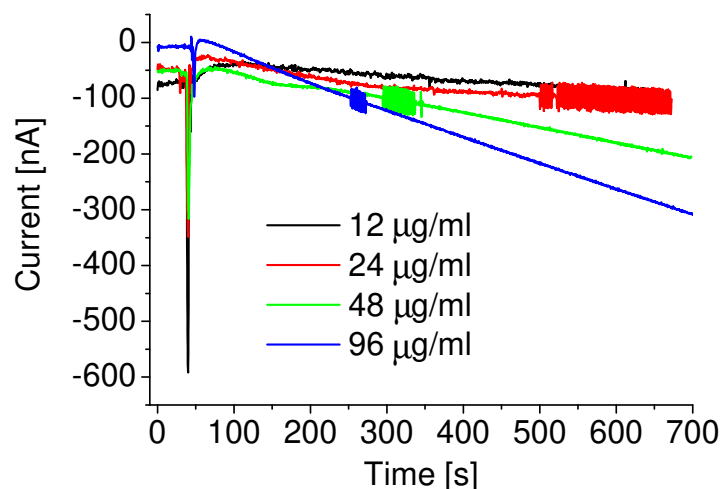


**Figure 5.13:** Chronoamperometry measurements with different vesicle concentrations. More enzyme functionalized vesicles led to a steeper slope. FC was used at a concentration of 1 mM. The observed large noise on some of the curves is an artefact of the instrument.

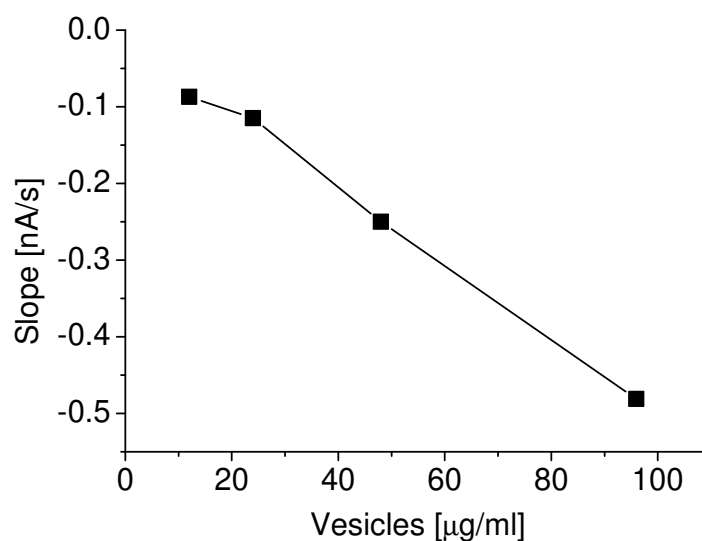


**Figure 5.14:** Slope during chronoamperometry measurement with 1 mM FC as a function of the vesicles concentration. Samples without GOx have a slope of 0.

constant at 0 mV; after one minute the GO/FC mixture was injected. The slope was determined from 1 until 10 minutes after the injection as shown in Figure 5.14. A higher vesicle (enzyme) concentration resulted in a steeper slope.

To estimate the minimum amounts of enzyme functionalized vesicles that are measurable with chronoamperometry, the connection between weight and molarity of the vesicles (400 nm) was calculated:

$$\text{Vesicle surface} = 4\pi \cdot r^2 = 5 \cdot 10^{-9} \text{cm}^2 \quad (5.1)$$

$$\text{Weight per vesicle} = 500 \text{ng/cm}^2 \cdot 5 \cdot 10^{-9} \text{cm}^2 = 2.5 \cdot 10^{-6} \text{ng} \quad (5.2)$$

$$\Rightarrow 12 \mu\text{g/ml} = 8 \text{pM} \quad (5.3)$$

These calculations, for 400 nm sized vesicles, are based on monolamellar vesicles (weight of bilayer 500 ng/cm<sup>2</sup> [227]). When the vesicles are extruded through 400 nm pores, their final size is slightly higher, since they are flexible and therefore deformed when squeezed through the pores. 450 nm final size would already improve the detection limit by about 10 %. Furthermore, in reality the vesicles are multilamellar. For bilamellar vesicles the detection limit would be half the estimated concentration, for trilamellar vesicles one third, etc. Thus, the detection limit is not 8 pM (as in the calculations above), but around 1-2 pM. This detection method is expected to be even more sensitive than the sensor with vesicles for mass amplification without enzymes.

## 5.3 Sandwich Assays with Enzymatic Detection

In Chapter 4 a sandwich based biosensor with vesicles for signal amplification was used. In order to use this sensor independent of the QCM-D in an array, GOx was introduced to the biosensor allowing for the electrochemical detection of antigens. First, the required modifications on the sensor are introduced, followed by EC measurements. Based on the sensitivity evaluation described in the previous section, in this section only chronoamperometry with ferrocyanide and CV with ferrocene were performed. Finally, in order to have a system that is stable for more than two weeks, polymeric instead of lipid vesicles were used.

### 5.3.1 Surface Modification

The buildup of the sandwich assay for enzymatic detection was similar to the biosensor with vesicles for mass amplification (Chapter 4). Additionally, GOx/b was bound to the vesicles via NA (see scheme in Figure 3.6). This extension was either performed step-by-step or with premixing the components. In case of the latter, first the NA and the GOx/b were mixed for 10 minutes, then the vesicles were added for another 10 minutes, before finally injecting the complexes. An example of a step-by-step injection is given in Figure 5.15. Injection steps i to vi represent the buildup of the mass amplification based vesicle sensor. In steps vii and viii NA and the biotinylated GOx were injected, respectively. In this example the maximum AG concentration ( $20\mu\text{g/ml}$ ) was used. Control experiments without the NA step showed that GOx/b did not adsorb unspecifically.

### 5.3.2 Enzymatic Detection

#### CV with Ferrocene

The EC-performance of the sensors, built up as shown above in Figure 5.15, was tested using CV with FE as a mediator. FE concentrations of 0.03 and 0.1 mM were combined with scan rates of 3 and 10 mV/s. The scans with 10 mV/s, especially in combination with 0.1 mM FE, were clearly less sensitive than the ones with 3 mV/s. Therefore, only the experiments where a scan rate of 3 mV/s was applied are further discussed here. Different sets of CV curves with FE concentrations of 0.03 and 0.1 mM are compared in

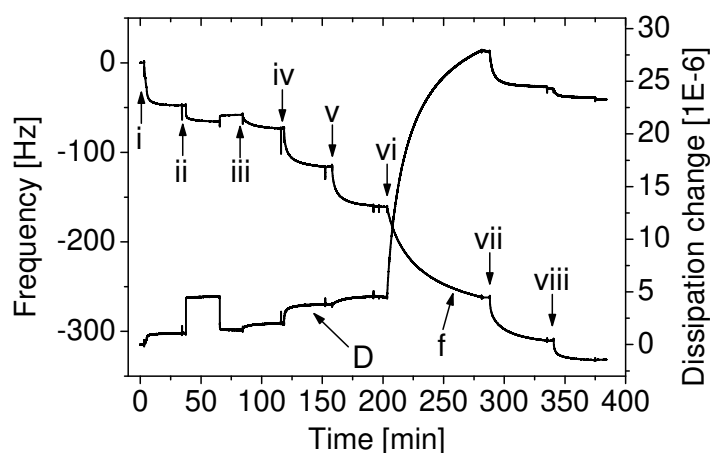


**Figure 5.15:** QCM-D adsorption curve of the sandwich-based enzymatic sensor: i) AB, ii) BSA, iii) AG, iv) 2nd AB (biotinylated), v) NA, vi) vesicles (biotinylated), vii) NA and viii) GOx/biotin.

Figure 5.16a and Figure 5.16b, respectively. With 0.03 mM FE a S/N ratio of around 3.0 was obtained (definition see Section 5.1.2), while it was around 2.5 for 0.1 mM FE. When NA, GOx/b and the vesicles were premixed prior to injection, the signal was slightly lower than for the step-by-step adsorption. The reason therefore is assumed to be that some of the NA bound to several GOx/b during the premixing and cannot bind to vesicles any more. On the other hand, too many GOx/b-NA complexes on the vesicle surface would not allow them to bind to the NA on the surface any more (compare also Section 5.2.1). To conclude, also for the enzyme based sandwich assay, for CV 0.03 mM FE and 3 mV/s turned out to be the parameters with which the highest sensitivity could be achieved within a reasonable detection time. CV measurements with FE did not reach a detection limit in the regime of most cancer antigens with the model sensor in Section 5.2.2. Thus, the here presented experiments only show the feasibility of this method in combination with a sandwich assay, but no detection limit was evaluated.

### Chronoamperometry with Ferrocyanide

Sandwich assays with enzyme functionalized vesicles were also performed in the chronoamperometry mode with ferrocyanide. In these assays with premixed reagents (NA, GOx/b and biotinylated vesicles) different antigen concentrations were used. The negative slope of the current during chronoamperometry as a function of the antigen concentration is given in Figure 5.17. For low antigen concentrations the signal increased linearly, before it levelled off at higher antigen concentrations, because of steric hindrance

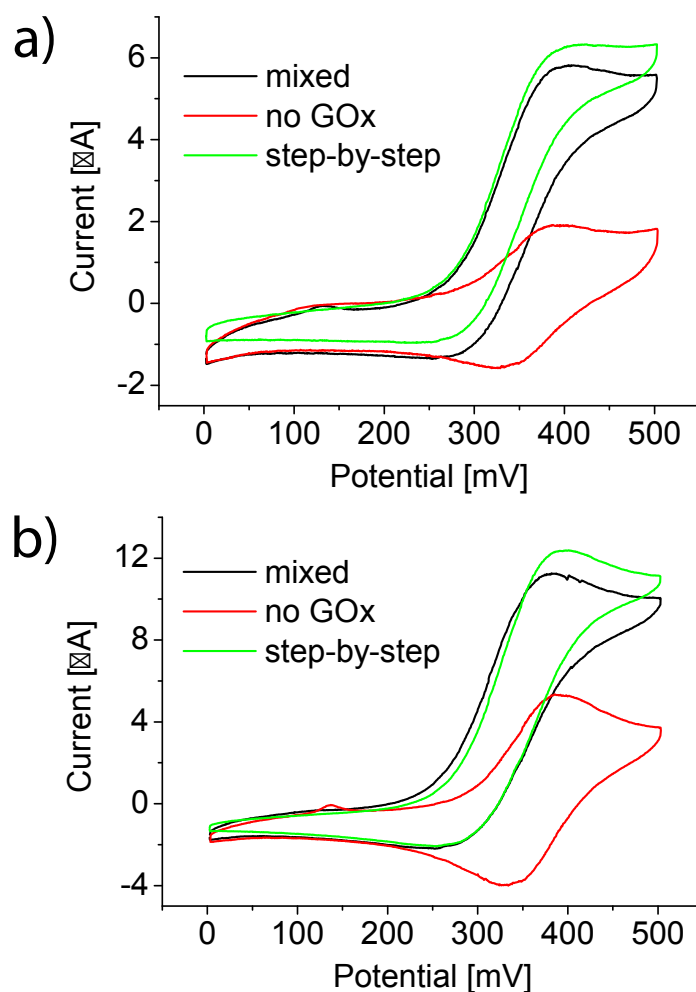


**Figure 5.16:** CV of GOx-functionalized vesicles in the sandwich sensor with a) 0.03 mM FE and b) 0.1 mM FE. The red curves represent a sensor without GOx, the black curves a sensor where NA, GOx/b and the vesicles were premixed and the green curves where the three species were adsorbed individually. The scan rate was 3 mV/s for all these measurements.

of the vesicles. This finding corresponds to the results from the sensor with vesicles for the mass amplification in Chapter 4. Because of the same amplification scheme, for an antibody-antigen system with low unspecific adsorption the detection limit corresponds to the one determined when the vesicles were directly adsorbed to NA (see Section 5.2.2). But when a whole sandwich assay is constructed, there are of course more influencing factors, such as unspecific adsorption of certain species. The lowest antigen concentration measured (except from no antigens) was 200 ng/ml, corresponding to 1.25 nM. However, from the linearity in the graph for low antigen concentrations and from the signal without enzymes, the detection limit is expected to be clearly lower than that.

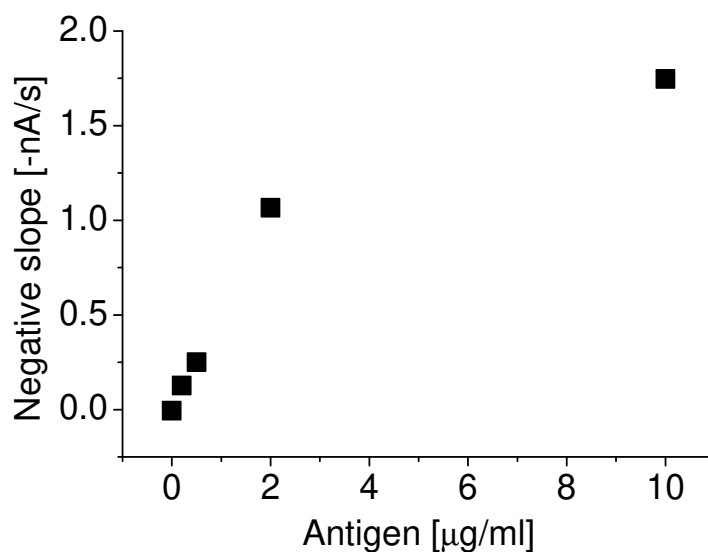


**Figure 5.17:** Chronoamperometry of GOx-functionalized lipidic vesicles in the sandwich assay: slope as a function of the antigen concentration.

### 5.3.3 Polymeric Vesicles for Increased Stability

To increase the lifetime of the enzymatic biosensor, the lipid vesicles were replaced by polymeric vesicles, which have a better stability against enzymatic attack and longer shelf-life stability. In this case we have incorporated the GOx inside the vesicles. OmpF pores (see Section 3.1.2) in the membrane make sure that the molecules contributing to the enzymatic reaction can diffuse through the membrane.

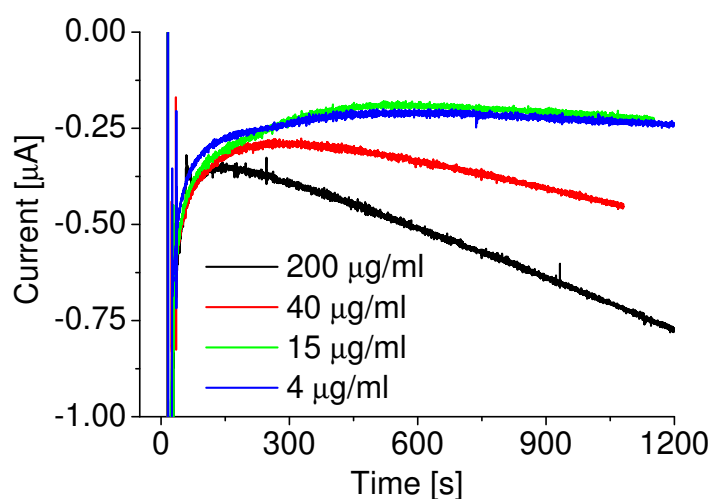


**Figure 5.18:** Chronoamperometry of different vesicle concentrations (polymeric vesicles) on NA. The electrode was kept at 0 V.

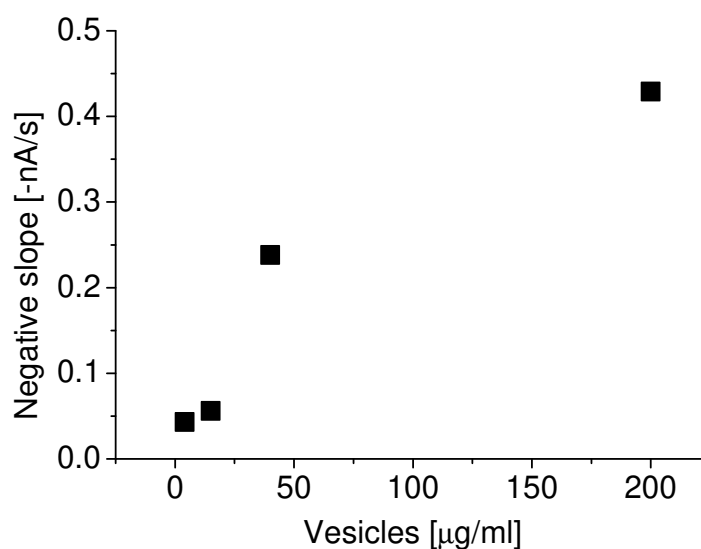


**Figure 5.19:** Negative slope of the chronoamperometry curves shown in Figure 5.18. The slope is taken from the linear part of the curves.

The performance of the polymeric vesicles was first tested by adsorbing them to NA, as described in Section 4.3. With this sensor setup, chronoamperometry with FC as a mediator was performed. The current as a function of time when a potential of 0 mV was applied is shown in Figure 5.18. The values of the slope, whereas a steeper slope corresponds to a higher number of active enzymes (compare also Section 5.1.1), are summarized in Figure 5.19. More enzyme functionalized vesicles resulted in a steeper slope, which indicated a higher number active enzymes.

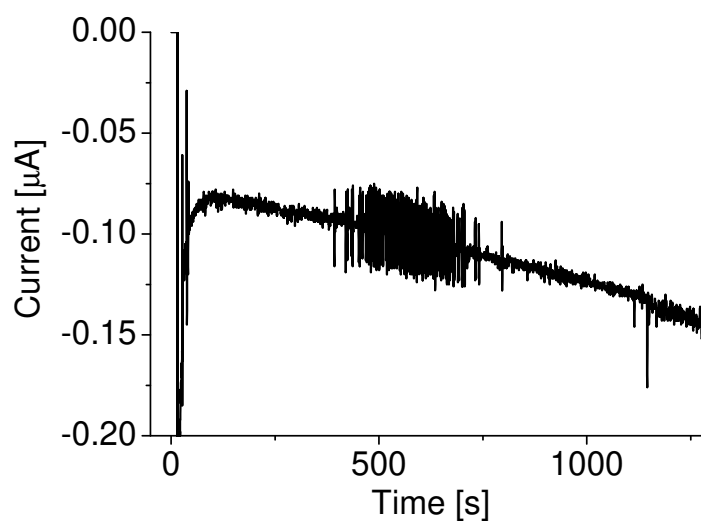


**Figure 5.20:** Chronoamperometry on a sandwich assay with polymeric vesicles containing GOx. A potential of 0 V was applied.

After successfully testing the electrochemical performance of the polymeric vesicles on NA, they were implemented into the sandwich assay. The sensor buildup was according to the experiments described in Section 4.3. The EC behaviour was evaluated by chronoamperometry with FC, as shown in a feasibility example in Figure 5.20. This clearly illustrates the potential of the polymeric vesicles in our sandwich assay with multiple enzymatic signal amplification.



## 5.4 Particles as Enzyme Carriers

Another approach to increase the number of enzymes coupled to a single recognition event is described in this section. Here, we used PS particles coated with enzymes. In these feasibility experiments the PS particles were coated with the biotinylated polymer PLL-*g*-PEG/biotin.

First, the adsorption performance of the polymer to PS particles was tested with the fluorescent PLL-*g*-PEG-TRITC (see schematics in Figure 5.21a). On the lower right in Figure 5.21 two particles were exposed to bleaching. It is clearly visible that the red colour disappeared. The green autofluorescence and a minor red autofluorescence still represented the PS core. Based on this, we can assume that PLL-*g*-PEG/biotin will coat the particles similarly.

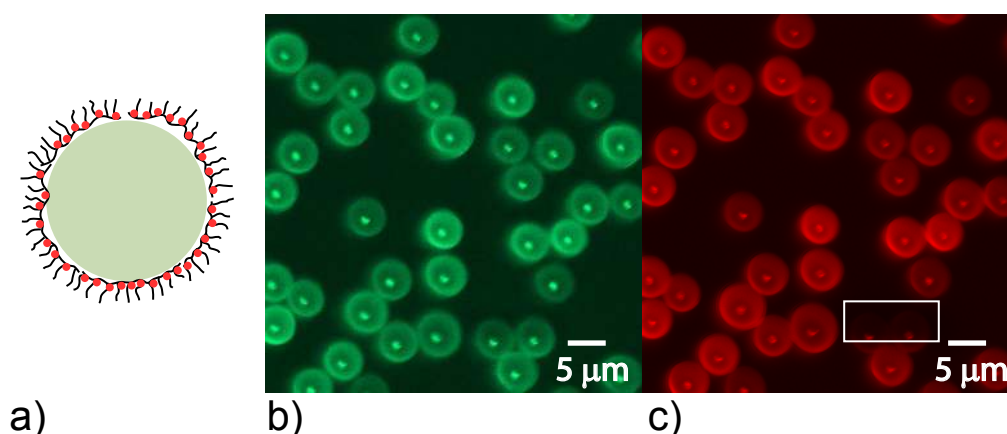


**Figure 5.21:** PS particles coated with the red fluorescent polymer PLL-*g*-PEG-TRITC. a) Scheme of the particle; b) autofluorescence of the particles at 488 nm excitation; c) fluorescence from the coating at 561 nm. Note the two photobleached particles in the bottom right of the image (white box).

The subsequent functionalization with GOx/b was performed the same way as with lipid vesicles (see Section 3.2.4). Then, particles coated with PLL-*g*-PEG/biotin and functionalized with GOx/b were injected into a flowcell with NA (saturated) on the substrate. The particles settled down and bound for about 10 min prior to rinsing. The particle density was 1079 particles per mm<sup>2</sup> after binding and 1065 particles per mm<sup>2</sup> after subsequent rinsing (see Figure 5.22). On the other hand, without this NA-biotin binding system the particles were rinsed off completely. This indicates that the particles really bound to the NA. In the shown example the density of the particles on the surface was limited by the particle concentration in the injected solution.

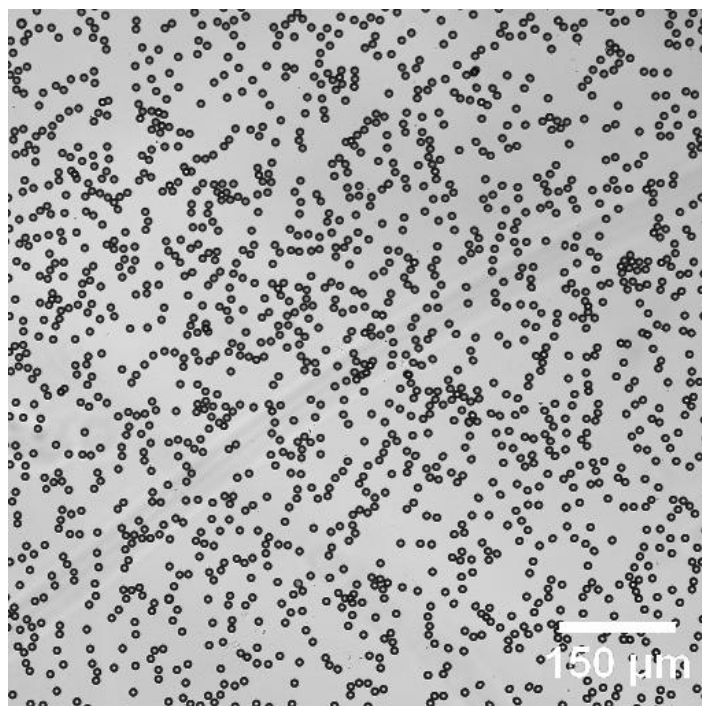


**Figure 5.22:** For the CV scan in Figure 5.23 a density of 1079 particles/mm<sup>2</sup> was reached after injection and 1065 particles/mm<sup>2</sup> after rinsing.

Finally, buffer with 200 mM glucose and 0.1 mM FE was injected to perform CV. A scan before the injection is compared to a scan after the binding of GOx functionalized particles in Figure 5.23. A high signal from the enzymatic reaction was achieved with a scan rate of 3 mV/s and a FE concentration of 0.1 mM. Because GOx/b and NA molecules were mixed in a 1:1 ratio, all the GOx/b are expected to have bound to NA during the particle preparation. It is possible that some NA bound to more than one GOx, which excludes them from binding to a particle, but this is not expected to interfere with the measurement.

In the example shown above, the particle concentration was 10 fM. Compared to a 400 nm vesicle, the surface of 10 μm particles is 5'000 times increased. Therefore, it makes sense that the signal per particle is accordingly higher. However, for the feasibility experiments surfaces fully coated with NA were used. This does not prove that such big particles could be captured by a single binding point, it only shows the promising proof of principle already without optimizing the system.

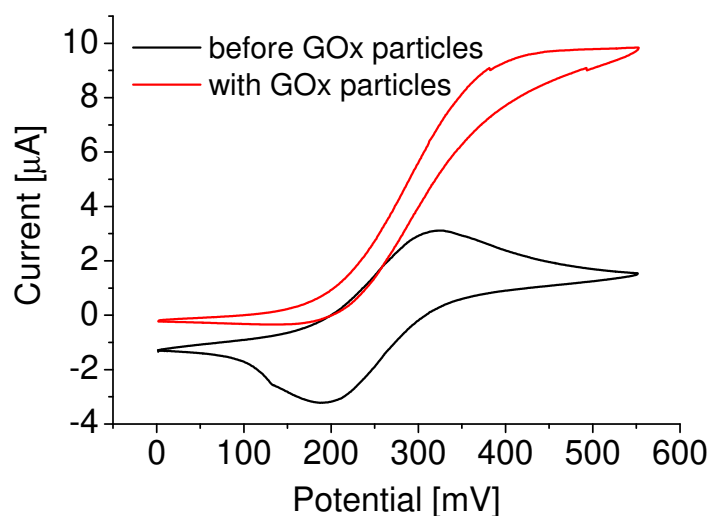


**Figure 5.23:** CV's before the injection and after the binding of GOx functionalized PS particles. A scan rate of 3 mV/s was applied.

## 5.5 Conclusion

In this chapter the most suitable EC detection methods have been evaluated with enzymes in solution. These findings were then transferred to "real" biosensors. An overview of the performance of the individual sensors and the different detection methods is presented in Table 5.2. In general, the main advantages of sensors with EC detection are connected to the possibility for measuring with a smaller and cheaper device and having a potential for array based detection.

The enzyme functionalized vesicles were adsorbed to NA to represent a simple model biosensor. It was used to test the feasibility and to adjust parameters, such as scan rate or concentration of the mediator. Ferrocyanide was successfully used in chronoamperometry measurements, ferrocene in both, CV and chronoamperometry. The first two were further followed, whereas with the third version no satisfying detection limit was achieved. In numbers this means, for chronoamperometry with FC, a detection limit of around 1-2 pM (0.2-0.4 ng/ml) could be achieved. CV with FE resulted in a detection limit of roughly 1.7 nM (30 ng/ml) NA with still some possibilities for improvements. Because of the clear differences, the chronoamperometry looks most promising. This knowledge was then transferred to the sandwich based assay, which was expanded by functionalizing the vesicles with enzymes. In terms of signal amplification, the same sensitivities as with the model system can be expected. However, since there is some unspecific binding during the sensor buildup, the current sensitivities were slightly lower. With the QCM-D a

**Table 5.2:** Overview of the detection limits of the different (enzymatic) sensors and the corresponding detection methods, including the mass amplification of the QCM-D from Chapter 4.

	QCM-D	FC, hold	FE, CV	FE, chronoamp.
Model assay with enzyme functionalized vesicles on NA	feasibility	1-2 pM	1.7 nM	< 85 nM <sup>a</sup>
Sandwich assay with enzyme functionalized vesicles	30 pM	< 1 nM (feasibility) <sup>b</sup>	feasibility	
Polymeric vesicles with enzymes on NA	0.2 pM			
Polymeric vesicles with enzymes in a sandwich assay	feasibility	feasibility		
Particles with enzymes on NA			< 10 fM (feasibility) <sup>c</sup>	

<sup>a</sup>This detection method was not sensitive enough; therefore, it was not used for the other sensor systems any more

<sup>b</sup>These measurements were focussed on the linear concentration dependence. The here given limit just represents the lowest measured concentration.

<sup>c</sup>This number only refers to the molarity of the particles to make it somehow comparable to the other sensors. It has not been shown that such a low molarity of antigens can be detected this way.

detection limit of 30 pM was achieved. Chronoamperometry with FC resulted in a signal with a linear dependence on the antigen concentration. Thus, it was successfully tested down to 1 nM; but the detection limit is expected to be clearly lower.

Later on, the lipid vesicles were replaced by polymeric vesicles. It was possible to integrate them into the biosensor system and achieve promising results (0.2 pM with the model sensor in the QCM-D) and feasibility results with electrochemical detection. Furthermore, compared to biosensors based on lipid vesicles, such modified systems have a better long-term stability. Finally, in a feasibility study it was demonstrated that enzyme functionalized PS particles can substitute the vesicles. With 10 fM vesicle solution the signal was saturated; there was no more reduction peak during CV. However, this result needs to be confirmed, because it only shows the strong signal enhancement effect of the enzyme coated particles; it does not prove that less than 10 fM antigens can be detected this way, i.e. the issue is, how many antigens are required to really bind such a particle.

---

In summary, from the evaluated detection methods chronoamperometry with FC was the most sensitive. Even though the system was first developed with lipid vesicles, polymeric vesicles or enzyme coated particles seem to be more promising in terms of shelf-life. Another advantage of the polymeric vesicles is the encapsulation of the enzymes. Through this, only the secondary antibody is bound to them via biotin/NA, which avoids a possible competition between enzymes and antibodies.



---

## Enzymes incorporated into Electroactive Polyelectrolyte Multilayers<sup>1</sup>

---

To further simplify the use of our biosensor, we intended to build a system where the mediator is already present when the enzymes bind. Therefore, we chose a polyelectrolyte multilayer (PEM) system with the aim to keep the mediator molecules within the film through electrostatic charges. We were not only successful in incorporating the mediator but also found that such PEMs showed electroactive behaviour. We then developed a new platform at the interface of PEM films and electroactive polymers (EAPs) by combining the easy buildup of PEM thin films and the deformation characteristics of the EAPs. The PEM films were made of Poly(L-glutamic acid) (PGA) and Poly-(allylamine hydrochloride) (PAH) by using the layer-by-layer (LbL) method which is already well established in biotechnology and biomaterial science. After adding  $[\text{Fe}(\text{CN})_6]^{4-}$  ions (FCIV), cyclic voltammetry (CV) was applied resulting in a reversible expansion and contraction of the film. The shape change as well as the film buildup prior to the cycling were *in situ* monitored using EC-QCM-D. Electrochemical atomic force microscopy (EC-AFM) images confirmed the rapid shape deformation. The process takes place in an aqueous environment under mild conditions (maximum potential of 600 mV and no pH change) which makes it a promising tool for biomedical applications.

After investigating this swelling/deswelling effect we went back to the original idea of having enzymes in or on PEM films. This can potentially be used for enzymatic sensing

---

<sup>1</sup>Parts of this chapter have been published in: D. Grieshaber, J. Vörös, T. Zambelli, V. Ball, P. Schaaf, J.C. Voegel, and F. Boulmedais, *Swelling and Contraction of Ferrocyanide Containing Polyelectrolyte Multilayers upon Application of a Potential*, *Langmuir*, **24**(23): 13668-13676, 2008.

of e.g. glucose. Furthermore, such films can protect the sensor from drying. We have introduced enzymes into the film and detected their activity by CV.

## 6.1 Swelling and Deswelling

The main focus of this section is on the swelling/deswelling behaviour of exponentially growing PGA/PAH films, containing FCIV ions, upon the application of an electric potential. First, the formation of the exponentially growing film is briefly documented. Then, different aspects of the swelling/deswelling phenomenon follow, describing when it is observed and the amplitude that is obtained depending on the scan rate of the CV or the number of bilayers. The results obtained from the EC-QCM-D are compared to EC-AFM and FTIR measurements. The influence of PSS/PLL, an almost linearly growing film, on the swelling/deswelling when it is adsorbed on top of the PGA/PAH film is studied. Finally, a mechanism is proposed based on the different observations.

The deposition of PEI-(PGA-PAH)<sub>10</sub> multilayer films was *in situ* monitored using the EC-QCM-D. Figure 6.1a represents the frequency shift and dissipation change directly obtained from the EC-QCM-D measurement; the modelled thickness (viscoelastic Voigt model [213, 214]) is shown in Figure 6.1b, whereas the density of the polymer film was assumed to be 1050 kg/m<sup>3</sup>. The frequency shift decreased after each adsorption step, which means that the adsorbed mass increased. PAH led to a high increase while the adsorption of PGA resulted in only a small increase of mass. All three curves - frequency shift, dissipation and modelled thickness - showed an exponential growth of the film. This deposition is based on the "in" and "out" diffusion of PGA molecules through the entire film during each deposition cycle [228]. By increasing the number of layers, the adsorption of PAH induced an increase in dissipation, whereas the subsequently adsorbed PGA led to a decrease. For 10 bilayers with incorporated FCIV the film was approximately 700 nm thick as shown in Figure 6.1b. There was no difference observed with and without buffer rinse in between the adsorption steps. That is why we did not use an additional rinsing step between the adsorption of the individual polymers (as described in the methods section).

After the film deposition a buffer solution, containing FCIV ions, was put into contact with the PEI-(PGA-PAH)<sub>10</sub> film (see last adsorption step in Figure 6.1a). The frequency shift increased whereas the dissipation decreased which could either indicate a loss of



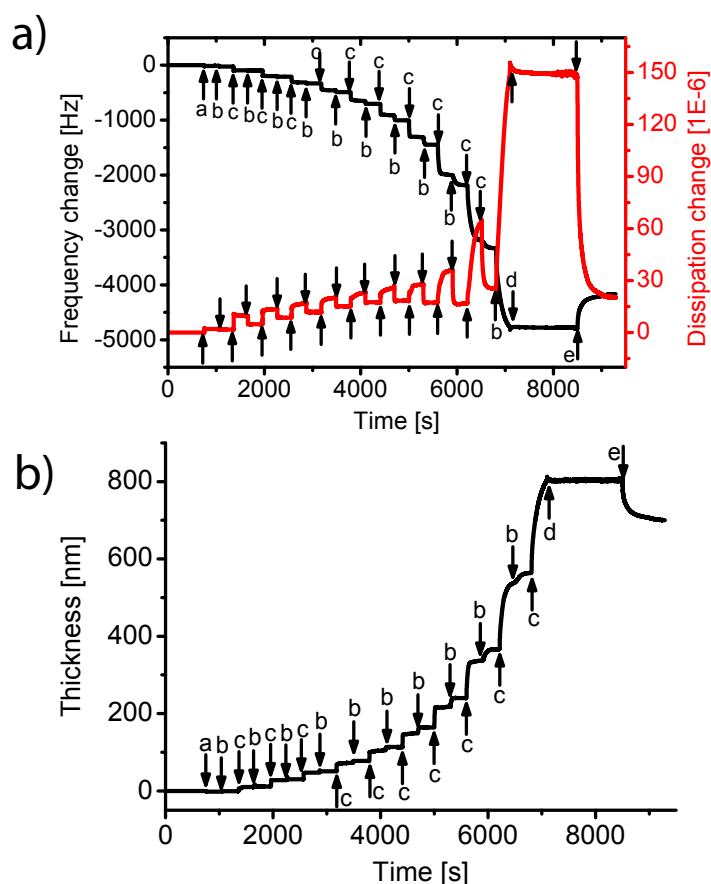


**Figure 6.1:** a) Adsorption of PEI-(PGA-PAH)<sub>10</sub>-FCIV. The frequency shift decreased with increasing mass, while the dissipation increased. The last step represents the adsorption of FCIV. The arrows indicate the adsorption of the polymer layers and the FCIV. The ones pointing to the frequency curve correspond to a: PEI, b: PGA, c: PAH, d: buffer and e: FCIV. b) Modelled thickness of the adsorbed PEM film using the viscoelastic Voigt model.

material or contraction of the film and less flexibility. In order to find out which reaction occurs, we performed the same experiment under FTIR observation. The spectra of PEI-(PGA-PAH)<sub>5</sub> after the adsorption of each PGA/PAH bilayer and after the uptake of FCIV ions and subsequent rinsing are shown in Figure 6.2. At each adsorption step of PGA/PAH bilayers, the absorbance peaks of PGA (at 1635 and 1560 cm<sup>-1</sup>, corresponding to amide I and COO<sup>-</sup> peaks, respectively) progressively increased. It appears that the absorbance increases in a non-exponential manner and even seems to level off after 4-5 layer pairs. In FTIR spectroscopy in ATR mode, the film deposited on the substrate (ZnSe crystal) is sensed by an evanescent wave with a penetration depth typically of the order of 1.5 μm. The intensity of light is a function of the separation distance from the ZnSe/solution interface ( $z$ ). In the case where  $z_2 > z_1$ , a PGA molecule located at the distance  $z_2$  contributes less to the light absorption than a molecule located at the distance  $z_1$ .

The exponential increase in the amount of deposited PGA molecules, combined with the exponential decrease of the intensity of light versus  $z$ , contributes to a measured linear increase of the absorbance up to 8 layer pairs (data not shown). When the PGA/PAH film was put in contact with FCIV containing buffer, the peak of FCIV at  $2033\text{ cm}^{-1}$  appeared. This means, that there was an uptake of FCIV by the film. At the same time, an increase of the PGA peaks was observed. This increase can only be interpreted by an increase in the PGA concentration in the region close to the ZnSe crystal. This strongly suggests that the film undergoes contraction with almost no film erosion upon FCIV loading. There is no indication of loss of material during the FCIV adsorption. Therefore, in combination with EC-QCM-D measurements, the results suggest that the addition of FCIV ions contracts the film and renders it more rigid.

During the contact of FCIV containing solution with a (PGA/PAH)<sub>10</sub> film, CV measurements were performed at different scan rates and monitored by EC-QCM-D to follow the frequency shift and the dissipation change (see Figure 6.3). The frequency shift decreased when the potential was increased from 0 to 600 mV, which means that the film expanded. Synchronically, the dissipation increased which indicates a less rigid film. The film reversibly contracted to its original thickness and rigidity when the potential was decreased back to 0 mV. Subsequently, CVs from 0 to 600 mV were applied at different scan rates ranging from 2 to 100 mV/s as shown in Figure 6.3i-iii. Independently of the scan rate, frequency shift and dissipation change followed the potential change.

The swelling/deswelling phenomenon of PGA/PAH films in contact with FCIV ions under CV was found to be reversible. The fact that even at high scan rates the same expansion and contraction occurred, indicates, that the film reacts instantly. Control runs of CV on PEI-(PGA-PAH)<sub>10</sub> before the injection of FCIV ions solution were also performed. Only a negligible effect in the dissipation ( $<1\text{E-}8$ ) and in the frequency shift (around 0.5 Hz) were observed. After being in contact with FCIV containing buffer, the flowcell was rinsed with buffer to remove the FCIV ions remaining in solution. Then, CV measurements were performed with the same scan rates as before. Without FCIV ions in the supernatant, the amplitudes of frequency shift and dissipation during CV were found to be even higher (see Figure 6.3iv-vii). This can be explained by the presence of different counter ions (chloride and FCIV ions) diffusing into the film upon oxidation of the FCIV ions. When FCIV ions are still in the supernatant, they will diffuse into the film and thereby reduce the swelling effect. On the other hand, without FCIV in the supernatant only chloride ions, which have no influence on the swelling, can diffuse into the film to maintain charge neutrality in the film. Like for the measurements with FCIV in

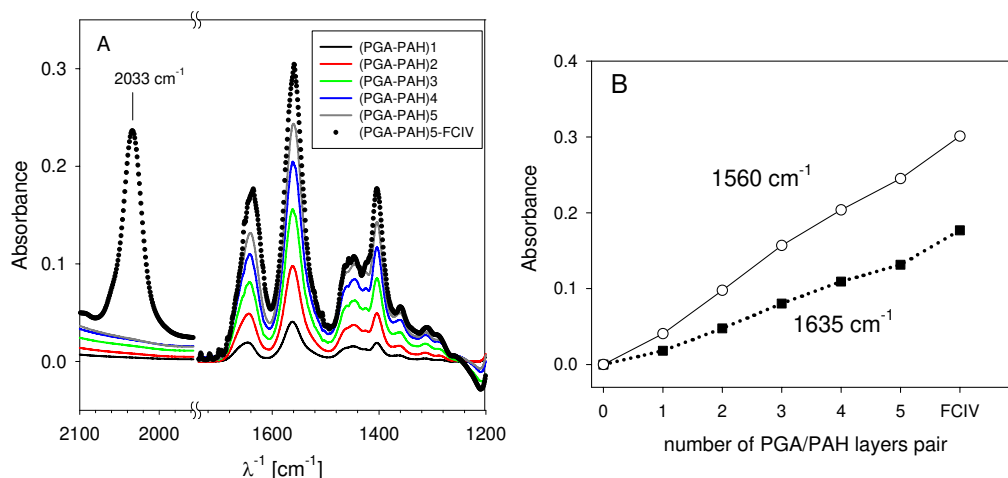


**Figure 6.2:** a) Absorbance spectra of a PEI-(PGA-PAH)<sub>5</sub> film obtained by FTIR in ATR mode. The peak at 2033 cm $^{-1}$  is attributed to FCIV. b) Evolution of the absorbance at 1560 cm $^{-1}$  (peak due to the COO $^{-}$  groups of PGA) and at 1635 cm $^{-1}$  (maximum of the amide I band of PGA) as a function of the number of PGA/PAH bilayer depositions and after loading with FCIV.

solution, the thickness expansion did not significantly depend on the scan rates when the FCIV in solution had been removed. In addition, Figure 6.3 shows that many successive oxidation/reduction cycles can be performed without changing the performance of the device.

The cyclovoltammogram monitored for a PEI-(PGA-PAH)<sub>10</sub> film after adsorption of FCIV ions is shown in Figure 6.4a. During the increase of the potential from 0 to 600 mV (scan rate 50 mV/s), FCIV ions were oxidized into FCIII ( $[\text{Fe}(\text{CN})_6]^{4-} \rightarrow [\text{Fe}(\text{CN})_6]^{3-} +$

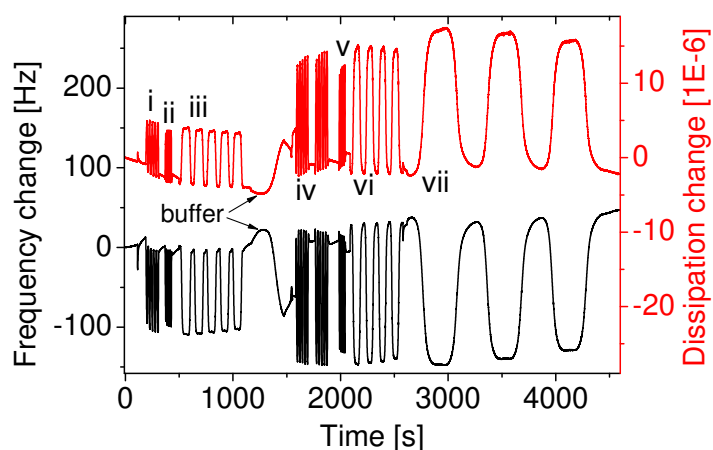


**Figure 6.3:** Frequency shift and dissipation change as a function of time on a PEM film consisting of 9 bilayers. First, CV was performed after adding FCIV (FCIV in the film and in solution) i) 50 mV/s, ii) 100 mV/s and iii) 10 mV/s. After buffer rinse the CV was repeated iv) 50 mV/s, v) 100 mV/s, vi) 10 mV/s and vii) 2 mV/s.

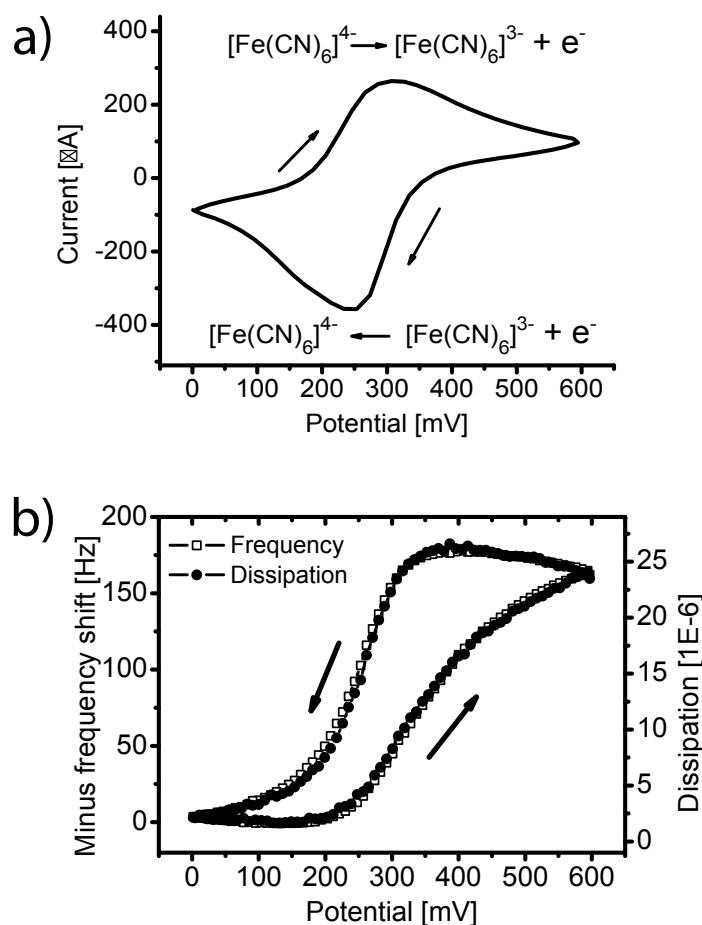


**Figure 6.4:** a) Voltammogram showing oxidation and reduction peaks of a film consisting of 10 bilayers (FCIV only in the film). b) Frequency shift and dissipation change as a function of the applied potential during CV (scan rate 50 mV/s). Please note that the left y-axis shows the negative values of the frequency shift. This allows for visualization of the frequency and dissipation changes occurring simultaneously.

$e^-$ ). This reaction resulted in an oxidation peak of almost 300  $\mu\text{A}$ . Since FCIII ions have one charge less compared to FCIV ions, the charge distribution in the film is disturbed. When the potential was decreased to 0 mV, FCIII ions were reduced to FCIV by gaining an electron leading to a reductive peak current. For the same film, Figure 6.4b represents the absolute values of frequency shift and dissipation change as a function of the applied potential. This figure shows the congruency of the two curves. The expansion and contraction of PGA/PAH films took place during oxidation/reduction of the FCIV/FCIII ions with a maximum of swelling/deswelling at the oxidation and the reduction potential of the FCIV ions. As described later (see Figure 6.6), this indicates that the expansion and contraction is directly related to the number of transferred electrons.

The swelling/deswelling effect was studied for 3 to 10 PGA/PAH bilayers. The frequency shift and dissipation amplitudes were measured during CV, while FCIV ions were in solution, and after the rinsing step. Figures 6.5a and 6.5b represent the frequency and dissipation shifts during CV with a scan rate of 50 mV/s. For the investigated films, the thickness increased more after removing free FCIV ions from the supernatant. Once these ions had been removed, no more changes in the swelling/deswelling behaviour were detected, even after repeated rinsing steps.

The frequency shift upon application of a potential increased exponentially with the number of layers of the film as did the thickness of the film itself. The dissipation change was almost negligible for thin films and increased exponentially above 7 bilayers. The amplitudes of changes in frequency and dissipation were also determined. In Figure 6.5c their change is plotted in percent of the total film frequency shift and dissipation change, respectively. By increasing the number of bilayers from 3 to 10, the frequency shift and the dissipation change were increased respectively from 2 to around 4 % and from 0 to 30-40 % with respect to the frequency and dissipation before the oxidation was performed. Additionally, CV measurements with PGA as the last layer were performed. After adsorption of FCIV ions and subsequent rinsing, the swelling/deswelling effect of PEI-(PGA-PAH)<sub>10</sub>-PGA was significantly lower than for PEI-(PGA-PAH)<sub>10</sub>. PGA as a last layer therefore dramatically decreased the swelling/deswelling effect. Recently, Hubsch *et al.* studied the diffusion kinetics of FCIV ions into PGA/PAH films with PGA or PAH as last layer by means of electrochemistry: as the films were brought into contact with buffer, containing FCIV ions, the diffusion of FCIV ions was followed as a function of the contact time. They found that with a contact time of 10 min between FCIV containing buffer and PGA/PAH films, the oxidation/reduction peaks were lower for a PGA terminal film than for a PAH terminal film [229]. Based on electrochemical measurements, Takita *et al.* also reported that PGA terminal bilayers take up less FCIV ions [230]. This effect could be explained with the fact that, prior to exposure to FCIV ions, the negatively charged PGA diffused into the film. Compared to PGA, chloride ions can diffuse out from the film much easier. Thus, less negatively charged FCIV ions can penetrate into a PGA saturated film. Subsequently, these fewer ions induce a lower current during CV and, what we showed for the first time now, a smaller swelling/deswelling effect.

We were also interested in knowing the extent of FCIV ions that need to be oxidized until there is a change in the film thickness. By integrating the CV curves, we calculated the number of electrons transferred. Because in the absence of FCIV ions there was no oxidation- and reduction-current detected from the film only, the number of transferred

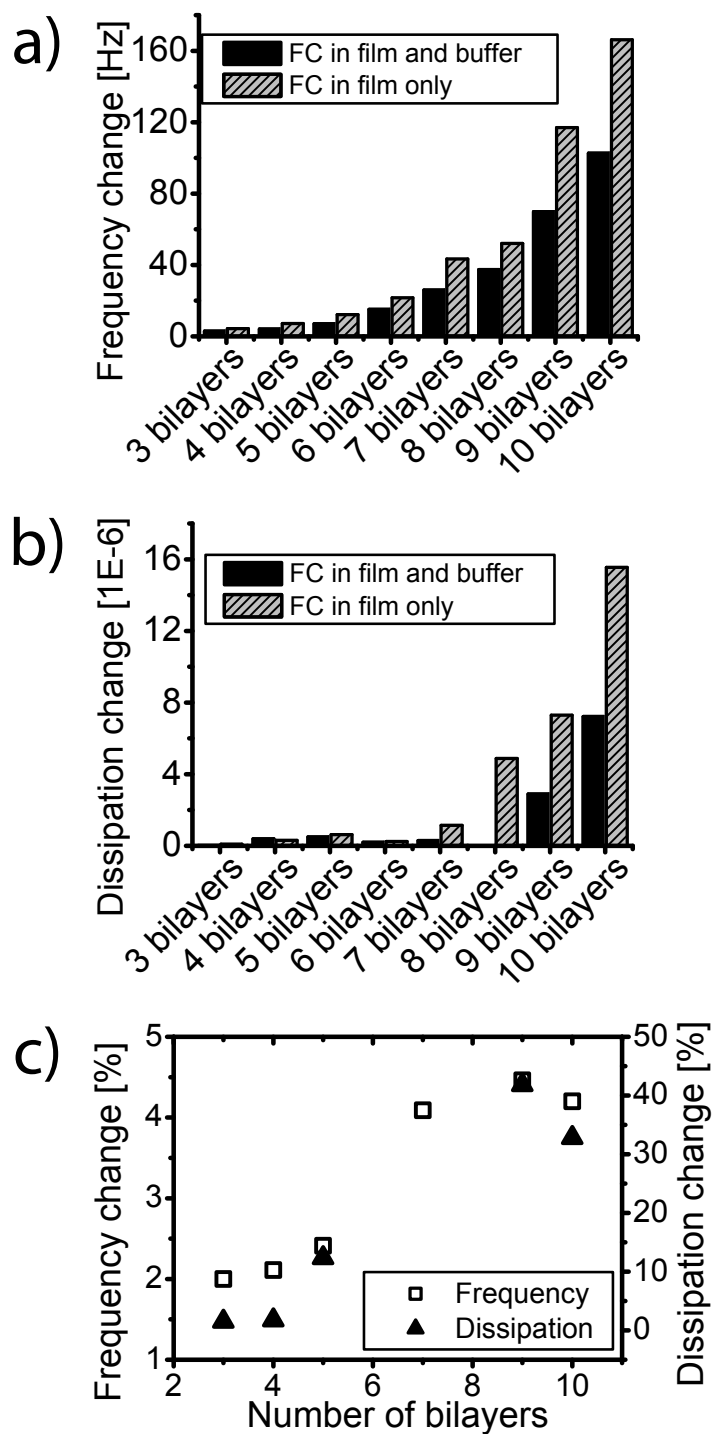


**Figure 6.5:** Absolute and percentage changes in frequency shift and dissipation change of films made of 3 to 10 bilayers upon application of a potential of 600 mV (CV, 50 mV/s). a) Change in frequency during CV as function of the number of layers when a positive potential was applied, b) the corresponding dissipation changes and c) frequency shift and dissipation change in percentages of the values for the total film at 0 mV.

electrons is identical to the number of FCIV ions that have been oxidized. Examples of experiments performed at different scan rates are given in Figure 6.6. Figure 6.6a depicts the changes in frequency and dissipation as a function of the number of transferred electrons with a scan rate of 10 mV/s. When the number of transferred electrons increased (through the increase of the potential applied), the absolute value of the frequency shift and the dissipation change increased too. When the number of electrons decreased, the frequency shift and the dissipation decreased. Moreover, the frequency shift and the dissipation change are clearly superposed, indicating that the swelling is directly proportional to the number of electrons transferred at 10 mV/s. Figures 6.6b and 6.6c show the same for scan rates of 50 mV/s and 100 mV/s, respectively. For low scan rates the swelling and deswelling was found to be a linear function of the number of transferred electrons. In case of higher scan rates, especially for 100 mV/s, the deswelling was not linear, but faster than the reduction of the FCIII ions. Furthermore, it needs to be mentioned that at higher scan rates the total number of transferred electrons was lower, i.e. for 100 mV/s only half of the number of electrons was transferred compared to 10 mV/s. This decrease in current at higher scan rates indicated that diffusion is the rate limiting process, i.e. the currents also might be a contribution of the capacitive current. In case of low scan rates, the film had enough time to more or less follow the oxidation and the reduction in equilibrium. At higher scan rates, where fewer electrons were flowing in total, the contraction took place faster than the expansion. The reason therefore might be that in the oxidized state the film did not have enough time to reach an equilibrium. Upon FCIV oxidation, negatively charged counter ions have to penetrate into the film to maintain charge neutrality. However, both monovalent counter ions (e.g. FCIII and especially  $\text{Cl}^-$ ) have reduced the ion bridge forming capability compared to the FCIV ions and therefore the film expands. However, the breaking of existing ion bridges in the polymer film during oxidation might take longer than the reformation during reduction. This can be an explanation for the asymmetric expansion curves at high scan rates. It means that the ions were oxidized and contributed to the swelling, but once the potential was reduced, they were immediately reduced and therefore the film contracted faster. Furthermore, since the layer thickness changes during the CV scan, this provides a moving boundary for the reservoir from which the FCIV ions diffuse to the electrode. This could explain why the swelling is slower than the contraction at higher scan rates. i.e. the ions have to move less when the thickness is smaller.

To further verify the results from the EC-QCM-D, the thickness of PGA/PAH films was monitored by EC-AFM before, during and after the application of 600 mV in liquid

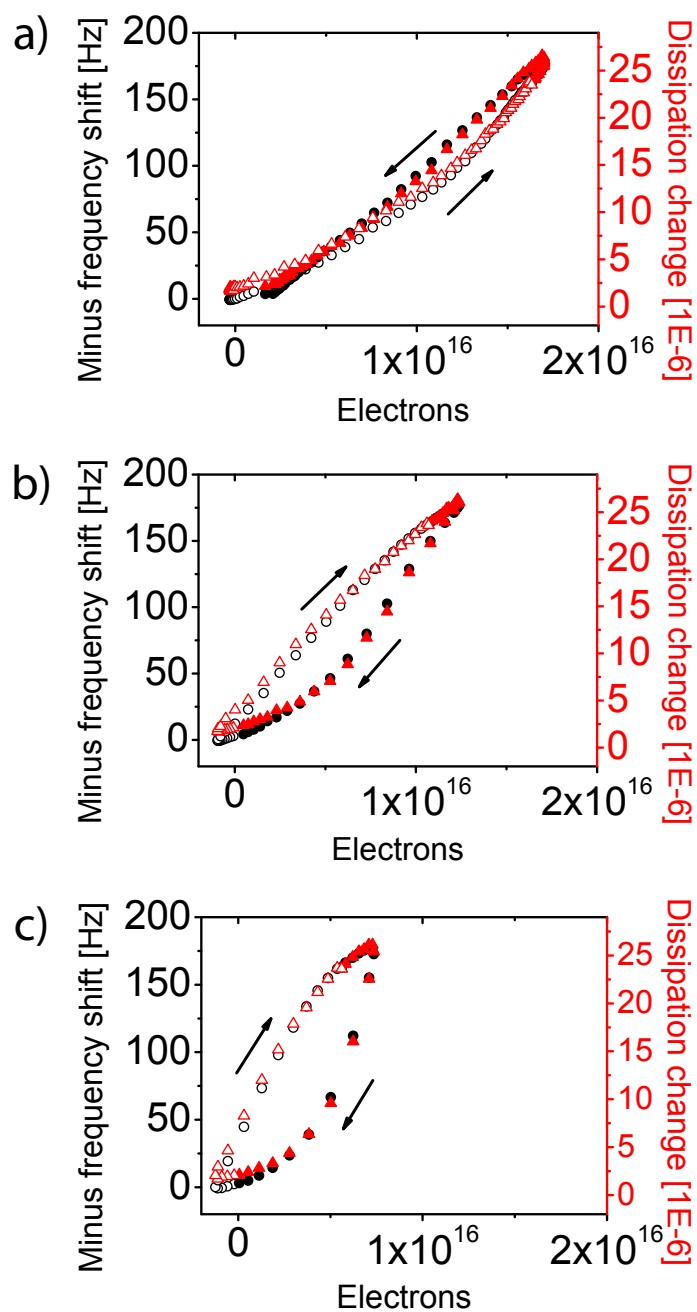


**Figure 6.6:** Absolute value of the frequency shift (o) and dissipation change ( $\Delta$ ) as a function of transferred electrons. Different scan rates were applied; a) 10 mV/s, b) 50 mV/s and c) 100 mV/s. Increase and decrease were close to linear. In case of higher scan rates the swelling was faster than the contraction. Note that the left y-axes show the negative values of the frequency shift.



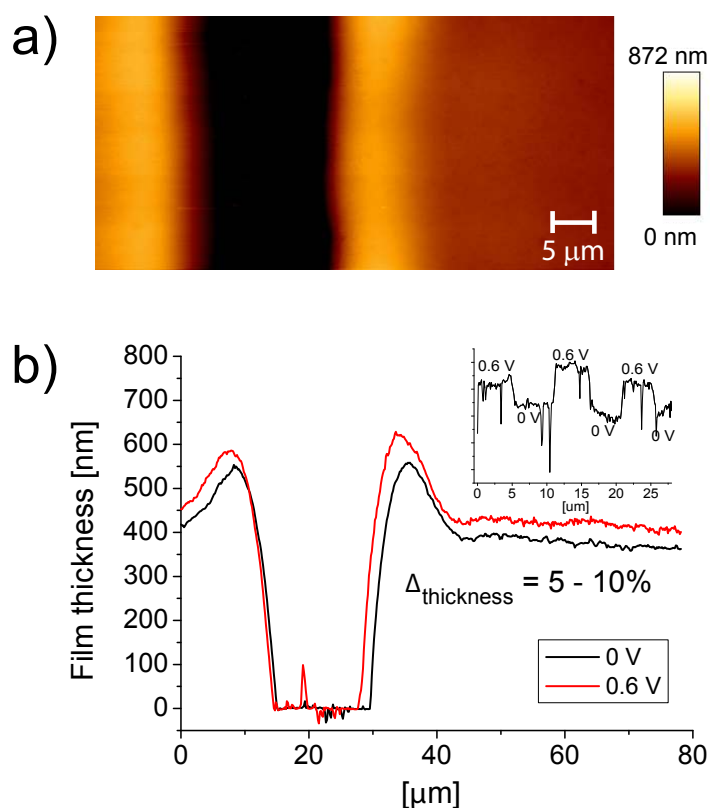


**Figure 6.7:** a) AFM image of a PGA/PAH film with 10 bilayers with a scratch to measure the film thickness obtained by tapping mode in liquid state. b) Cross-section of an FCIV containing film with 10 bilayers. Applying a potential of 600 mV induced a thickness increase of about 5-10%. In the insert the thickness change is monitored. During the scan the potential was repeatedly turned on and off.

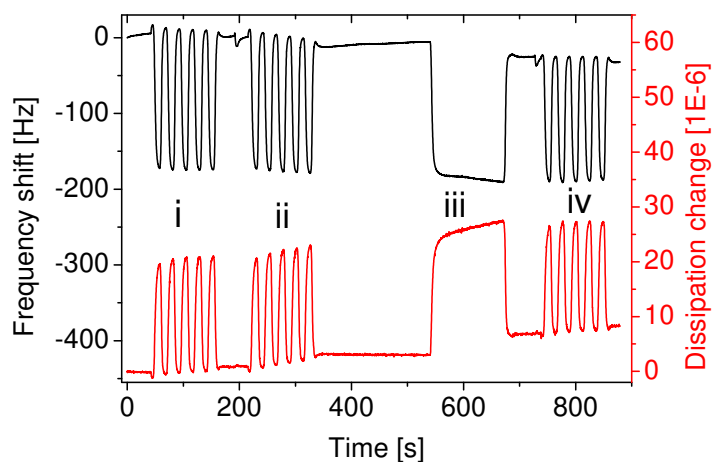
state. To obtain its thickness, the film was scratched and the height difference between the ITO substrate and the film surface was evaluated. A film surface with a scratch is shown in Figure 6.7a. Next to the scratch there was a bulge originating from the material in the scratch. Further away, the film consisting of 10 bilayers was flat and about 400 nm thick. The smaller thickness obtained by the AFM (i.e.  $\sim 400$  nm) in comparison to the QCM-D (i.e.  $\sim 700$  nm) might be attributed to the difference between the techniques, i.e. the AFM tip would probably sense thinner than the actual thickness because of the applied force, while the QCM-D is also sensitive to the few dangling polymer chains that might be at the outer surface of the film. Furthermore, the QCM-D thickness was obtained through a model.

Figure 6.7b shows the cross-section of a PEI-(PGA-PAH)<sub>10</sub>-FC film at 0 and 600 mV. The application of a potential of 600 mV caused swelling of PGA/PAH films of about 5-10% compared to the thickness at 0 mV. Lowering the potential back to 0 mV reversibly

decreased the film thickness to its original state. In the insert, a cross-section over several cycles (potential on/off) is shown. To obtain this graph, the AFM program took the surface of the film as the reference and imaged changes in the depth of the scratch. Therefore, the spikes in the profile are related to some impurities in the scratch (from film and/or solution) and do not represent an uneven film surface. When scanning only on the film without a scratch involved, no such peaks were observed.

One possible explanation for the swelling/deswelling effect could be that the FCIII ions, obtained by oxidation of FCIV, diffuse out of the film when a potential is applied and diffuse in again after reduction. To test this hypothesis, we performed another experiment, where flow was applied during the electrochemical measurements. After the deposition of a PEI-(PGA-PAH)<sub>10</sub> film, it was put into contact with buffer, containing FCIV ions. After a first rinsing step CV (50 mV/s) was applied with and without flow of buffer (see Figure 6.8i and 6.8ii). Then, a constant potential of 600 mV was applied for 2 min under flow (as shown in Figure 6.8iii). During this time the supernatant was exchanged about four times. No significant decrease in the swelling/deswelling behaviour was observed with a buffer flow, while the Faradic current was slightly higher (about 5%). This indicates that the oxidized FCIII ions remain in the film when a potential is applied. Otherwise, if the swelling had been induced by release of FCIII ions into the buffer, this would have occurred immediately and the concentration of these ions would have decreased significantly as soon as the supernatant was replaced. Subsequent CV without flow supported these findings by showing almost the same magnitude of swelling as before (see Figure 6.8iv).

Our proposed mechanism of the swelling/deswelling phenomenon is based on the formation of FCIV/FCIII ( $[\text{Fe}(\text{CN})_6]^{4-}/[\text{Fe}(\text{CN})_6]^{3-}$ ) ion bridges between the polymer chains (see Figure 6.9). As mentioned above, addition of FCIV ions led to a contraction of the film. This could be explained by the formation of FCIV ion bridges between positively charged PAH chains replacing  $\text{Cl}^-$  ions. Like that, the film contracts and water is expelled. Simultaneously, the stronger interactions in the film make it stiffer, as it can be deduced by the dissipation decrease monitored by QCM-D. Application of 600 mV induces oxidation of the FCIV ions. The less charged FCIII ions form weaker ion bridges, which partially get replaced by counter ions resulting in swelling of the film. The charge inside the film is compensated by diffusion of chloride ions from the supernatant into the film. When the potential is decreased to 0 mV, FCIII ions are reduced and at the same time chloride ions diffuse out of the film and the FCIV-PAH bridges are reformed again. Using the EC-QCM-D, we observed an increase in the dissipation during the oxidation process, whereas



**Figure 6.8:** i: CV of a PEI-(PGA-PAH)<sub>10</sub> film without flow, ii: with flow, iii: with a constant potential of 600 mV for 2 min with flow and iv: again CV without flow.

the dissipation decreased back to its original value upon reduction. This observation, as well as the associated frequency changes, suggest that the film becomes softer upon oxidation. Upon reduction, the film deswells and its stiffness increases.

The model proposed in Figure 6.9 is also able to explain our observation that the film swelling is of higher amplitude in the absence of FCIV in solution. When the electroactive FCIV ions are present in solution, they are in competition with the chloride ions diffusing

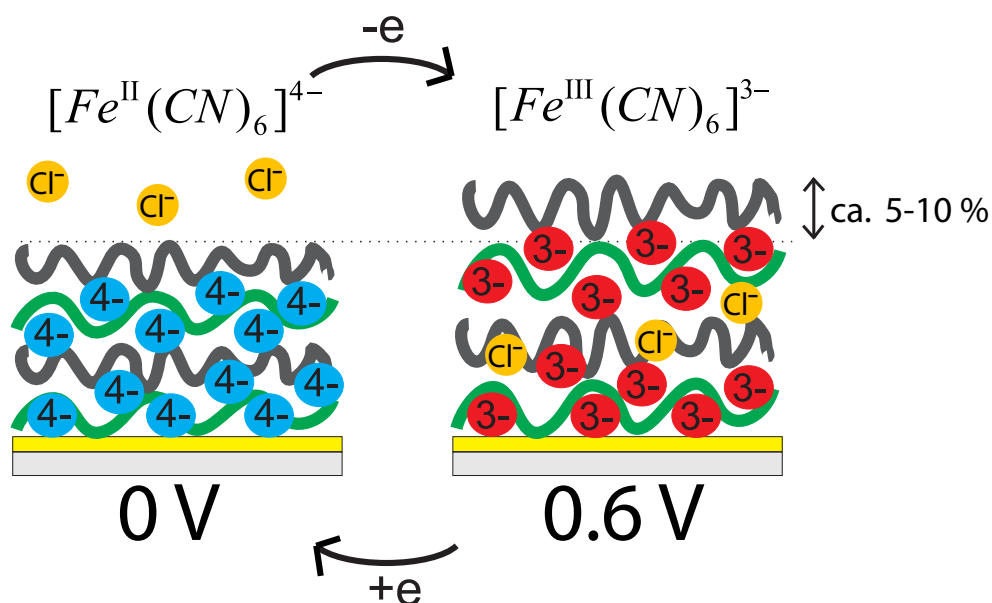


**Figure 6.9:** Schematics of a PGA/PAH multilayer with incorporated FCIV ions. When the FCIV ions are oxidized chloride ions enter the multilayer and the film swells.

into the film during the oxidation of FCIV. One FCIV diffusing into the film will have the same effect, from an electrostatic point of view, than four chloride ions. Thus, when FCIV ions are present in solution, a lower amount of anions has to diffuse into the film to maintain its electroneutrality. This will reduce the swelling effect in comparison to the case where only chloride ions can diffuse (absence of FCIV in solution) and more ion bridges will be maintained. The swelling behaviour under an electric potential related to ion uptake was also observed for polyelectrolyte-enzyme films as reported by Forzani *et al.* [231]. Compared to our system they used Osmium complexes, covalently attached to a polymer backbone, as redox-active compound and built alternating layers consisting of glucose oxidase and the PAH-Os complexes. Their complex Os compound led to swelling behaviour of a similar extent but slower than our system. The changes in thickness and refractive index during the oxidation of Os are associated to anion and water uptake and are proportional to the fraction of oxidized Os. In our case, instead of a covalent binding the redox probe is bound to the polyelectrolytes by electrostatic interactions with the same amplitude in swelling/contraction. The spontaneous entrapment seems to be easier to apply, provided that the redox probe is entrapped into the film.

Besides the PGA/PAH films we were also interested in the behaviour of PEMs consisting of different polymers. We investigated PSS/PLL films in contact with FCIV ions. CV was performed on a PEI-(PSS-PLL)<sub>5</sub> film during and after the contact with FCIV ions in solution. With FCIV in solution there was an oxidation/reduction peak, but about 10 times weaker than for PGA/PAH films. Moreover, the increased potential difference between the oxidation and the reduction peaks (compared to PGA/PAH) suggests that the charge transfer is diffusion limited. Once the FCIV ions in solution were replaced by buffer, the oxidation and reduction peaks disappeared, similar to a purely capacitive system (see Figure 6.10). This shows that PSS/PLL films, as PSS/PDAMAC [232] and PSS/PAH films [233], did not uptake FCIV ions. Moreover, EC-QCM-D measurements showed that the film did not react to an applied potential with an expansion and contraction effect. These results nicely illustrate that an uptake of FCIV ions of the film is a necessary condition to obtain a swelling/deswelling behaviour.

In a next step films consisting of two different multilayers were investigated, namely PSS/PLL and PGA/PAH, where up to five bilayers of PSS/PLL were adsorbed on top of five PGA/PAH bilayers. The film growth was found to be independent of the layers underneath, but the PSS/PLL film built on top of a PEI-(PGA-PAH)<sub>5</sub> film almost completely inhibited the swelling (only about 2 Hz frequency and 3E-7 dissipation change). Even though such films showed oxidation and reduction peaks in the presence of FCIV

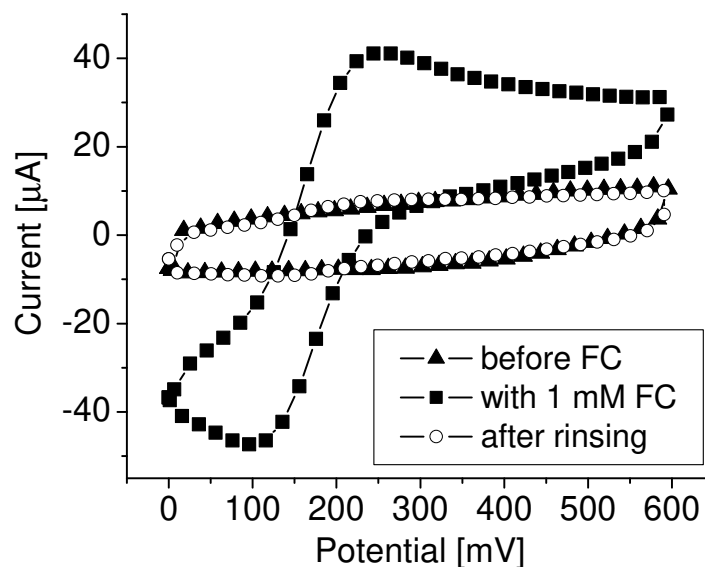


**Figure 6.10:** Voltammogram (50 mV/s) of a PSS/PLL film with 5 bilayers before, during and after being in contact with FCIV ions.

ions, after the rinsing step these peaks were smaller compared to PGA/PAH films without PSS/PLL on top. This means that PSS/PLL on top of PGA/PAH film retarded the diffusion of FCIV ions into the PGA/PAH film and towards the electrode, showing a limited permeability to FCIV ions. Already two PSS/PLL bilayers on top were enough to reduce the uptake of FCIV ions to around 30 %.

We have also studied the case when the PSS/PLL layers were built on top of a PGA/PAH film already containing the FCIV ions. Before the application of CV on this type of buildup, FTIR experiments allowed us to further verify that the FCIV ions remain in PGA/PAH films after the deposition of an overlaying PSS/PLL film (see Figure 6.11). After the uptake of FCIV into PGA/PAH films and a subsequent rinsing step, the first layer of PSS led to a small decrease in the FCIV peak (at  $2033\text{ cm}^{-1}$ ) in parallel with the increase of PSS peaks (at  $1035$  and  $1007\text{ cm}^{-1}$ ). During the 5 PSS/PLL bilayer depositions, the PSS peaks increased, showing presence of the terminal film. At the same time, the intensity of the FCIV peak showed only a small decrease of about 5 % during the buildup of PSS/PLL bilayers (see inset of Figure 6.11b).

The frequency shift and dissipation change during the application of CV on an FCIV containing PGA/PAH film with a PSS/PLL capping film, monitored by EC-QCM-D, are shown in Figure 6.12a. Upon application of CV, frequency shift and dissipation change followed the potential change but in a dramatically reduced manner compared to an FCIV containing PGA/PAH film without the PSS/PLL capping layer. Concerning the frequency

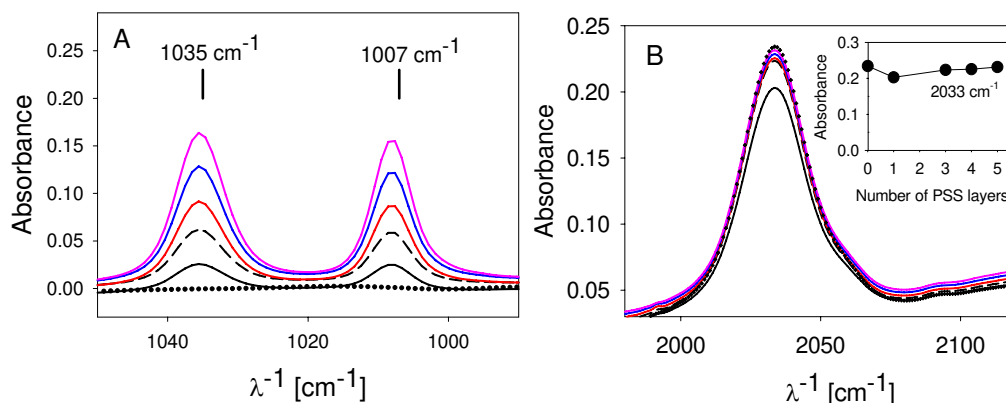


**Figure 6.11:** FTIR spectral regions characteristic of a) the absorbance peaks of the sulfonate groups of PSS (980-1080  $\text{cm}^{-1}$ ) and b) FCIV (1950-2100  $\text{cm}^{-1}$ ) obtained from a PEI-(PGA-PAH)<sub>5</sub> film after loading with FCIV (black dots) and after deposition of 1 (black line), 2 (black dashes), 3 (red line), 4 (blue line) and 5 (pink line) PLL/PSS bilayers. As the spectra did not change upon the deposition of PLL, they have been omitted for seek of clarity. The inset of b) represents the absorbance intensity of the band at 2033  $\text{cm}^{-1}$  (attributed to FCIV) upon further deposition of (PSS-PLL) layer pairs.

shift (and the dissipation change), the swelling/deswelling amplitudes with and without the PSS/PLL capping layer are 2 Hz (3E-7) and 14 Hz (7E-7), respectively. This inhibitory effect on the swelling/deswelling of FCIV containing PGA/PAH films is not related to the decrease in FCIV content inside the film as it has been confirmed by FTIR (Figure 6.11). In Figure 6.12b, the voltammogram of FCIV ions contained in a PGA/PAH film before and after the deposition of the PSS/PLL capping film shows a decrease of the Faradic current and an increase in the peak potential difference. This means that the charge transfer is limited by the diffusion which could explain the inhibiting effect of the PSS/PLL capping film. Overall, PSS/PLL films interfered with the diffusion of FCIV and counter ions and thus inhibited the swelling/deswelling effect.

In summary, we have built electroactive PEM films consisting of PGA and PAH. FE was found to diffuse from the supernatant into the film and stay there. Application of CV caused the film to reversibly swell and deswell, following the applied potential. PSS/PLL capping films disturbed the diffusion behaviour of FC and counter ions in the solution and therefore mainly inhibited the swelling/deswelling effect.

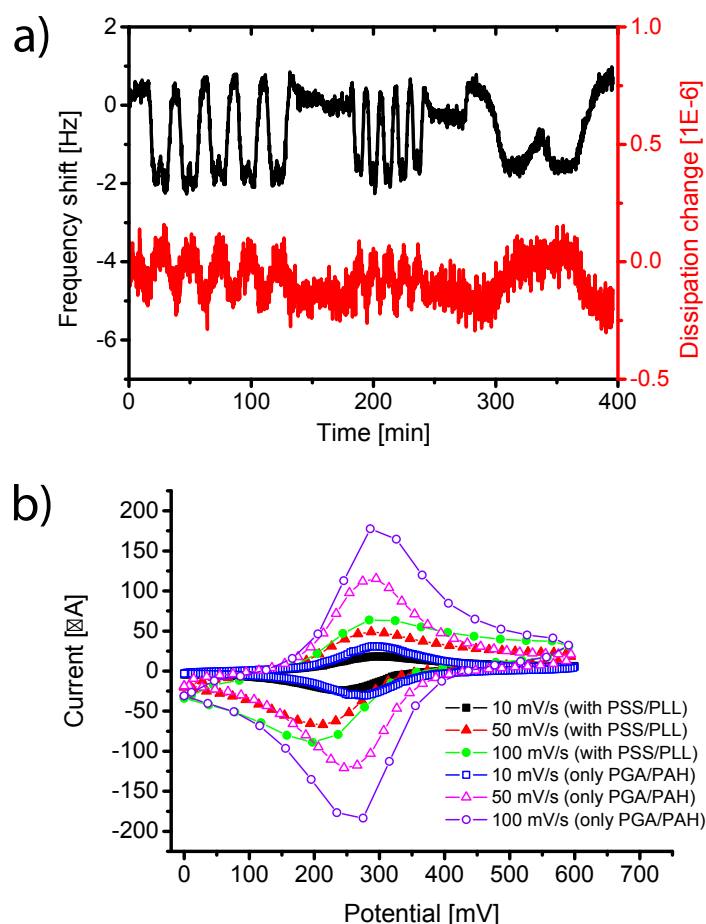


**Figure 6.12:** a) Frequency shift and dissipation change of a PGA/PAH film (containing FCIV ions) with a (PSS-PLL)<sub>5</sub> capping film during CV at 50, 10 and 100 mV/s. b) Voltammogram of a PGA/PAH film, containing FCIV, with and without a (PSS-PLL)<sub>5</sub> capping film.

## 6.2 Incorporation of Enzymes

In this section the combination of the above mentioned electroactive PEM films with enzymatic sensing is presented. The enzymes (GOx) have been electrostatically incorporated into the film. In this system CV does not only induce swelling and deswelling of the PEM film but also gives information about the activity of the enzymes.

From Chapter 5 we know that GOx requires ferrocene (FE) to be detected with CV. On the other hand, unlike FC, FE does not stay in PGA/PAH films. Thus, for experiments combining the swelling/deswelling effect with enzymatic detection, both mediators, FE and FC are required. Before combining the two techniques we had to verify that the two mediators do not interfere with each other.

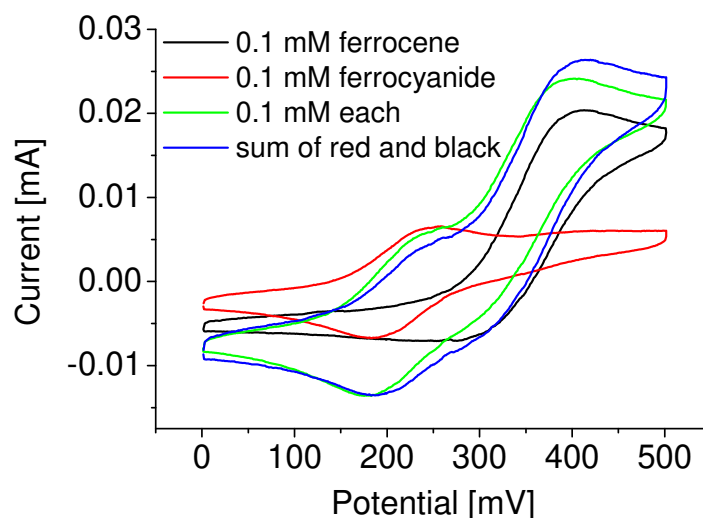


**Figure 6.13:** CV to compare mediator solutions with only ferrocene (black), only ferrocene (red), a mixture of both (green) and the sum (blue) of the current of the individual curves.

The cyclic voltammograms of FE, FC and a mixture of the two is shown in Figure 6.13. For both mediators a CV (10 mV/s) was run alone. Then, they were mixed together. Because the ferrocene has a higher oxidation potential than the ferrocyanide, the two peaks can clearly be distinguished in the cyclic voltammogram. The combined curve was then compared to the sum of the individual curves. It has the same shape but slightly different values. This is assumed to be because, except from the mediators, there are other minor contributions to the current - appearing in a CV with buffer - which are counted twice when the currents are summed up.

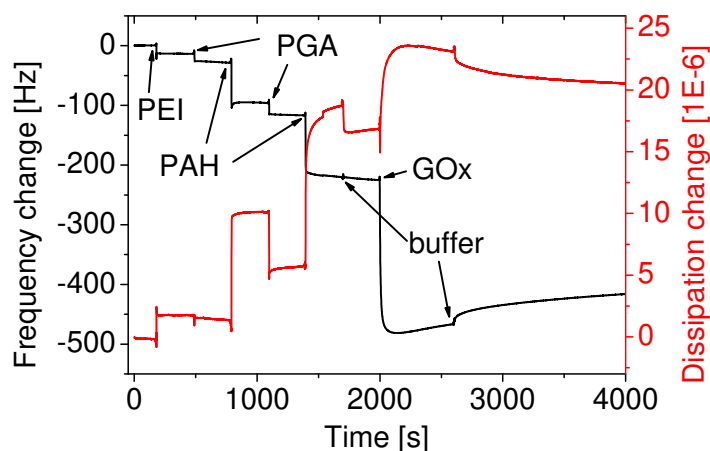


**Figure 6.14:** Frequency and dissipation change as a function of time for the buildup of a PEI-(PGA-PAH)<sub>2</sub>-GOx film.



First, the influence of the number of bilayers was investigated. We compared an empty gold surface to GOx adsorbed on PEI-(PGA-PAH)<sub>n</sub>, whereas n=2 and n=5 was measured. Because the isoelectric point (IEP) of GOx is around 4.2, it is negatively charged at pH 7.4. Thus, it was adsorbed to the positively charged PAH. A QCM-D curve showing frequency and dissipation changes during the PEM buildup with n=2 is given in Figure 6.14.

As described in Section 6.1, ferrocyanide causes swelling and deswelling when CV is applied to the film. On the other hand, if we want to detect GOx during CV, we need to use ferrocene. However, ferrocene did not irreversibly diffuse into the PEM films and therefore did not cause the formerly observed swelling/deswelling effect. Thus, we combined the two iron complexes: ferrocene to detect the enzymatic activity and ferrocyanide for the swelling/deswelling effect. This means, the ferrocene was in the supernatant during the CV measurements. Similar to ferrocyanide in solution it slightly decreased the swelling/deswelling effect. Since ferrocene interacts less actively with the PEM film than ferrocyanide, the decrease was only 5-10% - compared with almost 50 % for ferrocyanide.

After incubating ferrocyanide ions, a buffer solution containing 0.5 mM ferrocene and 200 mM glucose was injected. The cyclic voltammograms are shown in Figure 6.15. The applied scan rate was 10 mV/s. Compared to the empty surface, GOx/b adsorbed to NA induced some signal. A much larger signal was obtained from the enzymes on top of the film. Furthermore, it can be seen that the enzymatic signal does not depend on the thickness of the underlying film.

In a next step we were interested in the inhibition effect of the film when the GOx was not adsorbed on its top, but on the bottom or somewhere in between. Three films were compared: PEI-(PGA-PAH)<sub>5</sub>-GOx, PEI-GOx-PAH-(PGA-PAH)<sub>4</sub> and PEI-PGA-PAH-GOx-PAH-PGA-PAH-GOx-PGA-PAH-PGA-GOx (see Figure 6.16). When the GOx was below the PEM film, the electrochemical signal of the enzymatic reaction was significantly decreased. It is assumed that in this case the limiting factor is the diffusion of the non-charged glucose through the multilayer film. The second possible factor could be a different amount of adsorbed GOx. The frequency and dissipation changes were a factor 5-10 larger when GOx was adsorbed on top of the film. However, since it electrostatically interacts with the film, this huge change could also be related to conformational changes in the film. Having GOx not only on top but additionally in the film slightly increased the signal compared to GOx only on top.

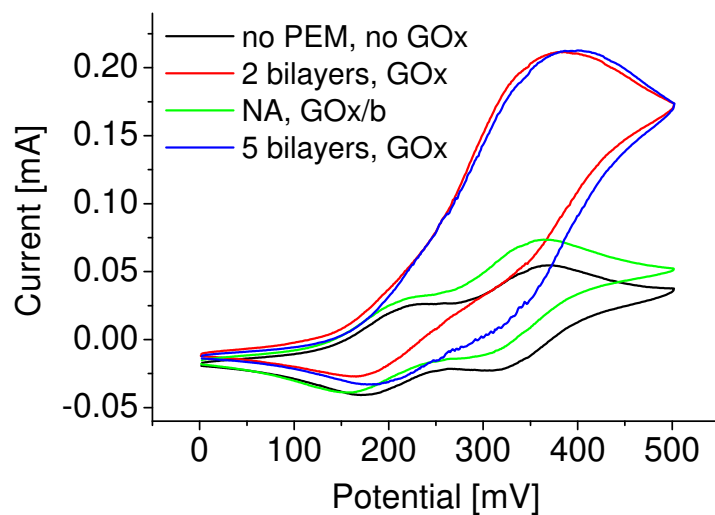


**Figure 6.15:** CV (scan rate 10 mV/s) of an empty surface, GOx on 2 and 5 bilayers as well as the comparison with GOx/biotin directly adsorbed to NA.

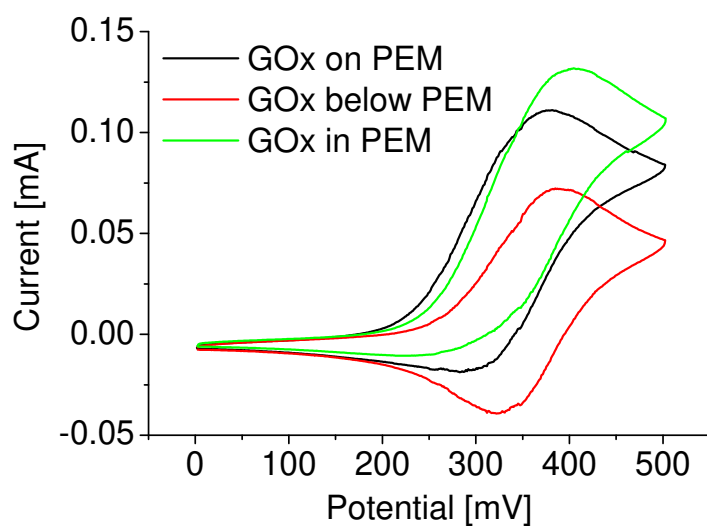


**Figure 6.16:** CV of films where the enzymes were adsorbed either on top of the PEM (black), before adsorbing the polymers (red) or both, two times in between and on top of the film (green). The films consisted of 5 polymeric bilayers.

**Table 6.1:** Frequency and dissipation change of a PEM film with 5 bilayers upon addition of GOx and FC, depending on the order of exposure.

GOx first	Frequency [Hz]	Dissipation [1E-6]
GOx	-569	7.1
FC	690	-24.2
FC first	Frequency [Hz]	Dissipation [1E-6]
FC	162	-11.5
GOx	-28.8	0.6

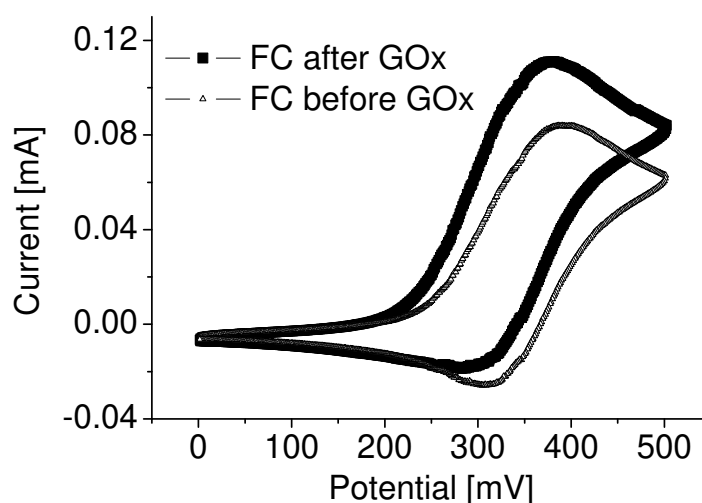


**Figure 6.17:** CV of PEI-(PGA-PAH)<sub>5</sub> films with FC adsorbed before or after GOx binding. The FE concentration was 0.5 mM.

We also investigated whether the order of adsorbing GOx and FC influences the performance of the system. When GOx was adsorbed first, the QCM-D signal was significantly higher (see summary in Table 6.1 for PEI-(PGA-PAH)<sub>5</sub>) and the following FC adsorption also resulted in a higher contraction compared to a film without GOx on top. For an explanation of this observation one needs to keep in mind that both species, GOx and FC, are negatively charged. Thus, when GOx is adsorbed first, a high amount will adhere to the film. The following FC could possibly replace part of the GOx, because both carry negative charges. This thesis is also supported by the fact that the decrease in adsorbed mass and dissipation upon adsorption of FC is much higher for films with GOx molecules on top than for a pure PEM film.

### 6.3 Conclusion

In this chapter we have introduced a platform to reversibly change the thickness of PEM films. We have achieved a similar thickness change as that for EAPs (i.e. up to 10 %) under mild conditions but with a significantly lower reaction time. From the tested polymer combinations, the PGA/PAH films were the only ones to show the ability of swelling and deswelling upon application of a low potential ( $< 600$  mV). The presented results were achieved by incorporating FCIV ions into the film that were subsequently oxidized and reduced during the applied CV. The films reacted immediately to the oxidation and the reduction even at high scan rates of 100 mV/s. During the oxidation of the FCIV ions the film expanded and contracted back to its original thickness during the reduction. According to the results from the EC-QCM-D, the film was less rigid in its expanded state than in the contracted form. The thickness change was also confirmed with an EC-AFM.

GOx was successfully incorporated into PEM films through the electrostatic interaction between the molecules. However, we did not succeed with putting the mediator for the enzymatic reaction into the PEM films. FE, which is required for the enzymatic reaction upon application of CV, did not stay in the film, whereas FC, which stayed in the film, could not be used for CV with GOx.

This new platform at the interface of EAPs and PEM films has the potential for various applications. It could be suitable for cell stretching because of its non cytotoxic components and the mild operating conditions, such as small pH change and low voltages. It might also be used for the creation of smart drug delivery particles which can change their size and/or their permeability upon enzymatic or electrochemical trigger. Because of the flexibility of the film, a possible application could also be the active control of surface topology, e.g. for optical applications.

## CHAPTER 7

---

### Summary

---

In this thesis a variable platform of enzymatic biosensors with various applications has been introduced. Sandwich assays for highly sensitive detection of antigens have been developed and later on combined with enzymes to allow for EC detection. A new type of electroactive PEM films has been introduced and combined with integrated, active enzymes. The buildup of the systems has mainly been followed *in situ* by QCM-D and characterized with EC methods.

The field of enzymatic biosensing has been reviewed in Chapter 1 and the various EC detection methods have been described. Then, the focus was on their combinations with techniques for adsorption measurements, such as QCM-D, SPR, AFM or OWLS. Different surface architectures have been introduced, ranging from EC signal transduction through enzymes to membrane based sensors. Also basic topics such as the reaction principle of enzymes and the role of antibodies in sandwich assays have been addressed. Finally, different possibilities to encapsulate enzymes, such as incorporation into vesicles or PEM capsules, have been discussed.

In Chapter 4 we have developed a high sensitivity biosensor with vesicles for signal amplification. The vesicles, bound to the secondary antibodies, drastically enhanced the signal. Like this, antigen concentrations down to 5 ng/ml or 30 pM could be detected in the QCM-D. Therefore, the dissipation signal was used; the changes in frequency were less sensitive to low amounts of vesicles. From different variations of premixing, the most accurate one has been chosen to decrease the assay time while still maintaining the sensitivity. Even though this system has been proven to work nicely under laboratory conditions, it is expected to suffer from a limited stability in biological samples because

the lipid vesicles are subject to e.g. enzymatic attack. Therefore, we have successfully replaced them with polymeric vesicles which have a better stability, improved non-specific binding and longer shelf-life.

Electrochemical methods, suitable for our biosensors, have been evaluated in Chapter 5 and the corresponding reaction schemes have been introduced. The methods include CV and chronoamperometry with ferrocyanide and ferrocene as mediators. After evaluating the performance with enzymes in solution, vesicles were functionalized with enzymes and adsorbed to NA as a model system in the QCM-D. The performance of this model biosensor was then tested by applying CV with ferrocene (FE) and chronoamperometry with both, ferrocyanide (FC) or FE. Chronoamperometry with FE was not followed any further because of lack of sensitivity. In CV mediator concentrations as low as 30  $\mu\text{M}$  were found to lead to the highest sensitivity.

This knowledge has then been successfully transferred to a sandwich assay with enzyme functionalized vesicles. Detection limits of 1-2 pM (0.2-0.4 ng/ml) and 30 ng/ml NA have been achieved for chronoamperometry with FC and CV with FE, respectively. Especially the former is promising, because it is about 20 times more sensitive than the vesicle amplification system. Also polymeric vesicles with incorporated enzymes have been found to behave accordingly. Feasibility experiments with enzyme functionalized microparticles have also successfully been performed.

Electroactive PEM films have been introduced in Chapter 6. Films consisting of the polyelectrolytes PGA and PAH have been found to show electroactive behaviour. After the film buildup FE ions were incorporated into the film through simple immersion. Within minutes the film was saturated with FE ions. Subsequently applied CV caused the film to swell and contract. With the chosen parameters, about 10 % of swelling due to changes in the ionic structures of the film has been observed. This behaviour occurred immediately and parallel to the oxidation and reduction of the FE ions; there was no delay measurable. Finally, the system has been expanded by adsorbing enzymes on top of the film or as intermediate layer(s). This allowed for synchronically swelling/deswelling the film and performing activity experiments of the enzymes.

Overall, in this thesis a variety of enzymatic biosensors have been developed. Thereby, the main focus has been on sandwich assays to detect low antigen concentrations down to 1 pM, as it was achieved with enzyme functionalized lipid vesicles for electrochemical signal amplification. The development has been made from simple vesicle based signal amplification over an enzymatic model system to the final enzyme enhanced signal

detection. Furthermore, the variation of enzymes combined with electroactive PEM films has been introduced.





### Outlook

---

In this thesis a sandwich-based enzymatic biosensor has been developed. We have shown the proof of principle and achieved promising results in terms of sensitivity, assay time and reliability.

Since in the presented system the limiting factor currently is unspecific binding and not the technique itself, lowering the unspecific adsorption would improve the performance of the sensor (compare Chapter 4). Therefore, more blocking steps or mixing the reagents with BSA might be a solution. Another approach could be the passivation of the surface, with e.g. PEG based polymers. To really estimate the required procedures, one will also need to replace the model antibody-antigen system with a specific, application focussed system.

Through equipping the initial vesicle based biosensor with enzymes for EC detection, the sensor is now prepared for array based testing. Thereby, different antibodies would be adsorbed to individually addressable electrodes in one flowcell. To reduce crosstalk it could also make sense to separate the individual points by using microfluidic channels. Like this, parallel testing for more than just one antigen will be possible. The motivation for this step is a cost reduction as well as a decrease of the required time.

For a commercial application the shelf life of lipid vesicles is likely to be a critical point. In this thesis some approaches into this direction have already been outlined. With both, polymeric vesicles and enzyme coated microparticles, promising results have been achieved. However, especially for the microparticles the protocol still needs to be optimized in terms of preparation (enzyme coverage that still enables binding in the sandwich assay) and size (number of required binding points) of the particles.

Furthermore, it will be necessary to transfer the system from a laboratory environment to an easy to use product for non-trained people. This means having all the components in one small device as well as offering the possibility of an automated readout.

With the electroactive PEM films promising results have been achieved. Due to a limited time frame to investigate this phenomenon, in this thesis only a small fraction of possible parameters could be investigated. Other variations, such as different mediators, other ions in solution, concentrations etc. are only few possibilities of further development. Because of the wide variety of ideas how to improve the performance of such films and to further develop the technique, e.g. with localized swelling, these topics are now being investigated by Raphael Zahn in a separate PhD thesis.

The combination of this system with enzymes has also been looked at in this thesis. At the moment one mediator is used for the swelling/deswelling effect and one for the enzymatic reaction. To simplify the method, it would help to tune it so that one mediator can serve for both, the deformation and the reaction with enzymes. This might even allow for achieving swelling/deswelling behaviour by enzymatically reduce or oxidize the ferrocyanide without applying a potential.

A completely different application of this system could go into the direction of coating other species than flat surfaces or particles, such as e.g. cells. Here the shape deformation could be combined with an enzymatic reaction or other functionalities still to implement into the films.

Another topic that has been mentioned in this thesis is the co-adsorption of proteins on surfaces. Depending on the order and the concentration the adsorbed amounts varied quite a lot, i.e. in some cases after blocking with BSA no binding to the previously adsorbed NA was observed. Some possible explanations have been proposed in this thesis. But to finally conclude what is going on on the surface, more experiments need to be performed. Because of a high number of experiments with different concentrations a microarray system will be more suitable than the QCM-D. This project is continued by Andreas Binkert. This study will give important information about adsorption and detection of low analyte concentrations.

---

## References

---

- [1] Lowe, C. R. Biosensors. *Trends in Biotechnology*, **2**(3), 59–65, 1984.
- [2] Thevenot, D. R., Toth, K., Durst, R. A. and Wilson, G. S. Electrochemical biosensors: recommended definitions and classification. *Biosensors & Bioelectronics*, **16**(1-2), 121–131, 2001.
- [3] Eggins, B. *Chemical sensors and biosensors*. Analytical Techniques in the Sciences. John Wiley & Sons, West Sussex, 2002.
- [4] Chaubey, A. and Malhotra, B. D. Mediated biosensors. *Biosensors & Bioelectronics*, **17**(6-7), 441–456, 2002.
- [5] Kasemo, B. Biological surface science. *Surface Science*, **500**(1-3), 656–677, 2002.
- [6] Lippa, P. B., Sokoll, L. J. and Chan, D. W. Immunosensors - principles and applications to clinical chemistry. *Clinica Chimica Acta*, **314**(1-2), 1–26, 2001.
- [7] Clark, L. C. and Lyons, C. Electrode Systems for Continuous Monitoring in Cardiovascular Surgery. *Annals of the New York Academy of Sciences*, **102**(1), 29, 1962.
- [8] Fang, A. P., Ng, H. T. and Li, S. F. Y. A high-performance glucose biosensor based on monomolecular layer of glucose oxidase covalently immobilised on indium-tin oxide surface. *Biosensors & Bioelectronics*, **19**(1), 43–49, 2003.
- [9] Wilson, M. S. Electrochemical immunosensors for the simultaneous detection of two tumor markers. *Analytical Chemistry*, **77**(5), 1496–1502, 2005.
- [10] D’Orazio, P. Biosensors in clinical chemistry. *Clinica Chimica Acta*, **334**(1-2), 41–69, 2003.
- [11] Schoning, M. J. and Poghossian, A. Recent advances in biologically sensitive field-effect transistors (BioFETs). *Analyst*, **127**(9), 1137–1151, 2002.
- [12] Clark, L. C. Monitor and Control of Blood and Tissue Oxygen Tensions. *Transactions American Society for Artificial Internal Organs*, **2**, 41, 1956.
- [13] Clark, L. C. and Clark, E. W. A Personalized History of the Clark Oxygen-Electrode. *International Anesthesiology Clinics*, **25**(3), 1–29, 1987.

- [14] Wang, J. Glucose biosensors: 40 years of advances and challenges. *Electroanalysis*, **13**(12), 983–988, 2001.
- [15] Mirsky, V. M., Riepl, M. and Wolfbeis, O. S. Capacitive monitoring of protein immobilization and antigen-antibody reactions on monomolecular alkylthiol films on gold electrodes. *Biosensors & Bioelectronics*, **12**(9-10), 977–989, 1997.
- [16] Guiseppi-Elie, A. and Lingerfelt, L. Impedimetric detection of DNA hybridization: Towards near-patient DNA diagnostics. In *Immobilisation of DNA on Chips I*, volume 260 of *Topics in Current Chemistry*, pages 161–186. Springer-Verlag Berlin, Berlin, 2005.
- [17] Ben, A. M., Korpan, Y., Gonchar, M., El'skaya, A., Maaref, M. A., Jaffrezic-Renault, N. and Martelet, C. Formaldehyde assay by capacitance versus voltage and impedance measurements using bi-layer bio-recognition membrane. *Biosensors & Bioelectronics*, **22**(5), 575–581, 2006.
- [18] Mehrvar, M. and Abdi, M. Recent developments, characteristics, and potential applications of electrochemical biosensors. *Analytical Sciences*, **20**(8), 1113–1126, 2004.
- [19] Patolsky, F., Zheng, G. F. and Lieber, C. M. Nanowire-based biosensors. *Analytical Chemistry*, **78**(13), 4260–4269, 2006.
- [20] Nair, P. and Alam, M. Dimensionally Frustrated Diffusion towards Fractal Adsorbers. *Physical Review Letters*, **99**(25), 256101, 2007.
- [21] Merkoci, A. Electrochemical biosensing with nanoparticles. *Febs Journal*, **274**(2), 310–316, 2007.
- [22] Park, S. J., Taton, T. A. and Mirkin, C. A. Array-based electrical detection of DNA with nanoparticle probes. *Science*, **295**(5559), 1503–1506, 2002.
- [23] Wanekaya, A. K., Chen, W., Myung, N. V. and Mulchandani, A. Nanowire-based electrochemical biosensors. *Electroanalysis*, **18**(6), 533–550, 2006.
- [24] Stadler, B., Solak, H. H., Frerker, S., Bonroy, K., Frederix, F., Voros, J. and Grandin, H. M. Nanopatterning of gold colloids for label-free biosensing. *Nanotechnology*, **18**(15), 6, 2007.
- [25] Heyrovsky, J. The Development of Polarographic Analysis. *Analyst*, **81**(961), 189, 1956.
- [26] Katz, E. and Willner, I. Probing biomolecular interactions at conductive and semiconductive surfaces by impedance spectroscopy: Routes to impedimetric immunosensors, DNA-Sensors, and enzyme biosensors. *Electroanalysis*, **15**(11), 913–947, 2003.
- [27] Pei, R. J., Cheng, Z. L., Wang, E. K. and Yang, X. R. Amplification of antigen-antibody interactions based on biotin labeled protein-streptavidin network complex using impedance spectroscopy. *Biosensors & Bioelectronics*, **16**(6), 355–361, 2001.
- [28] Liu, Y., Yuan, R., Chai, Y. Q., Tang, D. P., Dai, J. Y. and Zhong, X. Direct electrochemistry of horseradish peroxidase immobilized on gold colloid/cysteine/nafion-modified platinum disk electrode. *Sensors and Actuators B-Chemical*, **115**(1), 109–115, 2006.
- [29] Patolsky, F., Zayats, M., Katz, E. and Willner, I. Precipitation of an insoluble product on enzyme monolayer electrodes for biosensor applications: Characterization by faradaic impedance spectroscopy, cyclic voltammetry, and microgravimetric quartz crystal microbalance analyses. *Analytical Chemistry*, **71**(15), 3171–3180, 1999.
- [30] Bakker, E. and Pretsch, E. Potentiometric sensors for trace-level analysis. *Trac-Trends in Analytical Chemistry*, **24**(3), 199–207, 2005.

- 
- [31] Lorenz, W. and Schulze, K. D. Application of Transform-Impedance Spectrometry. *Journal of Electroanalytical Chemistry*, **65**(1), 141–153, 1975.
- [32] Willner, I. and Katz, E. e. *Bioelectronics*. Wiley-VCH, 1st edition, 2005.
- [33] Tlili, A., Abdelghani, A., Ameer, S. and Jaffrezic-Renault, N. Impedance spectroscopy and affinity measurement of specific antibody-antigen interaction. *Materials Science & Engineering C-Biomimetic and Supramolecular Systems*, **26**(2-3), 546–550, 2006.
- [34] Horenstein, M. *Microelectronic Circuits and Devices*. Prentice-Hall, Englewood Cliffs, 1990.
- [35] Lieber, C. M. and Wang, Z. L. Functional nanowires. *Mrs Bulletin*, **32**(2), 99–108, 2007.
- [36] Tansil, N. C. and Gao, Z. Q. Nanoparticles in biomolecular detection. *Nano Today*, **1**(1), 28–37, 2006.
- [37] Xiao, Y., Patolsky, F., Katz, E., Hainfeld, J. F. and Willner, I. Plugging into enzymes: Nanowiring of redox enzymes by a gold nanoparticle. *Science*, **299**(5614), 1877–1881, 2003.
- [38] Wang, D. H., Kou, R., Gil, M. P., Jakobson, H. P., Tang, J., Yu, D. H. and Lu, Y. F. Templated synthesis, characterization, and sensing application of macroscopic platinum nanowire network electrodes. *Journal of Nanoscience and Nanotechnology*, **5**(11), 1904–1909, 2005.
- [39] Patolsky, F., Timko, B. P., Zheng, G. F. and Lieber, C. M. Nanowire-based nanoelectronic devices in the life sciences. *Mrs Bulletin*, **32**(2), 142–149, 2007.
- [40] Zheng, G. F., Patolsky, F., Cui, Y., Wang, W. U. and Lieber, C. M. Multiplexed electrical detection of cancer markers with nanowire sensor arrays. *Nature Biotechnology*, **23**(10), 1294–1301, 2005.
- [41] Yeh, J. I., Zimmt, M. B. and Zimmerman, A. L. Nanowiring of a redox enzyme by metallized peptides. *Biosensors & Bioelectronics*, **21**(6), 973–978, 2005.
- [42] Arwin, H., Poksinski, M. and Johansen, K. Total internal reflection ellipsometry: principles and applications. *Applied Optics*, **43**(15), 3028–3036, 2004.
- [43] Elwing, H. Protein absorption and ellipsometry in biomaterial research. *Biomaterials*, **19**(4-5), 397–406, 1998.
- [44] Goodall, D. G., Stevens, G. W., Beaglehole, D. and Gee, M. L. Imaging ellipsometry reflectometry for profiling the shape of a deformable droplet as it approaches an interface. *Langmuir*, **15**(13), 4579–4583, 1999.
- [45] Pattnaik, P. Surface plasmon resonance - Applications in understanding receptor-ligand interaction. *Applied Biochemistry and Biotechnology*, **126**(2), 79–92, 2005.
- [46] McDonnell, J. M. Surface plasmon resonance: towards an understanding of the mechanisms of biological molecular recognition. *Current Opinion in Chemical Biology*, **5**(5), 572–577, 2001.
- [47] Liedberg, B., Nylander, C. and Lundstrom, I. Biosensing with Surface-Plasmon Resonance - How It All Started. *Biosensors & Bioelectronics*, **10**(8), R1–R9, 1995.
- [48] Campagnolo, C., Meyers, K. J., Ryan, T., Atkinson, R. C., Chen, Y. T., Scanlan, M. J., Ritter, G., Old, L. J. and Batt, C. A. Real-Time, label-free monitoring, of tumor antigen and serum antibody interactions. *Journal of Biochemical and Biophysical Methods*, **61**(3), 283–298, 2004.

- [49] Jung, L. S., Campbell, C. T., Chinowsky, T. M., Mar, M. N. and Yee, S. S. Quantitative interpretation of the response of surface plasmon resonance sensors to adsorbed films. *Langmuir*, **14**(19), 5636–5648, 1998.
- [50] De Feijter, J., Benjamins, J. and Veer, V. Ellipsometry as a Tool to Study the Adsorption Behaviour of Synthetic and Biopolymers at the Air-Water Interface. *Biopolymers*, **17**(7), 1759–1772, 1978.
- [51] Voros, J., Ramsden, J. J., Csucs, G., Szendro, I., De Paul, S. M., Textor, M. and Spencer, N. D. Optical grating coupler biosensors. *Biomaterials*, **23**(17), 3699–3710, 2002.
- [52] Georgiadis, R., Peterlinz, K. P. and Peterson, A. W. Quantitative measurements and modeling of kinetics in nucleic acid monolayer films using SPR spectroscopy. *Journal of the American Chemical Society*, **122**(13), 3166–3173, 2000.
- [53] Heaton, R. J., Peterson, A. W. and Georgiadis, R. M. Electrostatic surface plasmon resonance: Direct electric field-induced hybridization and denaturation in monolayer nucleic acid films and label-free discrimination of base mismatches. *Proceedings of the National Academy of Sciences of the United States of America*, **98**(7), 3701–3704, 2001.
- [54] Mullett, W. M., Lai, E. P. C. and Yeung, J. M. Surface plasmon resonance-based immunoassays. *Methods*, **22**(1), 77–91, 2000.
- [55] Lavers, C. R., Harris, R. D., Hao, S., Wilkinson, J. S., Odwyer, K., Brust, M. and Schiffrin, D. J. Electrochemically-Controlled Wave-Guide-Coupled Surface-Plasmon Sensing. *Journal of Electroanalytical Chemistry*, **387**(1-2), 11–22, 1995.
- [56] Badia, A., Arnold, S., Scheumann, V., Zizlsperger, M., Mack, J., Jung, G. and Knoll, W. Probing the electrochemical deposition and/or desorption of self-assembled and electropolymerizable organic thin films by surface plasmon spectroscopy and atomic force microscopy. *Sensors and Actuators B-Chemical*, **54**(1-2), 145–165, 1999.
- [57] Baba, A., Park, M. K., Advincula, R. C. and Knoll, W. Simultaneous surface plasmon optical and electrochemical investigation of layer-by-layer self-assembled conducting ultrathin polymer films. *Langmuir*, **18**(12), 4648–4652, 2002.
- [58] Peterlinz, K. A. and Georgiadis, R. In situ kinetics of self-assembly by surface plasmon resonance spectroscopy. *Langmuir*, **12**(20), 4731–4740, 1996.
- [59] Kurrat, R., Textor, M., Ramsden, J. J., Boni, P. and Spencer, N. D. Instrumental improvements in optical waveguide light mode spectroscopy for the study of biomolecule adsorption. *Review of Scientific Instruments*, **68**(5), 2172–2176, 1997.
- [60] Bearinger, J. P., Voros, J., Hubbell, J. A. and Textor, M. Electrochemical optical waveguide light-mode spectroscopy (EC-OWLS): A pilot study using evanescent-field optical sensing under voltage control to monitor polycationic polymer adsorption onto indium tin oxide (ITO)-coated waveguide chips. *Biotechnology and Bioengineering*, **82**(4), 465–473, 2003.
- [61] Brusatori, M. A. and Van Tassel, P. R. Biosensing under an applied voltage using optical waveguide lightmode spectroscopy. *Biosensors & Bioelectronics*, **18**(10), 1269–1277, 2003.
- [62] Ying, P. Q., Viana, A. S., Abrantes, L. M. and Jin, G. Adsorption of human serum albumin onto gold: a combined electrochemical and ellipsometric study. *Journal of Colloid and Interface Science*, **279**(1), 95–99, 2004.

- [63] Wang, Z. H., Viana, A. S., Jin, G. and Abrantes, L. M. Immunosensor interface based on physical and chemical immunoglobulin G adsorption onto mixed self-assembled monolayers. *Bioelectrochemistry*, **69**(2), 180–186, 2006.
- [64] Marx, K. Quartz Crystal Microbalance: A Useful Tool for Studying Thin Polymer Films and Complexes Biomolecular Systems at the Solution-Surface Interface. *Bio Macromolecules*, **4**(5), 1099–1120, 2002.
- [65] Wang, J., Rivas, G., Jiang, M. A. and Zhang, X. J. Electrochemically induced release of DNA from gold ultramicroelectrodes. *Langmuir*, **15**(19), 6541–6545, 1999.
- [66] Hook, F., Rodahl, M., Brzezinski, P. and Kasemo, B. Measurements using the quartz crystal microbalance technique of ferritin monolayers on methyl-thiolated gold: Dependence of energy dissipation and saturation coverage on salt concentration. *Journal of Colloid and Interface Science*, **208**(1), 63–67, 1998.
- [67] Hook, F., Voros, J., Rodahl, M., Kurrat, R., Boni, P., Ramsden, J. J., Textor, M., Spencer, N. D., Tengvall, P., Gold, J. and Kasemo, B. A comparative study of protein adsorption on titanium oxide surfaces using in situ ellipsometry, optical waveguide lightmode spectroscopy, and quartz crystal microbalance/dissipation. *Colloids and Surfaces B-Biointerfaces*, **24**(2), 155–170, 2002.
- [68] Dong, W. F., Ferri, J. K., Adalsteinsson, T., Schonhoff, M., Sukhorukov, G. B. and Mohwald, H. Influence of shell structure on stability, integrity, and mesh size of polyelectrolyte capsules: Mechanism and strategy for improved preparation. *Chemistry of Materials*, **17**(10), 2603–2611, 2005.
- [69] Schumacher, R. The Quartz Microbalance - a Novel-Approach to the Insitu Investigation of Interfacial Phenomena at the Solid Liquid Junction. *Angewandte Chemie-International Edition in English*, **29**(4), 329–343, 1990.
- [70] Beissenhirtz, M. K., Kafka, B., Schafer, D., Wolny, M. and Lisdat, F. Electrochemical quartz crystal microbalance studies on cytochrome c/polyelectrolyte multilayer assemblies on gold electrodes. *Electroanalysis*, **17**(21), 1931–1937, 2005.
- [71] Bott, A. Characterization of Films Immobilized on an Electrode Surface Using the Electrochemical Quartz Crystal Microbalance. *Current Separation*, **18**(3), 79–83, 1999.
- [72] Binnig, G. and Rohrer, H. Scanning Tunneling Microscopy. *Helvetica Physica Acta*, **55**(6), 726–735, 1982.
- [73] Binnig, G. and Rohrer, H. Scanning Tunneling Microscopy. *Ibm Journal of Research and Development*, **30**(4), 355–369, 1986.
- [74] Bae, S. E. and Gewirth, A. A. In situ EC-STM studies of MPS, SPS, and chloride on Cu(100): Structural studies of accelerators for dual damascene electrodeposition. *Langmuir*, **22**(25), 10315–10321, 2006.
- [75] Colton, R. J., Baselt, D. R., Dufrene, Y. F., Green, J. B. D. and Lee, G. U. Scanning probe microscopy. *Current Opinion in Chemical Biology*, **1**(3), 370–377, 1997.
- [76] Binnig, G., Quate, C. F. and Gerber, C. Atomic Force Microscope. *Physical Review Letters*, **56**(9), 930–933, 1986.
- [77] Rugar, D. and Hansma, P. Atomic Force Microscopy. *Physics Today*, **43**(10), 23–30, 1990.
- [78] Jalili, N. and Laxminarayana, K. A review of atomic force microscopy imaging systems: application to molecular metrology and biological sciences. *Mechatronics*, **14**(8), 907–945, 2004.

- [79] Bergamini, J. F., Ghilane, J., Guilloux-Viry, M. and Hapiot, P. In situ EC-AFM imaging of cathodic modifications of platinum surfaces performed in dimethylformamide. *Electrochemistry Communications*, **6**(2), 188–192, 2004.
- [80] Yamaguchi, Y., Shiota, M., Nakayama, Y., Hirai, N. and Hara, S. Combined in situ EC-AFM and CV measurement study on lead electrode for lead-acid batteries. *Journal of Power Sources*, **93**(1-2), 104–111, 2001.
- [81] Bard, A. J., Fan, F. R. F., Kwak, J. and Lev, O. Scanning Electrochemical Microscopy - Introduction and Principles. *Analytical Chemistry*, **61**(2), 132–138, 1989.
- [82] Kwak, J. and Bard, A. J. Scanning Electrochemical Microscopy - Apparatus and Two-Dimensional Scans of Conductive and Insulating Substrates. *Analytical Chemistry*, **61**(17), 1794–1799, 1989.
- [83] Kwak, J. and Bard, A. J. Scanning Electrochemical Microscopy - Theory of the Feedback Mode. *Analytical Chemistry*, **61**(11), 1221–1227, 1989.
- [84] Sun, P., Laforge, F. O. and Mirkin, M. V. Scanning electrochemical microscopy in the 21st century. *Physical Chemistry Chemical Physics*, **9**(7), 802–823, 2007.
- [85] Amemiya, S., Guo, J. D., Xiong, H. and Gross, D. A. Biological applications of scanning electrochemical microscopy: chemical imaging of single living cells and beyond. *Analytical and Bioanalytical Chemistry*, **386**(3), 458–471, 2006.
- [86] Kueng, A., Kranz, C. and Mizaikoff, B. Imaging of ATP membrane transport with dual micro-disk electrodes and scanning electrochemical microscopy. *Biosensors & Bioelectronics*, **21**(2), 346–353, 2005.
- [87] Macpherson, J. V. and Unwin, P. R. Combined scanning electrochemical-atomic force microscopy. *Analytical Chemistry*, **72**(2), 276–285, 2000.
- [88] Macpherson, J. V. and Unwin, P. R. Noncontact electrochemical imaging with combined scanning electrochemical atomic force microscopy. *Analytical Chemistry*, **73**(3), 550–557, 2001.
- [89] Kueng, A., Kranz, C., Lugstein, A., Bertagnolli, E. and Mizaikoff, B. AFM-tip-integrated amperometric microbiosensors: High-resolution imaging of membrane transport. *Angewandte Chemie-International Edition*, **44**(22), 3419–3422, 2005.
- [90] Kueng, A., Kranz, C., Lugstein, A., Bertagnolli, E. and Mizaikoff, B. Integrated AFM-SECM in tapping mode: Simultaneous topographical and electrochemical imaging of enzyme activity. *Angewandte Chemie-International Edition*, **42**(28), 3238–3240, 2003.
- [91] Kranz, C., Kueng, A., Lugstein, A., Bertagnolli, E. and Mizaikoff, B. Mapping of enzyme activity by detection of enzymatic products during AFM imaging with integrated SECM-AFM probes. *Ultramicroscopy*, **100**(3-4), 127–134, 2004.
- [92] Pavlickova, P., Schneider, E. M. and Hug, H. Advances in recombinant antibody microarrays. *Clinica Chimica Acta*, **343**(1-2), 17–35, 2004.
- [93] Lin, J. H. and Ju, H. X. Electrochemical and chemiluminescent immunosensors for tumor markers. *Biosensors & Bioelectronics*, **20**(8), 1461–1470, 2005.
- [94] Dai, Z., Yan, F., Hua, Y., Hu, X. Y. and Ju, H. X. Novel amperometric immunosensor for rapid separation-free immunoassay of carcinoembryonic antigen. *Journal of Immunological Methods*, **287**(1-2), 13–20, 2004.



- [95] Yang, L. J. and Li, Y. B. AFM and impedance spectroscopy characterization of the immobilization of antibodies on indium-tin oxide electrode through self-assembled monolayer of epoxysilane and their capture of *Escherichia coli* O157 : H7. *Biosensors & Bioelectronics*, **20**(7), 1407–1416, 2005.
- [96] Zhang, Y. Y., Fung, Y. S., Sun, H., Zhu, D. R. and Yao, S. Z. Study of protein adsorption on polymer coatings surface by combining quartz crystal microbalance with electrochemical impedance methods. *Sensors and Actuators B-Chemical*, **108**(1-2), 933–942, 2005.
- [97] Wink, T., van Zuilen, S., Bult, A. and van Bennekom, W. Self-assembled Monolayers for Biosensors. *Analyst*, **122**, 1997.
- [98] Pan, D. W., Chen, J. H., Yao, S. Z., Tao, W. Y. and Nie, L. H. An amperometric glucose biosensor based on glucose oxidase immobilized in electropolymerized poly(o-aminophenol) and carbon nanotubes composite film on a gold electrode. *Analytical Sciences*, **21**(4), 367–371, 2005.
- [99] Sotiropoulou, S. and Chaniotakis, N. A. Carbon nanotube array-based biosensor. *Analytical and Bioanalytical Chemistry*, **375**(1), 103–105, 2003.
- [100] Mena, M. L., Yanez-Sedeno, P. and Pingarron, J. M. A comparison of different strategies for the construction of amperometric enzyme biosensors using gold nanoparticle-modified electrodes. *Analytical Biochemistry*, **336**(1), 20–27, 2005.
- [101] Bauer, L. A., Birenbaum, N. S. and Meyer, G. J. Biological applications of high aspect ratio nanoparticles. *Journal of Materials Chemistry*, **14**(4), 517–526, 2004.
- [102] Yu, Y. Y., Chang, S. S., Lee, C. L. and Wang, C. R. C. Gold nanorods: Electrochemical synthesis and optical properties. *Journal of Physical Chemistry B*, **101**(34), 6661–6664, 1997.
- [103] Yi, G. C., Wang, C. R. and Park, W. I. ZnO nanorods: synthesis, characterization and applications. *Semiconductor Science and Technology*, **20**(4), S22–S34, 2005.
- [104] Kuznetsov, B. A., Shumakovich, G. P., Koroleva, O. V. and Yaropolov, A. I. On applicability of laccase as label in the mediated and mediatorless electroimmunoassay: effect of distance on the direct electron transfer between laccase and electrode. *Biosensors & Bioelectronics*, **16**(1-2), 73–84, 2001.
- [105] Ghindilis, A. L., Atanasov, P. and Wilkins, E. Enzyme-catalyzed direct electron transfer: Fundamentals and analytical applications. *Electroanalysis*, **9**(9), 661–674, 1997.
- [106] Patolsky, F., Weizmann, Y. and Willner, I. Long-range electrical contacting of redox enzymes by SWCNT connectors. *Angewandte Chemie-International Edition*, **43**(16), 2113–2117, 2004.
- [107] Alberts, B., Johnson, A., Lewis, J., Raff, M., Roberts, K. and Walter, P. *Molecular Biology of the Cell*. 2nd edition, 2002.
- [108] Heller, A. Amperometric biosensors. *Current Opinion in Biotechnology*, **7**(1), 50–54, 1996.
- [109] Azevedo, A., Martins, V., Prazeres, D., Vojinovic, V., Cabral, J. and Fonseca, L. Horseradish peroxidase: a valuable tool in biotechnology. *Biotechnology annual review*, **9**, 199–247, 2003.
- [110] Zhen, G. L., Egli, V., Voros, J., Zammaretti, P., Textor, M., Glockshuber, R. and Kuennemann, E. Immobilization of the enzyme beta-lactamase on biotin-derivatized poly(L-lysine)-g-poly(ethylene glycol)-coated sensor chips: A study on oriented attachment and surface activity by enzyme kinetics and in situ optical sensing. *Langmuir*, **20**(24), 10464–10473, 2004.

- [111] Chaniotakis, N. A. Enzyme stabilization strategies based on electrolytes and polyelectrolytes for biosensor applications. *Analytical and Bioanalytical Chemistry*, **378**(1), 89–95, 2004.
- [112] O’Fagain, C. Enzyme stabilization - recent experimental progress. *Enzyme and Microbial Technology*, **33**(2-3), 137–149, 2003.
- [113] Grieshaber, D., Reimhult, E. and Voros, J. Enzymatic Biosensors towards a Multiplexed Electronic Detection System for Early Cancer Diagnostics. In *2nd IEEE-NEMS*, volume 1, pages 402–405, Bangkok, 2007.
- [114] Sotiropoulou, S., Vamvakaki, V. and Chaniotakis, N. A. Stabilization of enzymes in nanoporous materials for biosensor applications. *Biosensors & Bioelectronics*, **20**(8), 1674–1679, 2005.
- [115] Sung, W. J. and Bae, Y. H. Glucose oxidase, lactate oxidase, and galactose oxidase enzyme electrode based on polypyrrole with polyanion/PEG/enzyme conjugate dopant. *Sensors and Actuators B-Chemical*, **114**(1), 164–169, 2006.
- [116] Kim, J., Grate, J. W. and Wang, P. Nanostructures for enzyme stabilization. *Chemical Engineering Science*, **61**(3), 1017–1026, 2006.
- [117] Lu, B., Smyth, M. R. and OKennedy, R. Oriented immobilization of antibodies and its applications in immunoassays and immunosensors. *Analyst*, **121**(3), R29–R32, 1996.
- [118] LaGraff, J. R. and Chu-LaGraff, Q. Scanning force microscopy and fluorescence microscopy of microcontact printed antibodies and antibody fragments. *Langmuir*, **22**(10), 4685–4693, 2006.
- [119] Wacker, R., Schroder, H. and Niemeyer, C. M. Performance of antibody microarrays fabricated by either DNA-directed immobilization, direct spotting, or streptavidin-biotin attachment: a comparative study. *Analytical Biochemistry*, **330**(2), 281–287, 2004.
- [120] Peluso, P., Wilson, D. S., Do, D., Tran, H., Venkatasubbaiah, M., Quincy, D., Heidecker, B., Poindexter, K., Tolani, N., Phelan, M., Witte, K., Jung, L. S., Wagner, P. and Nock, S. Optimizing antibody immobilization strategies for the construction of protein microarrays. *Analytical Biochemistry*, **312**(2), 113–124, 2003.
- [121] Padeste, C., Grubelnik, A., Steiger, B., Hefti, J. and Tiefenauer, L. Molecular architectures for enzyme sensors. Technical report, 2001.
- [122] Zacco, E., Pividori, M. I. and Alegret, S. Electrochemical biosensing based on universal affinity biocomposite platforms. *Biosensors & Bioelectronics*, **21**(7), 1291–1301, 2006.
- [123] Danczyk, R., Krieder, B., North, A., Webster, T., HogenEsch, H. and Rundell, A. Comparison of antibody functionality using different immobilization methods. *Biotechnology and Bioengineering*, **84**(2), 215–223, 2003.
- [124] Nielsen, U. B. and Geierstanger, B. H. Multiplexed sandwich assays in microarray format. *Journal of Immunological Methods*, **290**(1-2), 107–120, 2004.
- [125] Sarkar, P., Pal, P. S., Ghosh, D., Setford, S. J. and Tothill, I. E. Amperometric biosensors for detection of the prostate cancer marker (PSA). *International Journal of Pharmaceutics*, **238**(1-2), 1–9, 2002.
- [126] Haab, B. B. Applications of antibody array platforms. *Current Opinion in Biotechnology*, **17**(4), 415–421, 2006.
- [127] Peterson, J., Green, G., Iida, K., Caldwell, B., Kerrison, P., Bernich, S., Aoyagi, K. and Lee, S. R. Detection of hepatitis C core antigen in the antibody negative ‘window’ phase of hepatitis C infection. *Vox Sanguinis*, **78**(2), 80–85, 2000.

- 
- [128] Holliger, P. and Hudson, P. J. Engineered antibody fragments and the rise of single domains. *Nature Biotechnology*, **23**(9), 1126–1136, 2005.
- [129] Hamerscasterman, C., Atarhouch, T., Muyldermans, S., Robinson, G., Hamers, C., Songa, E. B., Bendahman, N. and Hamers, R. Naturally-Occurring Antibodies Devoid of Light-Chains. *Nature*, **363**(6428), 446–448, 1993.
- [130] Vikholm, I. Self-assembly of antibody fragments and polymers onto gold for immunosensing. *Sensors and Actuators B-Chemical*, **106**(1), 311–316, 2005.
- [131] Ellington, A. D. and Szostak, J. W. In vitro Selection of Rna Molecules That Bind Specific Ligands. *Nature*, **346**(6287), 818–822, 1990.
- [132] Tuerk, C. and Gold, L. Systematic Evolution of Ligands by Exponential Enrichment - Rna Ligands to Bacteriophage-T4 DNA-Polymerase. *Science*, **249**(4968), 505–510, 1990.
- [133] Tombelli, S., Minunni, A. and Mascini, A. Analytical applications of aptamers. *Biosensors & Bioelectronics*, **20**(12), 2424–2434, 2005.
- [134] O’Sullivan, C. K. Aptasensors - the future of biosensing. *Analytical and Bioanalytical Chemistry*, **372**(1), 44–48, 2002.
- [135] Caruso, F., Caruso, R. A. and Mohwald, H. Nanoengineering of inorganic and hybrid hollow spheres by colloidal templating. *Science*, **282**(5391), 1111–1114, 1998.
- [136] Donath, E., Sukhorukov, G. B., Caruso, F., Davis, S. A. and Mohwald, H. Novel hollow polymer shells by colloid-templated assembly of polyelectrolytes. *Angewandte Chemie-International Edition*, **37**(16), 2202–2205, 1998.
- [137] Antipov, A. A. and Sukhorukov, G. B. Polyelectrolyte multilayer capsules as vehicles with tunable permeability. *Advances in Colloid and Interface Science*, **111**(1-2), 49–61, 2004.
- [138] Heuberger, R., Sukhorukov, G., Voros, J., Textor, M. and Mohwald, H. Biofunctional polyelectrolyte multilayers and microcapsules: Control of non-specific and bio-specific protein adsorption. *Advanced Functional Materials*, **15**(3), 357–366, 2005.
- [139] Gao, C. Y., Liu, X. Y., Shen, J. C. and Mohwald, H. Spontaneous deposition of horseradish peroxidase into polyelectrolyte multilayer capsules to improve its activity and stability. *Chemical Communications*, **1**(17), 1928–1929, 2002.
- [140] Volodkin, D. V., Petrov, A. I., Prevot, M. and Sukhorukov, G. B. Matrix polyelectrolyte microcapsules: New system for macromolecule encapsulation. *Langmuir*, **20**(8), 3398–3406, 2004.
- [141] Walde, P. and Ichikawa, S. Enzymes inside lipid vesicles: Preparation, reactivity and applications. *Biomolecular Engineering*, **18**(4), 143–177, 2001.
- [142] Nasseau, M., Boublik, Y., Meier, W., Winterhalter, M. and Fournier, D. Substrate-permeable encapsulation of enzymes maintains effective activity, stabilizes against denaturation, and protects against proteolytic degradation. *Biotechnology and Bioengineering*, **75**(5), 615–618, 2001.
- [143] Winterhalter, M., Hilty, C., Bezrukov, S. M., Nardin, C., Meier, W. and Fournier, D. Controlling membrane permeability with bacterial porins: application to encapsulated enzymes. *Talanta*, **55**(5), 965–971, 2001.
- [144] Hill, K. J., Kaszuba, M., Creeth, J. E. and Jones, M. N. Reactive liposomes encapsulating a glucose oxidase-peroxidase system with antibacterial activity. *Biochimica Et Biophysica Acta-Biomembranes*, **1326**(1), 37–46, 1997.

- [145] Nardin, C., Hirt, T., Leukel, J. and Meier, W. Polymerized ABA triblock copolymer vesicles. *Langmuir*, **16**(3), 1035–1041, 2000.
- [146] Broz, P., Benito, S. M., Saw, C., Burger, P., Heider, H., Pfisterer, M., Marsch, S., Meier, W. and Hunziker, P. Cell targeting by a generic receptor-targeted polymer nanocontainer platform. *Journal of Controlled Release*, **102**(2), 475–488, 2005.
- [147] Meier, W., Nardin, C. and Winterhalter, M. Reconstitution of channel proteins in (polymerized) ABA triblock copolymer membranes. *Angewandte Chemie-International Edition*, **39**(24), 4599, 2000.
- [148] Nardin, C., Thoeni, S., Widmer, J., Winterhalter, M. and Meier, W. Nanoreactors based on (polymerized) ABA-triblock copolymer vesicles. *Chemical Communications*, **15**, 1433–1434, 2000.
- [149] Nardin, C., Widmer, J., Winterhalter, M. and Meier, W. Amphiphilic block copolymer nanocontainers as bioreactors. *European Physical Journal E*, **4**(4), 403–410, 2001.
- [150] Torchilin, V. P. PEG-based micelles as carriers of contrast agents for different imaging modalities. *Advanced Drug Delivery Reviews*, **54**(2), 235–252, 2002.
- [151] Torchilin, V. P. Targeted polymeric micelles for delivery of poorly soluble drugs. *Cellular and Molecular Life Sciences*, **61**, 2549–2559, 2004.
- [152] Gaucher, G., Dufresne, M. H., Sant, V. P., Kang, N., Maysinger, D. and Leroux, J. C. Block copolymer micelles: preparation, characterization and application in drug delivery. *Journal of Controlled Release*, **109**(1-3), 169–188, 2005.
- [153] Thurmond, K. B., Huang, H. Y., Clark, C. G., Kowalewski, T. and Wooley, K. L. Shell cross-linked polymer micelles: stabilized assemblies with great versatility and potential. *Colloids and Surfaces B-Biointerfaces*, **16**(1-4), 45–54, 1999.
- [154] Harada, A. and Kataoka, K. Novel polyion complex micelles entrapping enzyme molecules in the core: Preparation of narrowly-distributed micelles from lysozyme and poly(ethylene glycol)-poly(aspartic acid) block copolymer in aqueous medium. *Macromolecules*, **31**(2), 288–294, 1998.
- [155] Harada, A. and Kataoka, K. Pronounced activity of enzymes through the incorporation into the core of polyion complex micelles made from charged block copolymers. *Journal of Controlled Release*, **72**(1-3), 85–91, 2001.
- [156] Heller, A. Electrical Connection of Enzyme Redox Centers to Electrodes. *Journal of Physical Chemistry*, **96**(9), 3579–3587, 1992.
- [157] Dong, S. J. and Guo, Y. Z. Organic-Phase Enzyme Electrode Operated in Water-Free Solvents. *Analytical Chemistry*, **66**(22), 3895–3899, 1994.
- [158] Mano, N., Mao, F. and Heller, A. On the parameters affecting the characteristics of the "wired" glucose oxidase anode. *Journal of Electroanalytical Chemistry*, **574**(2), 347–357, 2005.
- [159] Mitala, J. J. and Michael, A. C. Improving the performance of electrochemical microsensors based on enzymes entrapped in a redox hydrogel. *Analytica Chimica Acta*, **556**(2), 326–332, 2006.
- [160] Mao, F., Mano, N. and Heller, A. Long tethers binding redox centers to polymer backbones enhance electron transport in enzyme "wiring" hydrogels. *Journal of the American Chemical Society*, **125**(16), 4951–4957, 2003.
- [161] Braun, S., Rappoport, S., Zusman, R., Avnir, D. and Ottolenghi, M. Biochemically Active Sol-Gel Glasses - the Trapping of Enzymes. *Materials Letters*, **10**(1-2), 1–5, 1990.

- [162] Avnir, D., Coradin, T., Lev, O. and Livage, J. Recent bio-applications of sol-gel materials. *Journal of Materials Chemistry*, **16**(11), 1013–1030, 2006.
- [163] Jin, W. and Brennan, J. D. Properties and applications of proteins encapsulated within sol-gel derived materials. *Analytica Chimica Acta*, **461**(1), 1–36, 2002.
- [164] Lei, C. X., Hu, S. Q., Gao, N., Shen, G. L. and Yu, R. Q. An amperometric hydrogen peroxide biosensor based on immobilizing horseradish peroxidase to a nano-Au monolayer supported by sol-gel derived carbon ceramic electrode. *Bioelectrochemistry*, **65**(1), 33–39, 2004.
- [165] Trojanowicz, M. Miniaturized biochemical sensing devices based on planar bilayer lipid membranes. *Fresenius Journal of Analytical Chemistry*, **371**(2), 246–260, 2001.
- [166] Xu, J., Wang, X. B., Ensign, B., Li, M., Wu, L., Guia, A. and Xu, J. Q. Ion-channel assay technologies: quo vadis? *Drug Discovery Today*, **6**(24), 1278–1287, 2001.
- [167] Howard, A. D., McAllister, G., Feighner, S. D., Liu, Q. Y., Nargund, R. P., Van der Ploeg, L. H. T. and Patchett, A. A. Orphan G-protein-coupled receptors and natural ligand discovery. *Trends in Pharmacological Sciences*, **22**(3), 132–140, 2001.
- [168] Schmitt, E., Nurbani, M., Bushby, R. and Steinem, C. Electrically insulating pore-suspending membranes on highly ordered porous alumina obtained from vesicle spreading. *Soft Matter*, **4**, 250–253, 2008.
- [169] Han, X., DiBernardino, M., Studer, A., Sehr, H., Geissbühler, I., Winkler, F. and Tiefenauer, L. Nanopore arrays for stable and functional free-standing lipid bilayers. *Advanced Materials*, **19**, 4466–4470, 2007.
- [170] Reimhult, E. and Kumar, K. Membrane biosensor platforms using nano- and microporous supports. *Trends in Biotechnology*, **26**(2), 82–89, 2008.
- [171] Castellana, E. T. and Cremer, P. S. Solid supported lipid bilayers: From biophysical studies to sensor design. *Surface Science Reports*, **61**(10), 429–444, 2006.
- [172] Ide, T. and Ichikawa, T. A novel method for artificial lipid-bilayer formation. *Biosensors & Bioelectronics*, **21**(4), 672–677, 2005.
- [173] Janshoff, A. and Steinem, C. Transport across artificial membranes - an analytical perspective. *Analytical and Bioanalytical Chemistry*, **385**(3), 433–451, 2006.
- [174] Sackmann, E. Supported membranes: Scientific and practical applications. *Science*, **271**(5245), 43–48, 1996.
- [175] Lang, H., Duschl, C. and Vogel, H. A New Class of Thiolipids for the Attachment of Lipid Bilayers on Gold Surfaces. *Langmuir*, **10**(1), 197–210, 1994.
- [176] Naumann, R., Schiller, S. M., Giess, F., Grohe, B., Hartman, K. B., Karcher, I., Koper, I., Lubben, J., Vasilev, K. and Knoll, W. Tethered lipid Bilayers on ultraflat gold surfaces. *Langmuir*, **19**(13), 5435–5443, 2003.
- [177] Naumann, R., Walz, D., Schiller, S. M. and Knoll, W. Kinetics of valinomycin-mediated K<sup>+</sup> ion transport through tethered bilayer lipid membranes. *Journal of Electroanalytical Chemistry*, **550**, 241–252, 2003.
- [178] Steinem, C., Galla, H. J. and Janshoff, A. Interaction of melittin with solid supported membranes. *Physical Chemistry Chemical Physics*, **2**(20), 4580–4585, 2000.

- [179] Steinem, C., Janshoff, A., Galla, H. J. and Sieber, M. Impedance analysis of ion transport through gramicidin channels incorporated in solid supported lipid bilayers. *Bioelectrochemistry and Bioenergetics*, **42**(2), 213–220, 1997.
- [180] Gritsch, S., Nollert, P., Jahnig, F. and Sackmann, E. Impedance spectroscopy of porin and gramicidin pores reconstituted into supported lipid bilayers on indium-tin-oxide electrodes. *Langmuir*, **14**(11), 3118–3125, 1998.
- [181] Yin, P., Burns, C. J., Osman, P. D. J. and Cornell, B. A. A tethered bilayer sensor containing alamethicin channels and its detection of amiloride based inhibitors. *Biosensors & Bioelectronics*, **18**(4), 389–397, 2003.
- [182] Glazier, S. A., Vanderah, D. J., Plant, A. L., Bayley, H., Valincius, G. and Kasianowicz, J. J. Reconstitution of the pore-forming toxin alpha-hemolysin in phospholipid/18-octadecyl-1-thiahexa(ethylene oxide) and phospholipid/n-octadecanethiol supported bilayer membranes. *Langmuir*, **16**(26), 10428–10435, 2000.
- [183] Hirano, A., Wakabayashi, M., Matsuno, Y. and Sugawara, M. A single-channel sensor based on gramicidin controlled by molecular recognition at bilayer lipid membranes containing receptor. *Biosensors & Bioelectronics*, **18**(8), 973–983, 2003.
- [184] Knapp, O., Benz, R., Gibert, M., Marvaud, J. C. and Popoff, M. R. Interaction of Clostridium perfringens iota-toxin with lipid bilayer membranes - Demonstration of channel formation by the activated binding component Ib and channel block by the enzyme component Ia. *Journal of Biological Chemistry*, **277**(8), 6143–6152, 2002.
- [185] Bayley, H. and Jayasinghe, L. Functional engineered channels and pores - (Review). *Molecular Membrane Biology*, **21**(4), 209–220, 2004.
- [186] Andersson, M., Keizer, H. M., Zhu, C. Y., Fine, D., Dodabalapur, A. and Duran, R. S. Detection of single ion channel activity on a chip using tethered bilayer membranes. *Langmuir*, **23**(6), 2924–2927, 2007.
- [187] Doyle, D. A., Cabral, J. M., Pfuetzner, R. A., Kuo, A. L., Gulbis, J. M., Cohen, S. L., Chait, B. T. and MacKinnon, R. The structure of the potassium channel: Molecular basis of K<sup>+</sup> conduction and selectivity. *Science*, **280**(5360), 69–77, 1998.
- [188] Cornell, B. A., BraachMaksyvtis, V. L. B., King, L. G., Osman, P. D. J., Raguse, B., Wieczorek, L. and Pace, R. J. A biosensor that uses ion-channel switches. *Nature*, **387**(6633), 580–583, 1997.
- [189] Woodhouse, G., King, L., Wieczorek, L., Osman, P. and Cornell, B. The ion channel switch biosensor. *Journal of Molecular Recognition*, **12**(5), 328–334, 1999.
- [190] Nikolelis, D. P., Siontorou, C. G., Krull, U. J. and Katrivanos, P. L. Ammonium ion minisensors from self-assembled bilayer lipid membranes using Gramicidin as an ionophore. Modulation of ammonium selectivity by platelet-activating factor. *Analytical Chemistry*, **68**(10), 1735–1741, 1996.
- [191] Blake, S., Mayer, T., Mayer, M. and Yang, J. Monitoring chemical reactions by using ion-channel-forming peptides. *ChemBiochem*, **7**(3), 433–435, 2006.
- [192] Boulmedais, F., Frisch, B., Etienne, O., Lavallo, P., Picart, C., Ogier, J., Voegel, J. C., Schaaf, P. and Egles, C. Polyelectrolyte multilayer films with pegylated polypeptides as a new type of antimicrobial protection for biomaterials. *Biomaterials*, **25**(11), 2003–2011, 2004.
- [193] Templin, M. F., Stoll, D., Schrenk, M., Traub, P. C., Vohringer, C. F. and Joos, T. O. Protein microarray technology. *Trends in Biotechnology*, **20**(4), 160–166, 2002.

- [194] Haab, B. B. Antibody Arrays in cancer research. *Molecular & Cellular Proteomics*, **4**(4), 377–383, 2005.
- [195] Romer, W., Lam, Y. H., Fischer, D., Watts, A., Fischer, W. B., Goring, P., Wehrspohn, R. B., Gosele, U. and Steinem, C. Channel activity of a viral transmembrane peptide in micro-BLMs: Vpu(1-32) from HIV-1. *Journal of the American Chemical Society*, **126**(49), 16267–16274, 2004.
- [196] Danelon, C., Perez, J. B., Santschi, C., Brugger, J. and Vogel, H. Cell membranes suspended across nanoaperture arrays. *Langmuir*, **22**(1), 22–25, 2006.
- [197] Malhotra, B. D., Singhal, R., Chaubey, A., Sharma, S. K. and Kumar, A. Recent trends in biosensors. *Current Applied Physics*, **5**(2), 92–97, 2005.
- [198] Botrã, F., Podestã, E., Silvestrini, B. and Bortã, C. Toxicity testing in environmental monitoring: the role of enzymatic biosensors. *Ann. Ist. Super. Sanitã*, **37**(4), 607–613, 2001.
- [199] Trojanowicz, M. Determination of pesticides using electrochemical enzymatic biosensors. *Electroanalysis*, **14**(19-20), 1311–1328, 2002.
- [200] Rasooly, A. and Jacobson, J. Development of biosensors for cancer clinical testing. *Biosensors & Bioelectronics*, **21**(10), 1851–1858, 2006.
- [201] Ray, S., Britschgi, M., Herbert, C., Takeda-Uchimura, Y., Boxer, A., Blennow, K., Friedman, L. F., Galasko, D. R., Jutel, M., Karydas, A., Kaye, J. A., Leszek, J., Miller, B. L., Minthon, L., Quinn, J. F., Rabinovici, G. D., Robinson, W. H., Sabbagh, M. N., So, Y. T., Sparks, D. L., Tabaton, M., Tinklenberg, J., Yesavage, J. A., Tibshirani, R. and Wyss-Coray, T. Classification and prediction of clinical Alzheimer's diagnosis based on plasma signaling proteins. *Nature Medicine*, **13**(11), 1359–1362, 2007.
- [202] Marquette, C. A. and Blum, L. J. State of the art and recent advances in immunoanalytical systems. *Biosensors & Bioelectronics*, **21**(8), 1424–1433, 2006.
- [203] Rongen, H. A. H., Bult, A. and vanBennekom, W. P. Liposomes and immunoassays. *Journal of Immunological Methods*, **204**(2), 105–133, 1997.
- [204] Wang, Y. J. and Caruso, F. Nanoporous protein particles through templating mesoporous silica spheres. *Advanced Materials*, **18**(6), 795–+, 2006.
- [205] Grieshaber, D., MacKenzie, R., Voros, J. and Reimhult, E. Electrochemical biosensors - Sensor principles and architectures. *Sensors*, **8**(3), 1400–1458, 2008.
- [206] Okuno, J., Maehashi, K., Kerman, K., Takamura, Y., Matsumoto, K. and Tamiya, E. Label-free immunosensor for prostate-specific antigen based on single-walled carbon nanotube array-modified microelectrodes. *Biosensors & Bioelectronics*, **22**(9-10), 2377–2381, 2007.
- [207] <http://www.thailabonline.com>.
- [208] Dai, Z., Yan, F., Chen, J. and Ju, H. X. Reagentless amperometric immunosensors based on direct electrochemistry of horseradish peroxidase for determination of carcinoma antigen-125. *Analytical Chemistry*, **75**(20), 5429–5434, 2003.
- [209] Schlageter, M. H., Larghero, J., Cassinat, B., Toubert, M. E., Borschneck, C. and Rain, J. D. Serum carcinoembryonic antigen, cancer antigen 125, cancer antigen 15-3, squamous cell carcinoma, and tumor-associated trypsin inhibitor concentrations during healthy pregnancy. *Clinical Chemistry*, **44**(9), 1995–1998, 1998.

- [210] <http://www.panomics.com>.
- [211] Nirschl, M., Bluher, A., Erler, C., Katzschner, B., Vikholm-Lundin, I., Auer, S., Voros, J., Pompe, W., Schreiter, M. and Mertig, M. Film bulk acoustic resonators for DNA and protein detection and investigation of in-vitro bacterial S-layer formation. *Euroensors XXII*, **Paper ID 644**, 2008.
- [212] Ronkainen-Matsuno, N. J., Thomas, J. H., Halsall, H. B. and Heinemann, W. R. Electrochemical immunoassay moving into the fast lane. *Trac-Trends in Analytical Chemistry*, **21**(4), 213–225, 2002.
- [213] Hook, F., Kasemo, B., Nylander, T., Fant, C., Sott, K. and Elwing, H. Variations in coupled water, viscoelastic properties, and film thickness of a Mefp-1 protein film during adsorption and cross-linking: A quartz crystal microbalance with dissipation monitoring, ellipsometry, and surface plasmon resonance study. *Analytical Chemistry*, **73**(24), 5796–5804, 2001.
- [214] Irwin, E. F., Ho, J. E., Kane, S. R. and Healy, K. E. Analysis of interpenetrating polymer networks via quartz crystal microbalance with dissipation monitoring. *Langmuir*, **21**(12), 5529–5536, 2005.
- [215] Sauerbrey, G. Verwendung Von Schwingquarzen Zur Wagung Dunner Schichten Und Zur Mikrowagung. *Zeitschrift Fur Physik*, **155**(2), 206–222, 1959.
- [216] Gewirth, A. A. and Niece, B. K. Electrochemical applications of in situ scanning probe microscopy. *Chemical Reviews*, **97**(4), 1129–1162, 1997.
- [217] Jones, C. W., Smolinski, D., Keogh, A., Kirk, T. B. and Zheng, M. H. Confocal laser scanning microscopy in orthopaedic research. *Progress in Histochemistry and Cytochemistry*, **40**(1), 1–71, 2005.
- [218] Larsson, C., Bramfeldt, H., Wingren, C., Borrebaeck, C. and Hook, F. Gravimetric antigen detection utilizing antibody-modified lipid bilayers. *Analytical Biochemistry*, **345**(1), 72–80, 2005.
- [219] Patolsky, F., Lichtenstein, A. and Willner, I. Amplified microgravimetric quartz-crystal-microbalance assay of DNA using oligonucleotide-functionalized liposomes or biotinylated liposomes. *Journal of the American Chemical Society*, **122**(2), 418–419, 2000.
- [220] Yun, K., Kobatake, E., Haruyama, T., Laukkanen, M. L., Keinänen, K. and Aizawa, M. Use of a quartz crystal microbalance to monitor immunoliposome-antigen interaction. *Analytical Chemistry*, **70**(2), 260–264, 1998.
- [221] Woodle, M. C., Engbers, C. M. and Zalipsky, S. New Amphipatic Polymer Lipid Conjugates Forming Long-Circulating Reticuloendothelial System-Evading Liposomes. *Bioconjugate Chemistry*, **5**(6), 493–496, 1994.
- [222] Kita-Tokarczyk, K., Grumelard, J., Haeefe, T. and Meier, W. Block copolymer vesicles - using concepts from polymer chemistry to mimic biomembranes. *Polymer*, **46**(11), 3540–3563, 2005.
- [223] Hamann, C. and Vielstich, W. *Elektrochemie*. WILEY-VHC Verlag GmbH und Co., 4 edition, 2005.
- [224] Green, N. M., Konieczn.L, Toms, E. J. and Valentin.Rc. Use of Bifunctional Biotinyl Compounds to Determine Arrangement of Subunits in Avidin. *Biochemical Journal*, **125**(3), 781, 1971.
- [225] Mayer, L. D., Hope, M. J. and Cullis, P. R. Vesicles of Variable Sizes Produced by a Rapid Extrusion Procedure. *Biochimica Et Biophysica Acta*, **858**(1), 161–168, 1986.
- [226] Hecht, H. J., Schomburg, D., Kalisz, H. and Schmid, R. D. The 3d Structure of Glucose-Oxidase from *Aspergillus-Niger* - Implications for the Use of God as a Biosensor Enzyme. *Biosensors & Bioelectronics*, **8**(3-4), 197–203, 1993.



- 
- [227] Q-Sense, a. n. Lipid Bilayer Formation; A Comparison between QCM-D, SPR and AFM.
- [228] Boulmedais, F., Ball, V., Schwinte, P., Frisch, B., Schaaf, P. and Voegel, J. C. Buildup of exponentially growing multilayer polypeptide films with internal secondary structure. *Langmuir*, **19**(2), 440–445, 2003.
- [229] Hubsch, E., Fleith, G., Fatisson, J., Labbe, P., Voegel, J. C., Schaaf, P. and Ball, V. Multivalent ion/polyelectrolyte exchange processes in exponentially growing multilayers. *Langmuir*, **21**(8), 3664–3669, 2005.
- [230] Takita, R., Yoshida, K. and Anzai, J. Redox properties of ferricyanide ion on layer-by-layer deposited poly(glutamic acid) film-coated electrodes and its use for electrocatalytic sensing of ascorbic acid. *Sensors and Actuators B-Chemical*, **121**(1), 54–60, 2007.
- [231] Forzani, E. S., Otero, M., Perez, M. A., Teijelo, M. L. and Calvo, E. J. The structure of layer-by-layer self-assembled glucose oxidase and Os(Bpy)(2)CIPyCH<sub>2</sub>NH-Poly(allylamine) multilayers: Ellipsometric and quartz crystal microbalance studies. *Langmuir*, **18**(10), 4020–4029, 2002.
- [232] Farhat, T. R. and Schlenoff, J. B. Ion transport and equilibria in polyelectrolyte multilayers. *Langmuir*, **17**(4), 1184–1192, 2001.
- [233] Han, S. and Lindholm-Sethson, B. Electrochemistry at ultrathin polyelectrolyte films self-assembled at planar gold electrodes. *Electrochimica Acta*, **45**(6), 845–853, 1999.



---

## PEM Coated Particles and PEM Capsules

---

As an alternative to enzymatic EC detection it might be possible to use the oxidation/reduction current of FC incorporated in PGA/PAH films for the signal amplification in the sandwich assay. Therefore, either microparticles coated with PGA/PAH or PEM capsules made from the same polyelectrolytes could be applied. In the following sections the investigated approaches with their different parameters such as core material, core size, polyelectrolytes or number of bilayers are described.

### **A.1 Calcium Carbonate Particles**

Since Calcium Carbonate ( $\text{CaCO}_3$ ) particles are porous, they would be ideal to incorporate enzymes. They were coated as described in the Materials and Methods Section.

To see whether the polymer really adsorbs to the particles, they were coated with PEI-PGA-PAH-PGA-(PLL-*g*-PEG-TRITC). The last polymer layer is visible when activated with a 561 nm laser. In Figure A.1a a CLSM image and the corresponding bright field image before the application of the fluorescent polymer layer is shown. The images in Figure A.1b were taken with the same settings after the adsorption of the fluorescent PLL-*g*-PEG-TRITC. From the fluorescent intensity it is clearly visible that the particles were well coated with the polymer.

On the other hand, especially on the bright field images, one can see some cubic crystals in between the spherical particles. Since in the very beginning these crystals were not abundant, they must have formed in the buffer and/or polymer solution. When

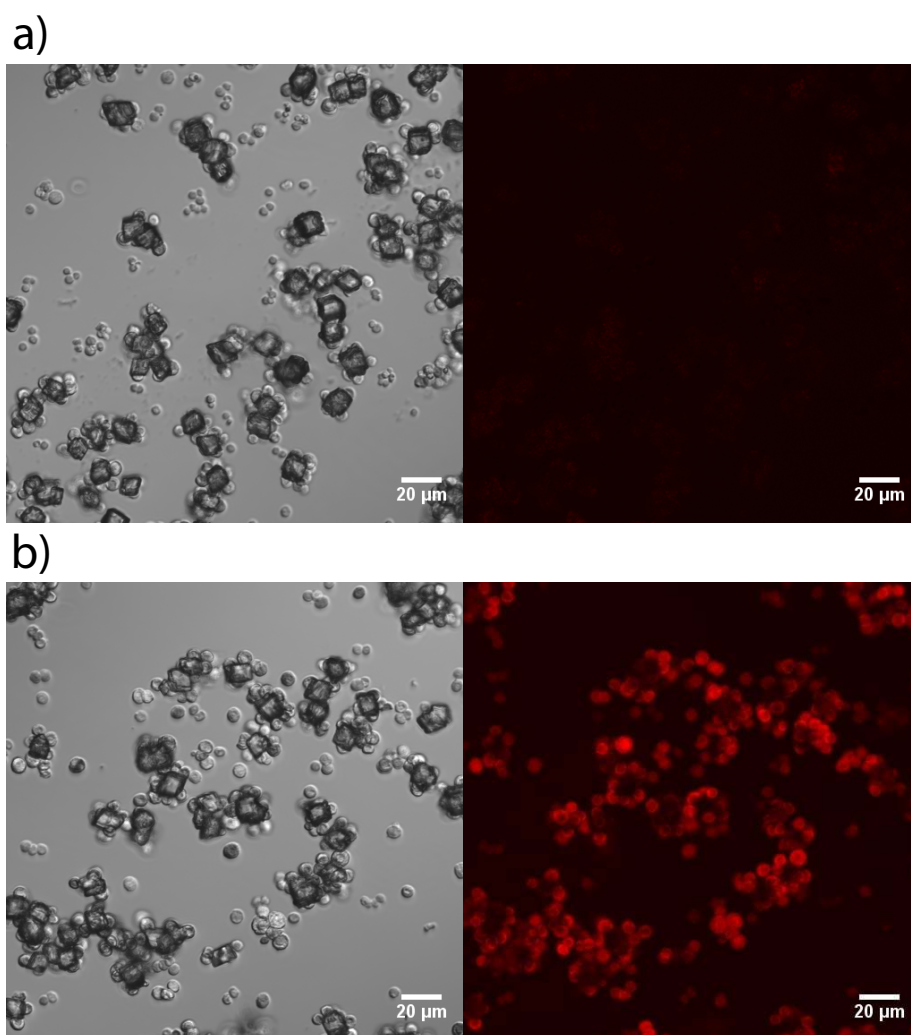


**Figure A.1:**  $\text{CaCO}_3$  particles coated with a) PEI-PGA-PAH-PGA and b) additionally with the fluorescent PLL-g-PEG-TRITC. From the fluorescence images on the right it is obvious that the particles were properly coated with polyelectrolytes. Furthermore, some  $\text{CaCO}_3$  crystals had already been formed.

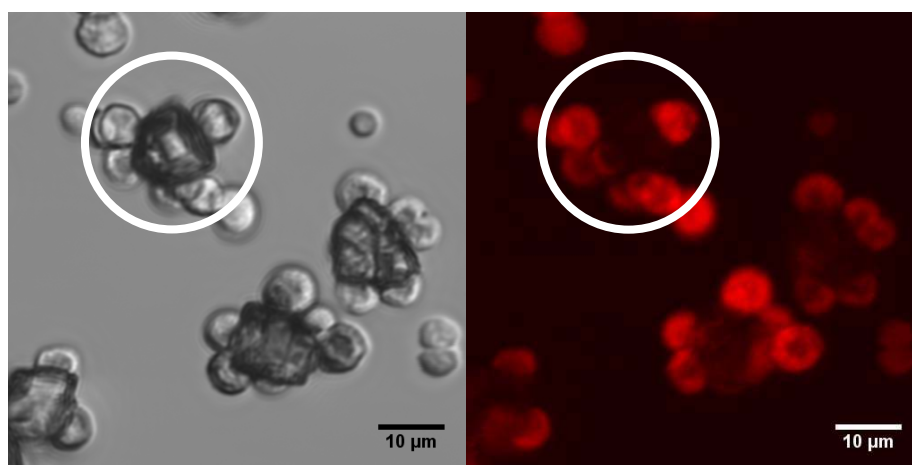


**Figure A.2:** Zoom in to a group of  $\text{CaCO}_3$  particles and crystals. As opposed to the particles, there was no polymer adsorbed to their surface.

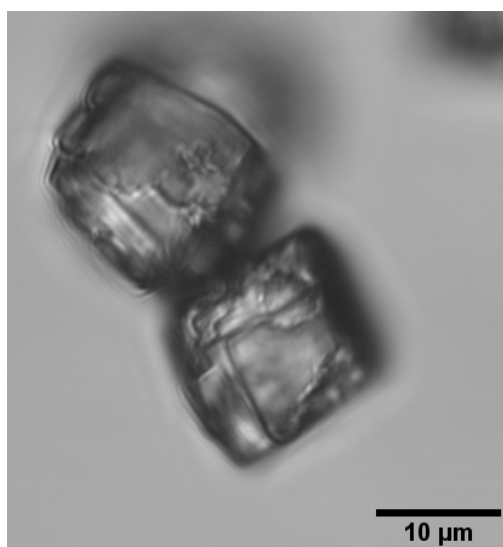


**Figure A.3:** Detailed view of two  $\text{CaCO}_3$  crystals. They all had a size of a bit more than  $10 \mu\text{m}$ .

having a closer look at these crystals (see Figure A.2), it is obvious that they had no fluorescent polymer coating. Thus, they cannot be used for the current system. After one day in buffer solution all particles had disappeared and new crystals had been formed. Once this process was finished, size and shape of the crystals did not change any more. A higher magnification image of such crystals is given in Figure A.3.

Even coating the particles instantly after getting into contact with the buffer solution did not prevent them from the conversion. Since the polymers did not adsorb to the crystals, which furthermore were not porous any more, this approach was not followed any further.

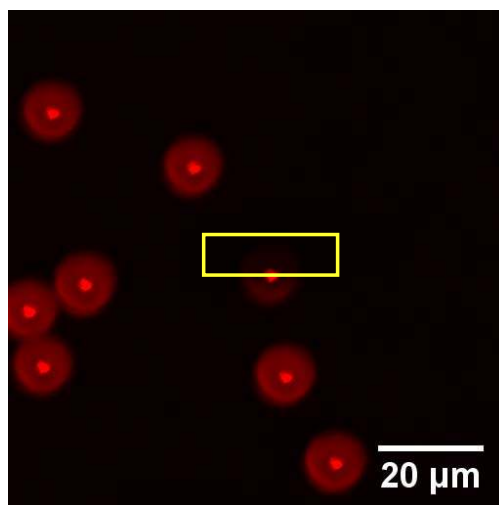


**Figure A.4:** PS particles coated with the fluorescent PLL-*g*-PEG-TRITC, where the yellow marked area had been bleached. Compared to a control measurement before bleaching the detected intensity within the rectangle was almost decreased to the background signal.

## A.2 Polystyrene Particles

Another approach was performed with Polystyrene (PS) particles. Differently sized particles (1, 2 and 10  $\mu\text{m}$ ) were coated with PGA/PAH multilayers. First, an experiment with the fluorescently labelled polymer PLL-*g*-PEG-TRITC was performed. Figure A.4 illustrates that it was possible to bleach the red colour of the polymer label in the yellow box.

When small microparticles were used, they built agglomerates already after the adsorption of few polyelectrolyte layers. Even with extensive vortexing and ultrasonic cleaning it was not possible to dissolve these agglomerates. With the 10  $\mu\text{m}$  particles however, no agglomerates were formed (see Figure A.5).

The mediator ferrocyanide was added to the coated particles and washed off after 10 minutes. Then, the particles were given into a flowcell to estimate their density on the surface. After letting them settle onto the surface (working electrode) CV was applied. However, no significant oxidation and reduction peaks were monitored. A possible explanation for this observation could be that the FC ions are not mobile enough to travel around the whole particle to interact with the electrode.

Therefore, THF was added to dissolve the PS cores in order to obtain PEM capsules. This would allow for a higher contact area of the PEM films and the electrode. An example of coated particles (PEI-(PGA-PAH)<sub>3</sub>-PGA) before the addition of THF is given

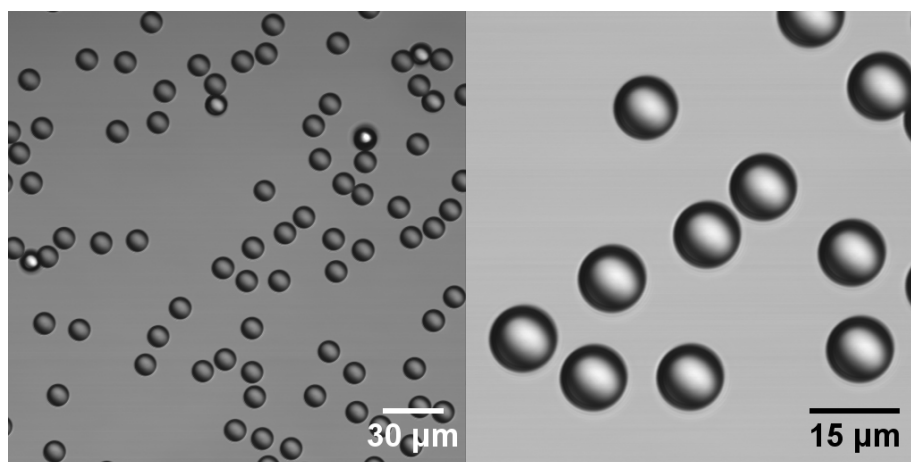


**Figure A.5:** Polyelectrolyte coated  $10\ \mu\text{m}$  particles. As opposed to smaller particles, these ones did not form agglomerates.

in Figure A.6a. The surface was flat and only the center of the core gave an autofluorescent signal. After the treatment with THF the core was partly dissolved (Figure A.6b). However, the single leftovers were too large to diffuse through the PEM shell. This result was independent of the last layer and also an exposure to a high concentration of THF during 24 hours did not significantly improve the result. To conclude, the PS particles were successfully coated with PEM, but it was not possible to completely dissolve and remove the core.

### A.3 Melamine Formaldehyde Particles

After the results with the PS particles, we were looking for a core suitable to form PEM capsules. Melamine formaldehyde (MF) particles are among the most common ones for such applications.

To stick with the most common system, the MF particles were first coated with PAH/PSS multilayers, before dissolving the cores with a diluted hydrogen peroxide solution. In case of eight bilayers the shells burst and the core was expelled (see time series in Figure A.7). The remaining capsules were all open, or in other words destroyed. Decreasing the number of bilayers to three prevented the capsules from exploding during the core dissolution (see also publication by Dong *et al.* [68]). The cores dissolved completely inside the shells as shown in the time series in Figure A.8.

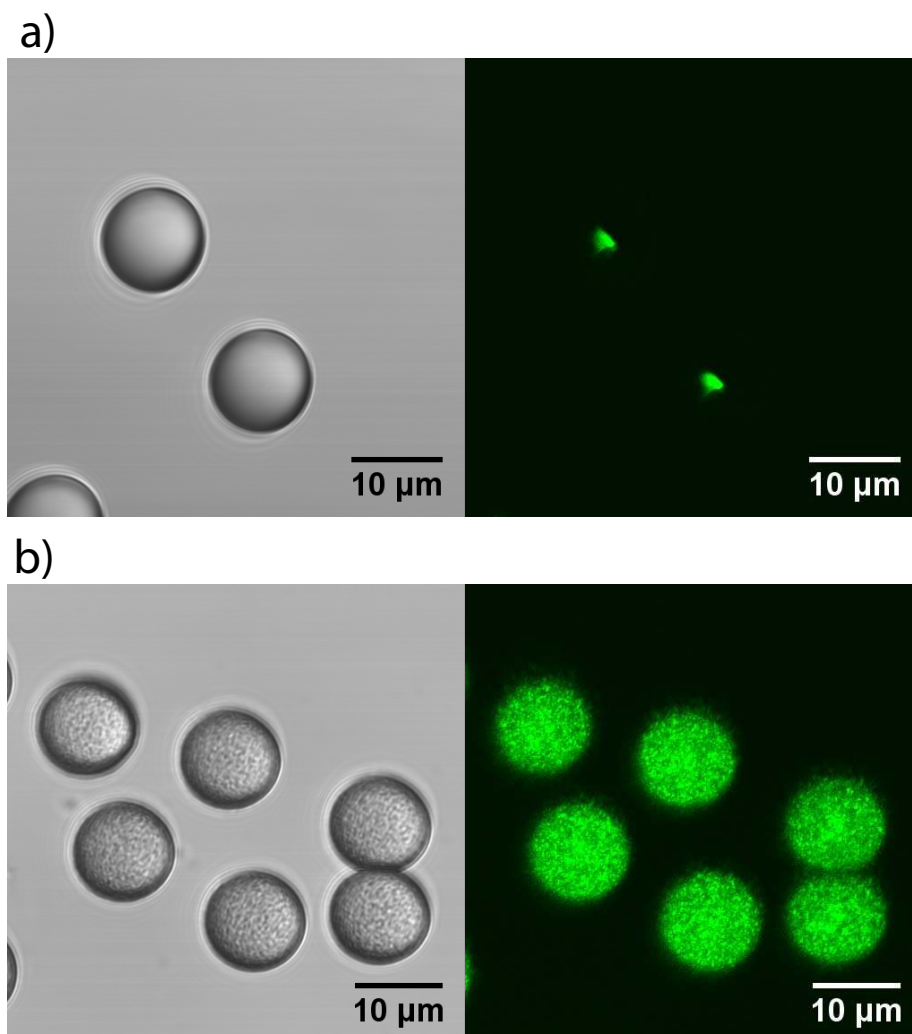


**Figure A.6:** Microscopy image and autofluorescence of PEM coated PS particles a) before and b) after the addition of THF. THF only partly dissolved the cores. The remaining parts stayed inside the capsules.

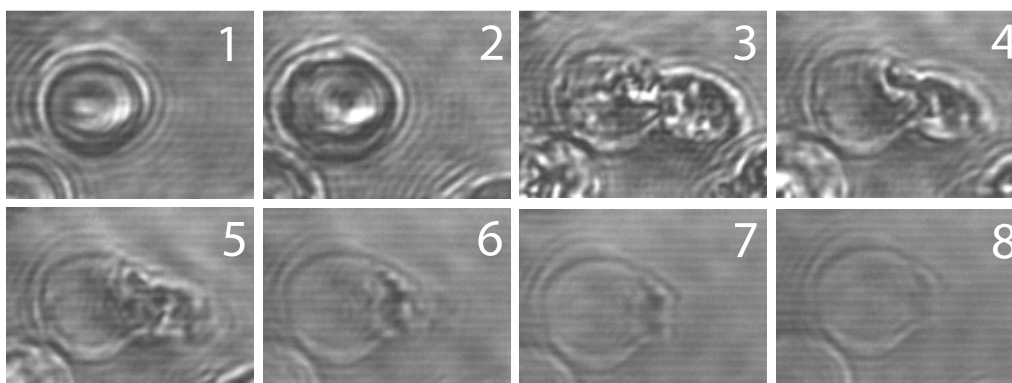


**Figure A.7:** Time series of core dissolution of MF particles coated with 8 PAH/PSS bilayers. Upon contact with a  $\text{H}_2\text{O}_2$  solution the shell burst and the core was expelled, resulting in opened capsules.



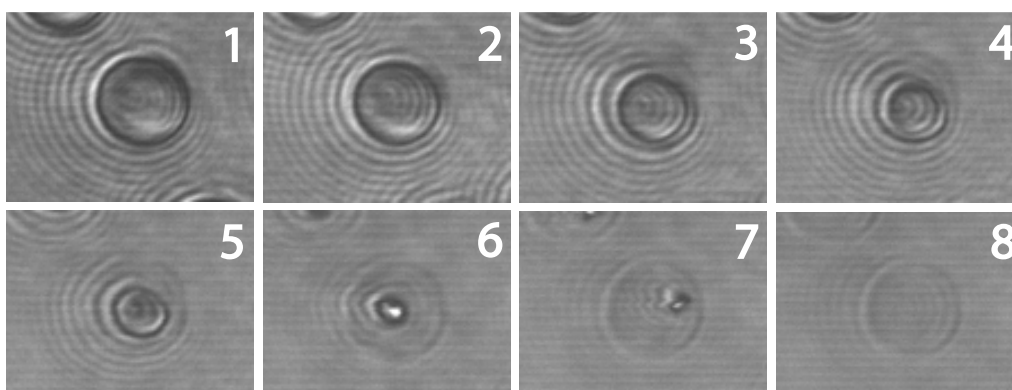


**Figure A.8:** Time series of core dissolution of MF particles coated with 3 PAH/PSS bilayers. The cores were slowly and completely dissolved inside the capsules.

With these positive results in mind the polyelectrolyte system was changed to PGA/PAH. With these polymers it was possible to successfully coat the MF particles. However, during dissolution of the core the PEM shell was dissolved as well. Since from the so far tested polyelectrolyte pairs PGA/PAH is the only combination showing the swelling/deswelling behaviour, it is not possible to change the composition of the PEM layers.

## A.4 Conclusion and Outlook

In this section several ways to finally use the oxidation/reduction of FC in PEM films for a sandwich assay were presented. It was possible to successfully coat microparticles with PGA/PAH multilayers. At the same time it became obvious that the limited contact area of the particles and the electrode would require PEM capsules. However, for different reasons all the approaches to fabricate PGA/PAH capsules were unsuccessful.

Of course it is possible that one day a solution will be found. But these investigations would have gone beyond the scope and time-frame of this thesis.



---

## Curriculum Vitae

---

### Personal

Name: Dorothea Niederberger (maiden name: Grieshaber)  
Date of Birth: 23. February 1981  
Nationality: Swiss, Citizen of Schaffhausen SH, Hallau SH and Dallenwil NW  
Present Address: Asylstrasse 18  
CH-8800 Thalwil  
Switzerland

### Education and Practical Experience

2005 – 2009      Doctoral student at the Laboratory of Biosensors and Bioelectronics, Institute for Biomedical Engineering, Department of Information Technology and Electrical Engineering, ETH Zürich  
2001 – 2005      Studies of Material Sciences at the ETH Zürich. Graduation with the degree Dipl. Werkstoff-Ing. ETH  
1996 – 2001      Gymnasium in Schaffhausen (SH), Switzerland, Matura Typus C

### Publications Related to this Thesis

#### Presentations

2008      Electroactive Polyelectrolyte Multilayers (*poster presentation*)  
**D. Grieshaber**, R. Zahn, J. Vörös, T. Zambelli, P. Schaaf, V. Ball, J.-C. Voegel, F. Boulmedais

SBE's 4th International Conference on Bioengineering and Nanotechnology,  
July 22–24, Dublin, Ireland

Electrochemical QCM-D for Electroactive Polyelectrolyte Multilayers and in  
Enzymatic Biosensing (*invited oral presentation*)

**D. Grieshaber**, J. Vörös

Scientific workshop - Surface Analytical Techniques, June 17, Dübendorf,  
Switzerland

Enzymatic Biosensors with Electrochemical Detection for Early Cancer Diagno-  
sis (*poster presentation*)

**D. Grieshaber**, V. de Lange, J. Vörös

The 10<sup>th</sup> World Congress on Biosensors, May 14–16, Shanghai, China

2007 Development of Enzymatic Biosensors with the Help of the QCM-D (*oral pre-  
sentation*)

**D. Grieshaber**, E. Reimhult, J. Vörös

Q-Sense user meeting, October 30–31, Toulouse, France

Enzyme Loaded Vesicles in Enzymatic Biosensing (*poster presentation*)

**D. Grieshaber**, E. Reimhult, J. Vörös

NanoEurope, September 12, St. Gallen, Switzerland

Increasing the Sensitivity of Enzymatic Biosensors by Working at the Phase  
Transition Temperature (*poster presentation*)

**D. Grieshaber**, E. Reimhult, J. Vörös

Biosurf VII, August 29–31, Zürich, Switzerland

Enzymatic Biosensors for early cancer detection (*poster presentation*)

**D. Grieshaber**, E. Reimhult, J. Vörös

2nd MRC meeting, June 27, Zürich, Switzerland

Ways to Improve the Substrate Permeability through a Vesicle Membrane, (*oral  
presentation*)

**D. Grieshaber**, E. Reimhult, J. Vörös

1st Joint Group Meeting University of Strasbourg - ETH Zurich, May 10–12, Albe, France

Enzymatic Biosensors towards a Multiplexed Electronic Detection System for Early Cancer Diagnostics (*oral presentation*)

**D. Grieshaber**, E. Reimhult, J. Vörös

2nd IEEE-NEMS conference, January 16–19, Bangkok, Thailand

2006 Different Immobilization Strategies of Enzymes to Evaluate their Activity in Variable Environments (*oral presentation*)

**D. Grieshaber**, E. Reimhult, B. Städler, J. Vörös

2nd Joint Group Meeting University of Twente - ETH Zurich, November 22–24, Wasserstelz, Germany

Patterning of DNA-tagged Vesicles towards Enzymatic Biosensors (*poster presentation*)

**D. Grieshaber**, B. Städler, E. Reimhult, J. Vörös

Gordon Research Conference on Bioanalytical Sensors, October 22–27, Les Diablerets, Switzerland

Micropatterns of DNA-tagged Vesicles towards Membrane Protein Microarrays, (*oral presentation*)

**D. Grieshaber**, B. Städler, M. Bally, J. Vörös

The 9<sup>th</sup> World Congress on Biosensors, May 10–12, Toronto, Canada

## Publications

T. Sannomiya, P. K. Sahoo, D. I. Mahcicek, **D. Grieshaber**, H. H. Solak, C. Hafner, and J. Vörös, Biosensing by Densely Packed and Optically Coupled Plasmonic Particle Arrays, *Small*, **2009**, accepted.

**D. Grieshaber**, V. de Lange, T. Hirt, Z. Lu and J. Vörös, Vesicles for Signal Amplification in a Biosensor for the Detection of Low Antigen Concentrations, *Sensors*, **2008**, 8: 7894-7903.

M. Bally, K. Bailey, **D. Grieshaber**, K. Sugihara, J. Vörös, and B. Städler, Synthetic and Functional Vesicle and Bilayer Arrays for Biosensing Applications, *Biointerphases*, **2008**, submitted.

**D. Grieshaber**, J. Vörös, T. Zambelli, V. Ball, P. Schaaf, J.-C. Voegel, and F. Boulmedais, Swelling and Contraction of Ferrocyanide-Containing Polyelectrolyte Multilayers upon Application of an Electric Potential, *Langmuir*, **2008**, 24(23): 13668–13676.

**D. Grieshaber**, R. MacKenzie, J. Vörös, and E. Reimhult, Electrochemical Biosensors - Sensor Principles and Architectures, *Sensors* **2008**, 8(3): 1400–1458.

B. Städler, M. Bally, **D. Grieshaber**, J. Vörös, A. Brisson, and H. M. Grandin, Creation of a functional heterogeneous vesicle array via DNA controlled surface sorting onto a spotted microarray, *Biointerphases* **2006**, 1(4): 142–145.

### Patents

**D. Grieshaber** and J. Vörös, Nanoparticle Based Amplification Scheme for the Detection of Low Concentration of Analytes, EP T-08-039, US provisional patent application.

**D. Grieshaber**, J. Vörös, T. Hirt, Z. Lu, US Patent Application Serial No. 12/315659 and PCT Application No. PCT/US08/13391.